1-1-2016

Functional Evaluation of the Peripheral Vasculature Using Magnetic Resonance Imaging

Erin Kristine Englund
University of Pennsylvania, eenglund@mail.med.upenn.edu

Functional Evaluation of the Peripheral Vasculature Using Magnetic Resonance Imaging

Abstract
Akin to cardiac stress testing, functional integrity of the peripheral vasculature can be interrogated by measuring the response to a stimulus. Recent reports suggest that the reactive hyperemia response, the physiologic reaction following induced ischemia, is associated with disease presence, correlated with disease severity, and may be a sensitive biomarker of pre-clinical disease.

In this dissertation, an innovative, interleaved magnetic resonance imaging method is developed, termed Perfusion, Intravascular Venous Oxygen saturation, and T2* (PIVOT), which simultaneously measures microvascular perfusion, venous oxygen saturation (SvO2), and the blood-oxygen-level dependent (BOLD) signal. PIVOT is first applied in healthy subjects to demonstrate its ability to measure reactive hyperemia response dynamics.

Next, reactive hyperemia perfusion is compared between the more temporally efficient pulsed arterial spin labeling (PASL) used in PIVOT and the more recently developed and preferred method for the brain, pseudo-continuous ASL (pCASL). Assessment of the impact of blood flow variability throughout the ischemia-reperfusion paradigm on pCASL perfusion quantification is investigated. Then, both PASL and pCASL sequences are used to measure reactive hyperemia perfusion in healthy subjects. No significant differences were detected between perfusion measured with PASL or pCASL despite different labeling strategies, temporal resolutions, and perfusion quantification models.

Subsequently, PIVOT is combined with a velocity-encoded dual-echo GRE to create an interleaved three-slice sequence that provides quantification of bulk blood flow in the arteries and veins in addition to the traditional PIVOT measures. This new sequence, termed Velocity and PIVOT (vPIVOT) is used to investigate the relationship of blood flow in the macro- and microvasculature and muscle oxygen consumption during the transition from exercise to rest.

Finally, PIVOT is applied clinically in a cohort of patients with varying degrees of severity of peripheral artery disease. Increasing disease severity was correlated with a prolongation of the hyperemic response time, measured as a lengthening of time to peak perfusion, SvO2 washout time, and time to peak T2*. In addition, peak perfusion and SvO2 upslope were significantly different between patients with PAD and healthy controls. These results suggest the potential for PIVOT to evaluate disease severity and may present a tool to assess response to therapeutic intervention.

Degree Type
Dissertation

Degree Name
Doctor of Philosophy (PhD)

Graduate Group
Bioengineering

FUNCTIONAL EVALUATION OF THE PERIPHERAL VASCULATURE USING MAGNETIC RESONANCE IMAGING

Erin K. Englund

A DISSERTATION

in

Bioengineering

Presented to the Faculties of the University of Pennsylvania in

Partial Fulfillment of the Requirements for the

Degree of Doctor of Philosophy

2016

Supervisor of Dissertation

_____

Felix W. Wehrli, Ph.D.

Professor of Radiology

Graduate Group Chairperson

_____

Jason A. Burdick, Ph.D. Professor of Bioengineering

Dissertation Committee

Hee Kwon Song, Ph.D., Associate Professor of Radiology (Chair)

Emile R. Mohler, III, M.D., Professor of Medicine

Victor A. Ferrari, M.D. Professor of Medicine

Bruce M. Damon, Ph.D. Associate Professor of Radiology & Radiological Sciences, Vanderbilt University

FUNCTIONAL EVALUATION OF THE PERIPHERAL VASCULATURE USING MAGNETIC RESONANCE IMAGING

COPYRIGHT

To my family.

ACKNOWLEDGEMENTS

I would like to express my gratitude to the people who helped to make this thesis possible, especially my advisor, Dr. Felix Wehrli. His unending curiosity, dedication to the scientific pursuit, and passion for the field is an inspiration. I would also like to acknowledge Dr. Bruce Damon, who first introduced me to the world of MRI research. Without a doubt I would not have ended up here if not for his support and encouragement. I have been fortunate to work with many brilliant colleagues including: Michael Langham, who initially guided me in the MRI assessment of the circulatory system; Zach Rodgers, who was always willing to talk through ideas, get a cup of coffee, go for a run, or volunteer for a scan; and Cheng Li, without whom several technical feats accomplished for the pursuit of this project would not have been possible. It was a pleasure to work alongside other members of the LSNI including Alan Seifert, Jeremy Magland, Varsha Jain, Erica Chirico, Yulin Chang, Xia Zhou, Chamith Rajapakse, Suliman Barhoum, and Yongxia Zhou. Additionally, a big thank you goes out to Holly Flachs, who always advocated for me and ensured that everything behind the scenes ran smoothly.

I would like to thank my thesis committee members, Dr. Hee Kwon Song, Dr. Emile Mohler, Dr. Victor Ferrari, and Dr. Bruce Damon, who provided insight and direction throughout my dissertation. I would also like to thank those who provided the funding for this research: Dr. Felix Wehrli, Dr. Emile Mohler, Dr. Tom Floyd, the American Heart Association, and HHMI-NIBIB Interfaces Scholars Program: Dr. Jim Gee, Dr. Andrew Maidment, Dr. Peter Davies, and Dr. Ann Tiao. This research would not have been possible without the team of study coordinators including Molly Fanning, Scott Welden, Liz Beothy, Elizabeth Medenilla, and Zeeshan Khan; or the MRI technologists, especially Pat O'Donnell, Doris Cain, Jacqui Meeks, and Norman Butler.

And finally, I want to thank my family for their love and support. To my Mom, Dad, and sister Anna, thank you for being my cheerleaders every step of the way, and to my fiancé and teammate Andy, thank you for your selflessness, creativity, and boundless enthusiasm.

ABSTRACT

FUNCTIONAL EVALUATION OF THE PERIPHERAL VASCULATURE USING MAGNETIC RESONANCE IMAGING

Erin K. Englund

Felix W. Wehrli, Ph.D.

Akin to cardiac stress testing, functional integrity of the peripheral vasculature can be interrogated by measuring the response to a stimulus. Recent reports suggest that the reactive hyperemia response, the physiologic reaction following induced ischemia, is associated with disease presence, correlated with disease severity, and may be a sensitive biomarker of pre-clinical disease.

In this dissertation, an innovative, interleaved magnetic resonance imaging method is developed, termed Perfusion, Intravascular Venous Oxygen saturation, and T_2* (PIVOT), which simultaneously measures microvascular perfusion, venous oxygen saturation (SvO_2), and the blood-oxygen-level dependent (BOLD) signal. PIVOT is first applied in healthy subjects to demonstrate its ability to measure reactive hyperemia response dynamics.

Next, reactive hyperemia perfusion is compared between the more temporally efficient pulsed arterial spin labeling (PASL) used in PIVOT and the more recently developed and preferred method for the brain, pseudo-continuous ASL (pCASL). Assessment of the impact of blood flow variability throughout the ischemia-reperfusion paradigm on pCASL perfusion quantification is investigated. Then, both PASL and pCASL sequences are used to measure reactive hyperemia perfusion in healthy subjects. No significant differences were detected between perfusion measured with PASL or pCASL despite different labeling strategies, temporal resolutions, and perfusion quantification models.

Subsequently, PIVOT is combined with a velocity-encoded dual-echo GRE to create an interleaved three-slice sequence that provides quantification of bulk blood flow in the arteries and veins in addition to the traditional PIVOT measures. This new sequence, termed Velocity and PIVOT (*v*PIVOT) is used to investigate the relationship of blood flow in the macro- and microvasculature and muscle oxygen consumption during the transition from exercise to rest.

Finally, PIVOT is applied clinically in a cohort of patients with varying degrees of severity of peripheral artery disease. Increasing disease severity was correlated with a prolongation of the hyperemic response time, measured as a lengthening of time to peak perfusion, SvO_2 washout time, and time to peak T_2*. In addition, peak perfusion and SvO_2 upslope were significantly different between patients with PAD and healthy controls. These results suggest the potential for PIVOT to evaluate disease severity and may present a tool to assess response to therapeutic intervention.

TABLE OF CONTENTS

LIST OF TABLES

LIST OF FIGURES

LIST OF ABBREVIATIONS

$\%HbO_2$	percent hemoglobin oxygen saturation
AC	anterior compartment
ASL	arterial spin labeling
BMI	body mass index
BOLD	blood-oxygen-level dependent
C_a	arterial oxygen content
CASL	continuous arterial spin labeling
COT	claudication onset time
CV	coefficient of variation
CVw	within-subject coefficient of variation
DCS	diffusion correlation spectroscopy
dHb	deoxyhemoglobin
eNOS	endothelial nitric oxide synthase
EPI	echo planar imaging
f	perfusion
FAIR	flow alternating inversion recovery
FMD	flow mediated dilation
fMRI	functional magnetic resonance imaging
FOV	field of view
GRE	gradient-recalled echo
Hb	hemoglobin
Hct	hematocrit
HD	hyperemic duration
HFV	hyperemic flow volume
ICC	intraclass correlation coefficient
MRI	magnetic resonance imaging
NIRS	near infrared spectroscopy
NO	nitric oxide
NS	non-selective
PAD	peripheral artery disease
PASL	pulsed arterial spin labeling
pCASL	pseudo-continuous arterial spin labeling
PET	positron emission tomography
PHF	peak hyperemic flow
PIVOT	perfusion, intravascular venous oxygen saturation, and T_2*
PLD	post labeling delay
PWT	peak walking time
RF	radiofrequency
ROI	region of interest
SATIR	saturation inversion recovery
SER	supervised exercise rehabilitation
SI	signal intensity
SMC	standard medical care
SS	slice-selective
SvO_2	venous oxygen saturation
TE	echo time
TTP	time to peak

TTP_{Perf}	time to peak perfusion
TTP_{T2*}	time to peak T_2*
TR	repetition time
TRUST	T_2 relaxation under spin tagging
v	velocity
VENC	velocity encoding
VO_2	oxygen consumption
VOP	venous occlusion plethysmography
vPIVOT	velocity and perfusion, intravascular venous oxygen saturation, and T_2*

PREFACE

Chapter 2 has been published as: Englund EK, Langham MC, Li C, Rodgers ZB, Floyd TF, Mohler ER, and Wehrli FW. Combined measurement of perfusion, venous oxygen saturation, and skeletal muscle T_2^* during reactive hyperemia in the leg. JCMR, 2013;15(70). DOI: 10.1186/1532-429X-15-70.

Chapter 3 has been submitted to the Journal of Magnetic Resonance Imaging and is currently under review as: Englund EK, Rodgers ZB, Langham MC, Mohler ER, Floyd TF, and Wehrli FW. Measurement of skeletal muscle perfusion dynamics with pCASL: Assessment of labeling efficiency in the peripheral vasculature and comparison to PASL.

Portions of Chapter 4 have been presented at the International Society for Magnetic Resonance in Medicine's 2014 Annual Scientific Meeting as: Englund EK, Rodgers ZB, Langham MC, Mohler ER, Floyd TF, and Wehrli FW. Simultaneous measurement of microvascular and macrovascular blood flow and oxygenation in the leg. Proceedings of the 22nd Annual Meeting of ISMRM, Milan, Italy, p. 722.

Chapter 5 has been published as: Englund EK, Langham MC, Ratcliffe SJ, Fanning MJ, Wehrli FW, Mohler ER, and Floyd TF. Multiparametric assessment of vascular function in peripheral artery disease: Dynamic measurement of skeletal muscle perfusion, blood-oxygen-level dependent signal, and venous oxygen saturation. Circulation: Cardiovascular Imaging, 2015;8:e002673. DOI: 10.1161/CIRCIMAGING.114.002673.

Erin K. Englund

February 10, 2016

CHAPTER 1: INTRODUCTION

1.1. Endothelial function and dysfunction

Blood flow is necessary to sustain life through the delivery of oxygen and nutrients essential for cellular metabolism, and for the removal of waste products. In fact, every cell in the body is separated from a blood vessel by only 1-3 cell widths, corresponding to approximately 40 micrometers (1). The regulation of blood flow to the tissue is a complex and dynamically controlled process mediated in large part by the innermost layer of the artery, the vascular endothelium (2) (**Figure 1.1**). Only one cell-layer thick, the endothelium is responsible for the maintenance of vascular homeostasis and among other roles serves to regulate vascular tone, the balance between vasodilation and vasoconstriction (3).

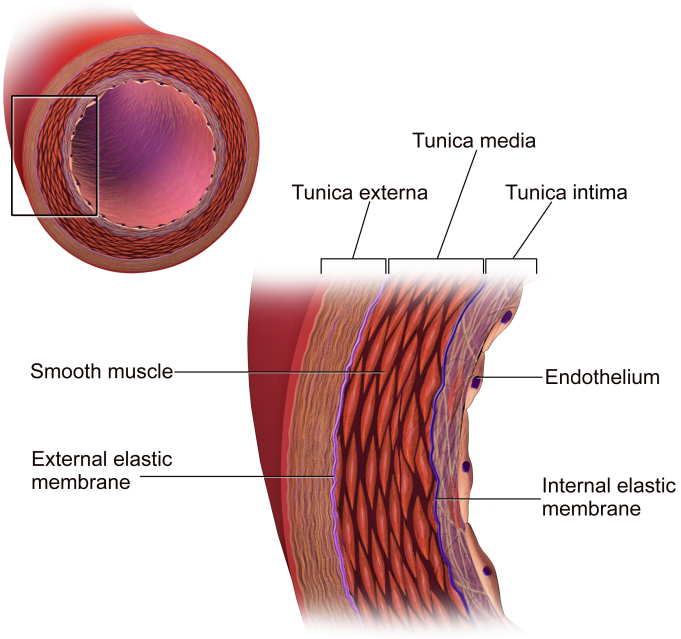

Figure 1.1. The structure and composition of the arterial wall. The endothelium is the innermost layer of cells, and acts to maintain vascular tone and overall homeostasis. In healthy vessels, shear stress due to blood flow in the artery causes production and release of nitric oxide from the endothelial cells, promoting vasodilation. Image from (4).

To maintain appropriate vascular tone the endothelium produces and secretes several vasoactive molecules, chief among which is nitric oxide (NO) (5). NO is a potent vasodilator produced in the endothelium, which diffuses into the vascular smooth muscle, causing relaxation and subsequent vasodilation. NO is produced enzymatically from L-arginine by endothelial NO synthase (eNOS), which is activated by chemical (e.g. acetylcholine) or mechanical (e.g. shear stress) stimulus. Balancing the effects of NO are factors that promote vasoconstriction including endothelin-1 and angiotensin II, however in general the baseline state of endothelial function is one of relative quiescence (6).

Endothelial dysfunction is the general term for the phenotypic presentation of a vasoconstricted, pro-inflammatory, thrombogenic state, and is purported to be the earliest stage of cardiovascular disease, preceding overt atherosclerotic plaque formation (3). A reduced bioavailability or activity of NO is thought to be the predominant mechanism underlying endothelial dysfunction, resulting in reduced vasodilation and delayed vascular reactivity (7). Endothelial dysfunction exists in many diseases including diabetes (8) and atherosclerosis (9), and is present in patients with significant risk factors for cardiovascular disease including aging and hypertension (10). One disease in particular, peripheral artery disease (PAD) is the focus of this thesis.

1.1.1. Peripheral artery disease

PAD, generally a manifestation of atherosclerosis in vessels supplying the lower limbs, affects over 20% of the population over 70 and is thought to be the most under-diagnosed and undertreated atherosclerotic disease (11-14). In PAD, atherosclerotic plaques develop at branch points in the peripheral arteries, resulting in occlusions or stenoses that increase vascular resistance and decrease blood flow to downstream skeletal muscle (15) (**Figure 1.2**). To meet the baseline oxygen and nutrient delivery demands of the muscle, the decrease in arterial flow is compensated by vasodilation of collateral arteries (15,16); but due to reduced vasoreactivity

caused by endothelial dysfunction, the vasculature is unable to quickly respond to increases in flow or metabolic demand (e.g. following a transient ischemia or during exercise). This creates an oxygen supply-demand mismatch resulting in ischemia and causing patients to present with the characteristic symptom of PAD – intermittent claudication, or pain on walking that is relieved by rest (17,18).

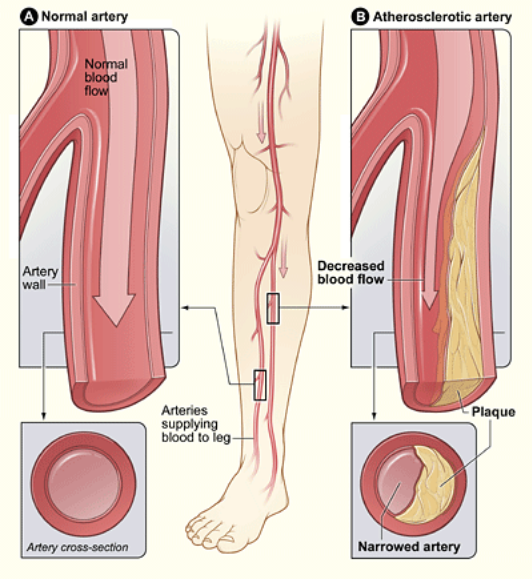

Figure 1.2. The primary feature of PAD is the presence of atherosclerotic plaques in the macrovasculature, which narrow the vessel lumen and reduce blood flow to downstream skeletal muscle. Image from (19).

Although endothelial dysfunction coexists (20), the presence of occlusions or stenoses due to atherosclerotic plaque formation in the peripheral circulation is the hallmark of PAD. In fact, diagnosis, staging, and standard clinical monitoring of PAD are based solely upon manifestations of macrovascular lesions even though those lesions are generally unchanged by therapeutic interventions that improve patient symptomatology (21,22). Thus, the investigation of endothelial function in patients with PAD may be critically important in yielding insight into the mechanism of action of various therapeutic approaches, and providing better tools for clinical monitoring.

1.2. Measurement of endothelial function

1.2.1. Endothelium-dependent vasodilation

To investigate endothelial function, a state of increased blood flow known as hyperemia is induced via a mechanical or chemical stimulus. In the coronary circulation, chemical stimulation through intra-arterial infusion of acetylcholine is the typical method used to assess endothelial function. Administration of acetylcholine triggers competing effects: vasoconstriction by activation of the muscarinic receptors in vascular smooth muscle and vasodilation by stimulation of NO production. Typically, the vasodilatory response dominates, however in the absence of the endothelium or in endothelial dysfunction, vasoconstriction occurs (2). Quantitative angiography can be used to directly measure the diameter of the artery before and after acetylcholine administration, providing a measure of the coronary endothelial function.

In contrast to the coronary circulation, mechanical stimulation is feasible in the peripheral circulation by means of temporary external compression of the arteries, commonly known as an ischemia-reperfusion paradigm. In such a protocol, proximal arterial occlusion is sustained for several minutes using either supra-systolic pressure applied via a sphygmomanometer cuff secured around the subject's arm or thigh, or invasively using an arterial clamp to occlude only the vessel of interest. During the period of arterial occlusion, blood flow in the arteries, capillaries, and veins is halted. The stagnant blood in the capillary bed is subjected to continued oxygen extraction, though the oxygen diffusion gradient between blood and tissue decreases with increasing ischemic duration. Additionally, there is local accumulation of vasodilators and a reduction in arteriolar pressure, causing an overall decrease in vascular resistance.

Following cuff release, reactive hyperemia ensues with a transient surge of macrovascular flow owing to the decrease in vascular resistance downstream. This increases shear stress at the vessel wall, which activates eNOS, promoting NO production and release, and

triggering arteriolar vasodilation (23). The return of blood flow causes an increase in perfusion, delivering oxygenated blood to the ischemic tissue and driving out the accumulated vasodilators and deoxygenated capillary blood. As deoxygenated blood exits the capillary bed, there is a sharp decrease in intravascular venous oxygen saturation (SvO_2) in the draining veins, which then quickly recovers, reflecting the hyperperfusion of oxygenated arterial blood in the capillary bed and the recovery of tissue oxygenation. SvO_2 continues to rise and eventually surpasses the baseline value during the time that blood velocity exceeds the oxygen extraction rate. The kinetics and magnitude of the reactive hyperemic response provide insight about vascular reactivity and endothelial function (24).

Alternatively, exercise can act as a stimulus to investigate the regulation of blood flow. During exercise there is a decrease in tissue partial pressure of oxygen due to a local increase in oxygen consumption. This triggers a metabolic response that demands increases of blood flow to the muscle, resulting in additional capillary recruitment by relaxing the terminal arterioles. The response to exercise is prolonged compared to the response elicited by transient ischemia due to the increase in metabolic demand that accompanies exercise, which is not present in the ischemic state. However, exercise is a subject-effort dependent paradigm and given the more combined and coordinated effort to change the local blood flow, it maybe a more difficult paradigm to investigate. In fact, Lopez et al recently investigated the response to ischemia compared to exercise hyperemia and found that the microvascular perfusion response was more repeatable following ischemia (25).

1.2.2. Early measures of endothelial function and control of muscle blood flow

The vital function of the endothelium in mediating vasodilation was not discovered until Furchgott and Zawadzki's seminal report in 1980 (2), and the specific role of NO was subsequently uncovered by other investigators (5). Pivotal experiments were conducted prior to that breakthrough to study the regulation of blood flow in the skeletal muscle capillary bed. Krogh,

who later won the Nobel Prize in Physiology for his contribution to the field, suggested that under baseline conditions not all capillaries are perfused, that is, blood flows only through select channels within the capillary bed (26,27). Augmentation of flow largely served to increase the flow through those open capillaries rather than through previously unopened channels (26,28). Follow-up studies found that in response to an increase in metabolic demand, recruitment of additional capillaries was realized through vasodilation at the level of the terminal arteriole (29-31), however this continues to be an active area of research (32).

Early studies in humans estimated muscle perfusion through venous occlusion plethysmography (VOP), first described by Hewlett and van Zwaluwenburg in 1909 (33). In VOP, relatively low external pressure is applied to the limb of interest, serving to occlude only venous blood flow. The early rate of change of the distal limb circumference, measured via strain gauge, relates to perfusion. VOP continues to be a standard to which other measures of perfusion are compared, as it is noninvasive, inexpensive, and easy to combine with other methods (34). However VOP-measured perfusion may overestimate skeletal muscle perfusion since its measurement includes blood flow to the skin.

In 1964, Lassen, et al conducted the first study to specifically quantify skeletal muscle perfusion during reactive hyperemia in healthy subjects and patients with PAD (35). Radioactive ^{133}Xe was injected locally into the muscle, and its clearance rate was measured both at baseline and during reactive hyperemia. Perfusion at baseline was not significantly different between healthy subjects and patients with PAD, but the hyperemia response was significantly reduced and delayed in patients.

As understanding of the underlying physiology and technology advanced, the methods developed to investigate vascular function expanded as well. Several imaging-based methods have emerged for the measurement of endothelial function and vascular reactivity. Flow-mediated dilation (FMD) of the brachial artery is perhaps the most common measure of macrovascular

reactivity. To measure FMD, the diameter of the brachial artery is measured using Doppler ultrasound before and after a period of ischemia. In patients with PAD, low brachial artery FMD was associated with an increased risk for future cardiovascular event (36). However, the precise measurement of the artery's diameter can be difficult, requiring technical expertise, and in general the brachial artery is spared from macrovascular atherosclerotic disease.

Other imaging-based approaches to investigate blood flow in skeletal muscle include positron emission tomography (PET) or near infrared spectroscopy (NIRS). PET can quantify perfusion through an adaptation of the Kety-Schmidt model (37) following injection of ^{15}O-water (38). However, the obligatory injection of a radiotracer and the need for an on-site cyclotron for ^{15}O due to its short half-life has limited its application to only a few studies (38-42). Optical imaging-based approaches on the other hand are noninvasive, the equipment is portable and relatively inexpensive, and patient is not subjected to ionizing radiation. NIRS or near-infrared diffusion correlation spectroscopy (DCS) have been used to measure relative changes in muscle oxygenation and blood flow, respectively (43,44). However, the quantification of these physiologic parameters requires complicated models and even so measurements are generally reported in relative rather than absolute physiologic units. Furthermore, optical imaging is restricted to relatively superficial structures therefore, while skeletal muscle is generally amenable, measurements may be prone to error if there is substantial subcutaneous fat.

Magnetic resonance imaging (MRI) methods have also been utilized to investigate vascular function. MRI is entirely non-invasive, produces tomographic images, does not require injection of contrast, and does not expose the subject to ionizing radiation. MRI affords a wide variety of different structural and functional contrasts, depending on the particular pattern of magnetic field gradients and radiofrequency pulses, together known as a MRI pulse sequence.

Among the MRI methods is arterial spin labeling (ASL), a method for quantification of perfusion in absolute physiologic units of mL blood per minute per 100 g of tissue. Only a few

years after it was introduced by Detre, et al for the measurement of perfusion in the brain (45), Toussaint and colleagues applied a variation of the technique for the measurement of skeletal muscle perfusion during reactive hyperemia (46). Since then, several groups have continued to investigate the post-ischemia perfusion response (25,34,47,48), and have additionally looked into the response to exercise (25,49), hypoxia (50), various states of vascular filling (51), and in disease states such as PAD (52).

Other MRI methods to assess vascular function include phase contrast flow measurements (53-57), MR susceptometry for dynamic measurement of intravascular venous oxygen saturation (SvO_2) (58,59), and skeletal muscle blood-oxygen-level dependent (BOLD) imaging, which uses relative changes in the effective transverse relaxation time (T_2*) as a surrogate for capillary bed oxygen content (60-65). Alterations in the dynamics of each of these parameters have been associated with the presence of PAD during reactive hyperemia studies. Patients exhibited a blunted and delayed hyperemic response in bulk arterial blood flow (66), perfusion (52), dynamic SvO_2 (67) , and T_2* (68,69). The technical foundations of each of these methods are described subsequently.

1.4. MRI measures of vascular function

1.4.2. Phase contrast MRI for quantification of flow

Unlike many of the previously mentioned responses, which are only altered due to endothelial dysfunction in the post-stimulus state, the measurement of macrovascular blood flow velocity provides insight into vascular health both at rest and during hyperemia. In young healthy subjects, the baseline blood flow waveform of arteries in the peripheral circulation is triphasic, with high velocity antegrade flow during the systolic phase of the cardiac cycle, followed by flow reversal and then low velocity forward flow during diastole. In contrast to healthy subjects, patients with PAD generally present with a monophasic flow waveform, where blood flow velocity

drops during diastole, but remains antegrade throughout the entire cardiac cycle (70). In addition to this baseline measurement of the arterial flow waveform, the dynamics of the arterial blood flow response during reactive hyperemia or following exercise provide insight into endothelial function and vascular reactivity, as pointed out earlier.

1.4.2.1. Quantification of blood flow velocity

Blood flow velocity can be quantified using phase-contrast MRI (53-55,71). Generally, the temporal evolution of the phase of the MRI signal can be expressed as:

$$\varphi(t) = \gamma\left(m_0 x_0 + m_1 v_0 + \frac{1}{2} m_2 a_0 + \cdots\right) \qquad [1.1]$$

where γ is the gyromagnetic ratio, m_0, m_1, and m_2 represent the zeroth, first, and second order gradient moments, respectively ($m_n = \int_0^t G(\tau)\tau^n d\tau$ and G is the gradient amplitude at time, t), x_0 is the position of the spin, v_0 is the velocity, and a_0 represents acceleration. The relationship can be expanded to include higher order time derivatives of position such as jerk, however these terms are generally disregarded.

By using bipolar gradients, it is possible to create a situation with $m_0 = 0$, but a non-zero m_1. In this case, stationary spins will have complete phase restoration, but moving spins will accumulate phase as a function of velocity (**Figure 1.3**).

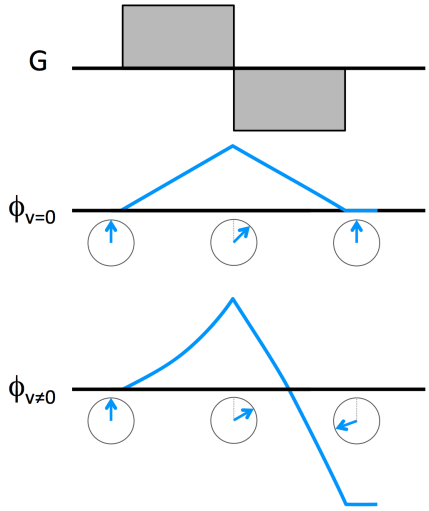

Figure 1.3. Diagram showing the effect of bipolar gradients on stationary and moving spins. The phase evolution of stationary spins is shown in the center, and that of moving spins is shown in bottom. Bipolar gradients are balanced, having no net area and therefore imparting no residual phase onto stationary spins. However there is a non-zero first gradient moment, causing accumulation of phase in moving spins.

In this special situation, moving spins will accrue phase simply as: $\varphi(t) = \gamma m_1 v$. In phase contrast MRI, the first gradient moment is changed (typically toggled) between otherwise identical image acquisitions. The phase difference between these two images attenuates phase variation from background field gradients and accentuates the phase accrual due to motion. The range of velocities that can be measured without phase wrapping is given by a user-defined parameter related to the difference in m_1 between the two acquisitions, the velocity encoding (VENC) as:

$$VENC = \frac{\pi}{\gamma \cdot \Delta m_1} \qquad [1.2]$$

Thus for toggled gradients, $\Delta m_1 = m_1 - (-m_1) = 2m_1$.

1.4.2.2. Gated and ungated methods

Velocity maps can be acquired in several different forms. By gating the phase contrast acquisition to the electrocardiogram, several images can be reconstructed at different time points in the cardiac cycle, providing cine images of blood flow throughout the cardiac cycle (72). Image acquisition generally takes several seconds to minutes depending on the apparent temporal resolution desired, as k-space data are acquired over several heartbeats and synthesized together to create images of a single cardiac phase. Furthering this technique, velocity can be resolved in 3 dimensions along with 3-dimensional spatial encoding to create 4D flow images (73,74).

If the acquisition is not gated to the cardiac cycle, the velocity will be weighted by the phase of the cardiac cycle during the acquisition of the center portion of k-space. Alternatively, ungated projection phase contrast can generate time-resolved beat-to-beat velocity measurements (56,57). In Langham, et al's approach to quantify velocity via k-space projections a fully phase encoded reference image is first obtained, followed by acquisition of only the centerline of k-space (k-space projection) (57). The reference image is used to create a static tissue k-space projection by masking out the vessels of interest, then taking the inverse Fourier transform and isolating the center k-space line (k_y=0). This static tissue k-space projection is subtracted from every dynamically acquired velocity-encoded projection to isolate blood signal. The phase difference between adjacent positive and negative velocity-encoded projections is computed and the average velocity across the vessel of interest can be quantified temporal resolution equal to the pulse sequence repetition time (TR), using a temporal window of two TRs.

Reactive hyperemia bulk flow or blood flow velocity time courses can provide insight into the vascular reactivity and endothelial function (75). Parameters of interest include the time to peak flow and the duration of forward flow, which are increased in the presence of PAD (66).

1.4.3. Arterial spin labeling for perfusion quantification

ASL is a well-established method for noninvasive perfusion imaging (45,76-79). Several variations of ASL exist, employing various labeling strategies, but generally perfusion is quantified by pairwise subtraction between two images – one acquired after magnetically-labeling the inflowing arterial blood (label) and an otherwise identical image without the label (control). The resultant signal difference cancels out the contribution from static tissue, leaving behind a signal that is related to the amount of perfusion, that is microvascular flow and exchange between blood water and tissue water, that occurred during the time between the label and image acquisition (**Figure 1.4**). This signal can be converted into perfusion in units of mL/min/100g through application of various models that describe the exchange between arterial blood water and tissue water (34,47,80,81).

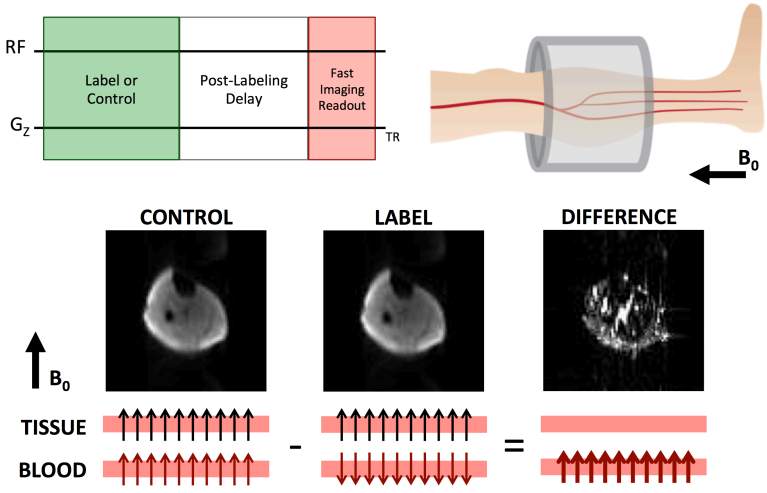

Figure 1.4. General experimental setup for ASL MRI-based perfusion measurement. Identical images are acquired with or without magnetically labeling arterial blood in the label and control conditions, respectively. Static tissue signal is unchanged between these two images, thus subtraction cancels out its contribution, leaving behind only the signal from exchange of blood and tissue water during the post labeling delay.

The ASL labeling method scan be divided into two general categories: those that label by flow-driven adiabatic inversion of blood as it passes through a labeling plane, as in continuous

ASL (CASL) or pseudo-continuous ASL (pCASL), or those that use spatially selective inversion of blood as in pulsed ASL (PASL) (**Figure 1.5**). Skeletal muscle perfusion during hyperemia has been quantified with all of these methods (25,34,47,48), and there are benefits and drawbacks to each. CASL and pCASL methods utilize a long pulse or series of pulses to achieve inversion, thereby reducing labeling efficiency to approximately 85% (82) and limiting temporal resolution to 6-8 seconds (47,48,52). CASL or pCASL methods do offer an increase in theoretical signal-to-noise ratio compared to PASL as the labeled blood water spins accumulate in the tissue throughout the longer labeling duration (83). PASL on the other hand uses a single RF pulse for nearly instantaneous and complete inversion, allowing perfusion measurement at a temporal resolution of up to 2 second (34).

Both PASL and pCASL or CASL methods have an unavoidable post-labeling delay (PLD). The PLD is dead time between the arterial labeling pulse and the image acquisition required to allow the transit of blood from the labeling location into the imaging slice location. The temporal resolution of PASL is largely limited by the duration of the PLD. For pCASL and CASL, the labeling duration and PLD are typically approximately the same at about 1-2 seconds each (81).

Due to the transient nature of the hyperemic response, high temporal resolution sampling of the time course is necessary. Furthermore, there is baseline signal variation over the course of the ischemia reperfusion experiment due to the changing oxygen saturation and vascular volume in the capillaries causing changes in the BOLD signal. To correct for the baseline signal variation, temporal matching of the label and control datasets is performed by linear interpolation of the control dataset (47). Interpolation works well when the signal change is negligible or linear between the time points, however when signal variation changes rapidly, as seen immediately following cuff release, linear temporal matching does not compensate for the dynamic changes. Given that the offset between label and control images is approximately 3 – 4

seconds in CASL or pCASL, and only 1 – 1.5 seconds in PASL, the BOLD signal changes are more accurately adjusted in PASL (84).

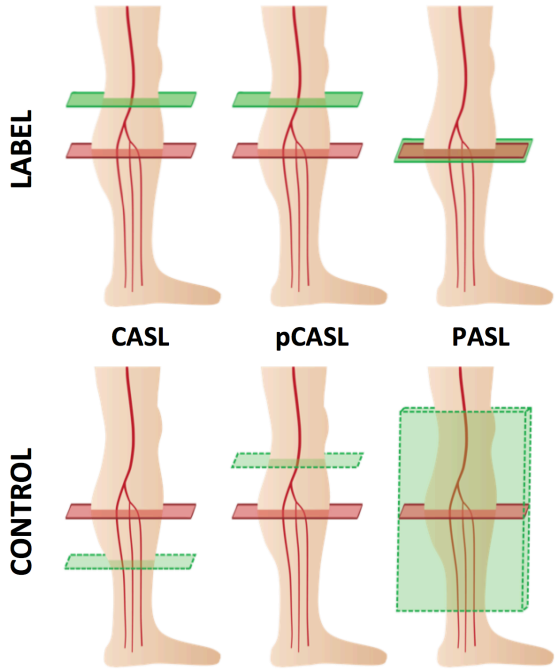

Figure 1.5. Description and location of label and control locations in CASL, pCASL, and PASL experiments. In CASL and pCASL, flow-driven adiabatic inversion causes blood in the artery to be inverted as it passes through the proximal labeling plane. In the control condition for CASL, the labeling plane is located distal to the imaging slice location. For the pCASL control condition, the location of the labeling plane remains unchanged, but no net labeling of blood is achieved. In contrast, the label condition of the PASL sequence is a slice-selective inversion, causing inversion of tissue, but inflowing blood is uninverted. In the control condition of PASL both the inflowing blood and tissue signal are inverted.

1.4.3.1. Continuous and pseudo-continuous ASL

In CASL, inflowing arterial blood is selectively inverted in the label condition through flow-driven adiabatic inversion (85), in which a continuous low B_1 field is played alongside a constant amplitude gradient to drive spins moving perpendicularly through the labeling plane to the

negative Z axis (**Figure 1.6a**). An adiabatic inversion is achieved in the presence of a constant gradient and B_1 field, as long as the velocity of the spin meets the adiabatic condition:

$$\frac{1}{T_2} \ll \frac{Gv}{|B_{eff}|} \ll \gamma |B_{eff}| \quad [1.4]$$

where T_2 is the transverse relaxation time of blood water protons, v is the velocity of the spin, G is the average gradient amplitude, B_{eff} is the effective magnetic field, and γ is the proton gyromagnetic ratio. Implications of this will be further discussed in Chapter 3.

Labeling generally lasts one to two seconds. Current MRI transmit coils are incapable of playing out such a long continuous B_1 field, thus pCASL was introduced as an adaptation of CASL (82). pCASL also relies on flow-driven adiabatic inversion, but rather than continuous radiofrequency (RF) excitation for the duration of a second or so, the excitation period is broken up into a train of short RF pulses along with oscillating gradients with a non-zero net amplitude are used (**Figure 1.6b**) to label blood.

To prevent errors due to magnetization transfer effects, the low flip angle RF pulse or pulses must be matched between the label and control image acquisitions (86). In CASL, the simplest option uses gradients of opposed polarity or RF of opposite phase; either option causes the labeling plane to be distal to the imaging location (**Figure 1.6d**). For the control condition in pCASL, spins remain uninverted through application of similar RF pulses as in pCASL labeling, but alternating in phase by 180°, and zero net gradient amplitude (**Figure 1.6e**) (82), thereby imparting no net excitation.

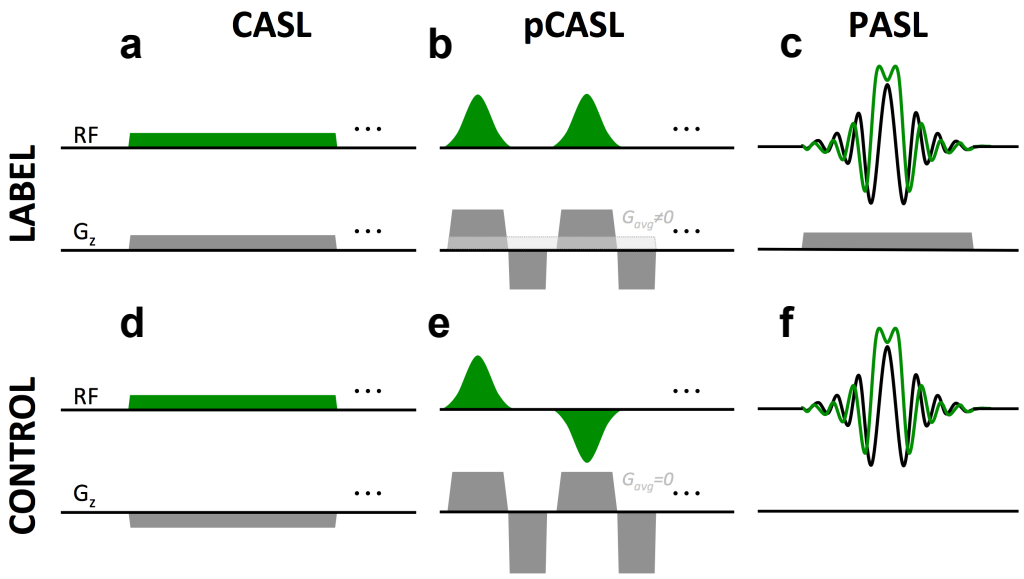

Figure 1.6. Pulse sequence diagrams of label and control schemes for CASL, pCASL, and PASL. Flow-driven adiabatic inversion is used to label arterial blood water spins in both CASL and pCASL. In the control condition, spins in inflowing blood remain unperturbed either by labeling distal to the imaging slice (as in CASL) or by producing no net excitation (as in pCASL). Spatially selective or non-selective adiabatic inversion pulses are used for PASL label and control, respectively.

1.4.3.2. Pulsed ASL

There are several variants of pulsed arterial spin labeling. The method that has been most widely applied for skeletal muscle perfusion is Flow-Alternating Inversion Recovery (FAIR) or offshoots of that method (25,34,49,51). In contrast to CASL and pCASL, PASL labeling is achieved via application of a single spatially-selective inversion pulse, meaning that the duration of the label or control module is much shorter, spins are inverted regardless of the flow velocity, and the transit distance between the locations of the label and the image acquisition is generally much smaller. Thus, PASL methods have faster labeling and thus higher potential temporal resolution, and higher and more consistent labeling efficiency.

In FAIR (77) a RF pulse inverts the magnetization either slice-selectively (SS) for the label condition, or non-selectively (NS) for the control condition (**Figure 1.6 c, f**). Thus for the

label condition, the tissue signal is recovering from inversion, but inflowing blood remains uninverted, and in the control condition both the inflowing blood and tissue are recovering from inversion. Saturation Inversion Recovery, a method developed for the measurement of skeletal muscle perfusion by Raynaud, et al (34) uses the same control and label conditions as in FAIR, and additionally includes a slice-selective saturation pulse after each imaging readout to ensure presence of the same initial magnetization in each dynamic acquisition.

1.4.3.3. Quantification of perfusion

To determine perfusion in physiologic units, several models have been proposed that derive from the general solution to the Bloch equation for longitudinal magnetization of blood including a term for inflow and outflow of blood, originally described by Detre, et al (45):

$$\frac{dM_z}{dt} = \frac{M_0 - M_z}{T_1} + f(M_a - M_v) \qquad [1.5]$$

where M_z is the longitudinal magnetization of water in tissue, M_a is that of arterial blood water, M_v is that of venous blood water ($M_v = \frac{M}{\lambda}$, where λ is the tissue partition coefficient), T_1 is the relaxation time of tissue, and f represents perfusion.

Assuming a one-compartment model for blood (e.g. blood water is delivered and accumulates in tissue), pCASL perfusion can be quantified as described by Buxton, et al (80) as:

$$f = \frac{\lambda \cdot (M_{control} - M_{label}) \cdot e^{\frac{PLD}{T_{1,blood}}}}{2 \cdot \alpha \cdot T_{1,blood} \cdot M_{control} \cdot \left(1 - e^{\frac{-\tau}{T_{1,blood}}}\right)} \qquad [1.6]$$

where *PLD* represents the post labeling delay – the time between the end of the labeling period and image acquisition, $T_{1,blood}$ is the longitudinal relaxation time of blood, α is the labeling efficiency, and τ is the labeling duration. An alternate form of this model can be used to quantify perfusion using the SATIR PASL sequence (34). Using a similar one-compartment model and

assuming the T_1 of blood and tissue can be approximated as equal, perfusion can be quantified as:

$$f = \frac{\lambda}{PLD} \cdot \ln\left[\frac{M_{label} - M_{control}}{M_{label} + M_{control}} \cdot \left(1 - e^{\frac{PLD}{T_{1,blood}}}\right) + 1\right] \quad [1.7]$$

In the brain the interest is generally in high accuracy measurement of spatially resolved perfusion, therefore several repeats are averaged to create a voxelwise map of perfusion. In skeletal muscle, although spatial localization of the signal is important, the interest is generally in the dynamic measurement of perfusion changes over time. Thus, each label and control image pair is used to calculate perfusion, yielding time-resolved perfusion in muscles of interest. In reactive hyperemia experiments, the time course is analyzed to determine the speed of response, measured as the time to peak perfusion, and the response magnitude, measured as the peak perfusion. Prior studies have uncovered an association between peak perfusion and PAD disease presence and severity, showing a decrease in peak perfusion with the presence of PAD and a further decrease with increasing disease severity. A similar trend was reported for the time to peak perfusion – with increasing disease severity there was an increase in the time to peak perfusion (52).

1.4.4. Dynamic oximetry

SvO_2 is an important physiologic parameter, providing information about oxygen utilization in tissue (58,87). During the ischemia reperfusion paradigm, supra-systolic pressure halts arterial inflow and oxygen extraction continues in the stationary blood of the capillary bed, but due to the stagnation of blood flow there is no observed change in SvO_2 of the draining vein. Upon cuff release, the hyperemic arterial inflow drives deoxygenated blood in the capillary bed into the collecting veins, causing the measured SvO_2 to drop sharply. This response is followed by an overshoot as the increased flow velocity exceeds the maximum oxygen extraction rate. The SvO_2 then normalizes back to the baseline value. Oxygen extraction only occurs in the capillary

bed, thus the dynamic measurement of SvO_2 allows intravascular blood to act as an endogenous tracer, providing information about endothelial function and vascular reactivity (66,67,75,88).

There are two main methods that have been introduced and reduced to practice for measurement of oxygen saturation in the large draining veins. These are MR susceptometry-based oximetry (58,87), and T_2-based oximetry (89), such as T_2 relaxation under spin tagging, commonly called TRUST (90) or projection T_2 (91). The T_2-based oximetry method requires a sequence-specific calibration between the measured T_2 and $\%HbO_2$ (92). On the other hand, MR susceptometry quantifies SvO_2 by modeling the relationship between the venous oxygen saturation and the induced magnetic field shift (58,87). Thus susceptometry-based oximetry is more limited in the geometry of vessels to which it can be applied, but does not require any sequence-specific calibration. For applications in skeletal muscle, MR susceptometry is preferred owing to the fact that the vessels are generally long and oriented parallel to the main magnetic field, thus an analytical solution can equate the MRI measurement to SvO_2. Furthermore, MR susceptometry has higher feasible temporal resolution than T_2-based methods, which typically require a lengthy T_2 prep and image acquisition. Maximum temporal resolution of T_2-based oximetry is limited to 12 seconds (93), while a temporal sampling rate exceeding 2 seconds can be obtained with MR susceptometry (94).

1.4.4.1. Susceptometry-based oximetry

MR susceptometry-based oximetry is a recently developed method for quantifying SvO_2, measured in units of percent-oxygenated hemoglobin ($\%HbO_2$) (58,87). Due to the different electron spin configurations of the Fe^{2+} heme iron in the oxygenated versus deoxygenated state (95), the magnetic properties of arterial and venous blood differ. Specifically, deoxyhemoglobin is paramagnetic thus creating a magnetic susceptibility difference between it and diamagnetic oxyhemoglobin and tissue. The susceptibility difference $(\Delta\chi)$ is related to the content of deoxygenated hemoglobin in the blood as:

$$\Delta\chi = \Delta\chi_{do}\,\mathrm{Hct}\,(1 - \mathrm{SvO_2}) \qquad [1.8]$$

where $\Delta\chi_{do}$ represents the susceptibility difference between fully oxygenated and fully deoxygenated blood ($\Delta\chi_{do}$ = 4π·0.27 ppm (SI units) (96,97)) and Hct is the hematocrit. The susceptibility difference induces a local magnetic field ΔB in the draining vein relative to the tissue, which, by modeling the vein as a long paramagnetic cylinder, can be described as:

$$\Delta\mathrm{B} = \frac{1}{6}\Delta\chi\;\mathrm{B_0}\;(3\cos^2\theta - 1) \qquad [1.9]$$

where B_0 is the main magnetic field strength, and θ is the angle of the vessel with respect to B_0. The incremental field ΔB can be determined by subtracting the phase accumulation of the MRI signal in surrounding tissue from that inside the vein (Δϕ) as:

$$\Delta\phi = \gamma\,\Delta\mathrm{B}\,\Delta\mathrm{TE} \qquad [1.10]$$

where the phase is measured from successive echoes separated in echo time by ΔTE (**Figure 1.7**). Combining equations 1.8-1.10, one can relate the intra/extravascular inter-echo phase difference to SvO_2 as:

$$\mathrm{SvO_2} = \left[1 - \frac{2\,\Delta\phi/\Delta\mathrm{TE}}{\gamma\,\Delta\chi_{do}\,\mathrm{B_0}\,(\cos^2\theta - 1/3)}\right] \times 100 \qquad [1.11]$$

It has been shown that for small angles, the induced field outside of the vessel is approximately homogeneous and independent of the susceptibility difference between the vein and tissue (98). Therefore SvO_2 can be measured using a field-mapping sequence, such as a multi-echo gradient-recalled echo (GRE). With this technique, one can quickly, directly, and noninvasively quantify intravascular SvO_2 at high-temporal resolution. Due to inhomogeneities in the main magnetic field, background phase accumulation can occur. In the image processing of multi-echo GRE oximetry data, the background phase modulation is fitted and subtracted out as described

by Langham, et al (99).

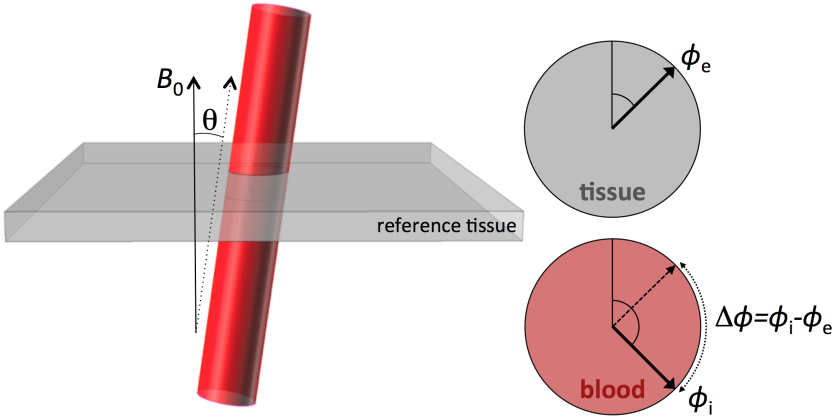

Figure 1.7. Diagram depicting the vein as a long, relatively parallel, paramagnetic cylinder. The inter-echo phase accrual of intravascular blood (ϕ_i) is compared to that of background tissue (extravascular phase, ϕ_e). The difference between intra- and extravascular phase accrual is proportional to the incremental magnetic field shift inside the vessel, which can be related to susceptibility and hence SvO_2.

Washout time (time to minimum SvO_2), upslope – representing the rate of resaturation (maximum slope during recovery), and overshoot (peak SvO_2 minus baseline SvO_2) can be extracted from the SvO_2 time course data. These metrics reflect the reactivity of the microvessels to NO-mediated vasodilation. Langham et al revealed an association between alterations in the SvO_2 time course-derived metrics in the femoral vein and the presence of PAD (66,67). Compared to age-matched healthy controls and young healthy subjects, patients with PAD had a longer washout time, diminished upslope, and lower overshoot, suggesting endothelial dysfunction.

1.4.5. BOLD MRI

In the microvasculature, as in the large veins, the paramagnetism of deoxyhemoglobin causes inhomogeneities in the local magnetic field. Because the microvessels are small compared to the MR imaging resolution, it is not possible to directly measure a change in signal

phase as was described above for MR susceptometry. However, changes in the concentration of deoxyhemoglobin will modify the local magnetic field to cause incoherent phase accrual, resulting in intravoxel phase dispersion, which causes the MRI magnitude signal to decay more rapidly (60,61). This can be measured as a reduction in the effective transverse relaxation time, T_2*, and represents the contrast mechanism commonly known as the BOLD response. The BOLD signal originates not only from changes in blood oxygen level, it is also sensitive to changes in perfusion, cellular pH, vessel diameter, and vessel orientation (100-103). It has been postulated, however, that the skeletal muscle BOLD signal primarily results from changes in the concentration of deoxyhemoglobin in the capillary bed (103).

BOLD imaging has been extensively applied for functional activation studies in the brain, and can additionally be used to investigate activation of other organs including skeletal muscle. Changes in T_2* in response to an ischemia-reperfusion paradigm can serve as a relative marker of tissue oxygenation (104). The multifactorial contrast mechanism and the fact that the measured response is relative, rather than in physiologic units, however, can make the interpretation of the BOLD signal more complicated than perfusion or dynamic SvO_2.

Quantification of T_2* can be achieved by fitting signal intensity (SI) data from a multi-echo gradient-recalled echo acquisition to a monoexponential function: $S(\mathrm{TE}) = S_0 e^{-\mathrm{TE}/T_2^*}$ where TE is the echo time of the acquisition. Prior studies have shown the utility of investigating dynamic skeletal muscle BOLD during exercise (105-107), ischemia (69), reactive hyperemia (46), and in disease states (68,69). Important metrics that may provide information about vascular function in reactive hyperemia experiments include relative T_2* maximum and the time to maximum T_2*. Previous work by Ledermann and colleagues showed that patients with PAD had a reduction in the peak T_2* and a prolongation in the time to peak T_2* compared to healthy subjects (68).

1.4.6. Combined measures of flow and oxygenation

The combination of measures of flow and oxygenation can provide additional information regarding the vascular function. Some MRI protocols explored the combination of imaging and spectroscopy to assess either metabolism directly, or tissue oxygen saturation. Specifically, a method proposed by Richardson, et al combined the measurement of ASL-based perfusion and 31P spectroscopy to assess changes in blood flow and ATP and its metabolites, respectively, in response to exercise (108). Another approach pursued the measurement of perfusion, through MRI-based plethysmography, and of deoxymyoglobin concentration through non-localized spectroscopy, providing a quantitative measure of microvascular and skeletal muscle tissue oxygen saturation and hence muscle oxygen consumption (109). Several other methods have been introduced that measure two of the previously introduced processes simultaneously.

1.4.6.1. Perfusion and BOLD

Duteil, et al described a method to measure both the perfusion and BOLD response from the same series of images: either the subtraction of label and control images to quantify perfusion, or the addition of these two images to assess BOLD signal changes (51). As the BOLD response is a multi-factorial in mechanism, the authors postulated that the combined method might help to distinguish the different contribution of perfusion increases to the change in the BOLD contrast or of changes in oxygen saturation in the capillary bed.

Other methods have been proposed for the combined measurement of perfusion and BOLD changes. For example, a double excitation sequence for simultaneous quantification of ASL and BOLD was proposed by Walvick, et al (110), and later refined by Mendes, et al for the additional measurement of T_2 (111,112). In the more recent adaptation (112), the image acquisition for perfusion quantification is followed by a separate dual-echo acquisition to quantify T_2*. The subsequent NS or SS inversion also acts to refocus the magnetization for quantification of T_2.

1.4.6.2. Flow and SvO_2

Combined measure of flow and SvO_2 can be achieved using several different methods. Langham, et al introduced a method to measure time resolved flow via projections and field maps for SvO_2 quantification using susceptometry-based oximetry, as detailed earlier (88). This method was applied in patients and healthy controls during an ischemia-reperfusion paradigm, and results of flow and SvO_2 were analyzed independently (66).

More recently, Mathewson, et al (113) utilized a similar combined flow and SvO_2 method to investigate the off-kinetics of exercise, that is the transition between exercise and rest. Flow and SvO_2 were measured in the femoral vein following quadriceps exercise, and from these data, muscle oxygen consumption ($\dot{V}O_2$) was calculated via the Fick principle as:

$$\dot{V}O_2 = C_aO_2 \cdot flow \cdot (SaO_2 - SvO_2) \qquad [1.12]$$

where C_aO_2 is the arterial oxygen content. It is important to note that the calculation of oxygen consumption cannot be so easily computed from reactive hyperemia studies since the measured changes in SvO_2 reflects the aggregate effect of the desaturation during ischemia rather than reflecting the current capillary bed oxygen saturation.

Others have investigated an approach that quantifies muscle oxygen consumption either by empirical calibration (49) or theoretical relationship between $\%HbO_2$ and T_2', the RF-reversible component of the transverse relaxation time $\left(\frac{1}{T_2^*} = \frac{1}{T_2} + \frac{1}{T_2'}\right)$ (114). Therefore, instead of bulk flow and draining vein SvO_2, perfusion and microvascular SvO_2 were measured via a combined ASL and T_2'-based methods (115,116). T_2'-based oximetry methods have been used to quantify oxygen saturation on a voxel-wise basis in the brain (114), and combined with ASL-based perfusion can quantify the rate of oxygen consumption either in the steady state of an isometric contraction (115), or in response to the transition between exercise and rest (116).

1.4.6.3. Bulk flow and perfusion

Another interesting combined measurement is the assessment of blood flow in the large arteries and blood flow in the capillaries, measured for instance as the combination of phase contrast flow and ASL perfusion. Zhang et al pursued a method to investigate these two parameters through Doppler ultrasound to quantify bulk arterial flow in the popliteal artery, and ASL MRI was used to determine perfusion (117). Although these investigations are still in an early stage, this combined measurement may provide insight into the specific reactivity of the microvasculature.

1.3. Outline of Dissertation Chapters

This dissertation describes the development and application of MRI-based methods for the measurement of peripheral vascular function. In **Chapter 2**, an interleaved pulsed arterial spin labeling and multi-echo GRE method, termed perfusion, intravascular venous oxygen saturation, and T_2* (PIVOT) is described, evaluated compared to standard non-interleaved approaches, and applied to a small cohort of young healthy subjects and patients with peripheral artery disease. In **Chapter 3**, the PASL method for perfusion quantification is compared to pseudo-continuous ASL (pCASL) and implications of the changes in average arterial blood flow on the precision of pCASL quantified perfusion are investigated. In **Chapter 4**, the original PIVOT sequence is expanded to include an upstream velocity-encoded multi-echo GRE outside of the PASL portion of the sequence. This expanded three-slice interleaved sequence permits quantification of perfusion, SvO_2, and T_2* alongside arterial and venous bulk flow at four second temporal resolution, providing a comprehensive tool for evaluation of peripheral vascular function. Using both post-ischemia reactive hyperemia and post-exercise functional hyperemia stimuli, the relationship between blood flow in the macro- and microvasculature was investigated, and oxygen consumption was quantified following exercise. Finally, in **Chapter 5**, the PIVOT method outlined in Chapter 2 was applied in a cohort including 96 patients with varying degrees of peripheral

artery disease and 10 healthy subjects. Results show that the reactive hyperemia timing response is highly correlated with the clinical measure of disease severity.

CHAPTER 2: COMBINED MEASUREMENT OF PERFUSION, VENOUS OXYGEN SATURATION, AND SKELETAL MUSCLE T_2* DURING REACTIVE HYPEREMIA IN THE LEG

2.1. Abstract

Purpose: To develop and evaluate an MRI technique for simultaneous measurement of perfusion, venous oxygen saturation (SvO_2), and skeletal muscle T_2*.

Methods: Perfusion, Intravascular Venous Oxygen saturation, and T_2* (PIVOT) is comprised of interleaved pulsed arterial spin labeling (PASL) and multi-echo gradient-recalled echo (GRE) sequences. During the PASL post-labeling delay, images are acquired with a multi-echo GRE to quantify SvO_2 and T_2* at a downstream slice location. Thus time-courses of perfusion, SvO_2, and T_2* are quantified simultaneously within a single scan. The new sequence was compared to separately measured PASL or multi-echo GRE data during reactive hyperemia in five young healthy subjects. To explore the impairment present in peripheral artery disease patients, five patients were evaluated with PIVOT.

Results: Comparison of PIVOT-derived data to the standard techniques shows that there was no significant bias in any of the time-course-derived metrics. Preliminary data show that PAD patients exhibited alterations in perfusion, SvO_2, and T_2* time-courses compared to young healthy subjects.

Conclusion: Simultaneous quantification of perfusion, SvO_2, and T_2* is possible with PIVOT. Kinetics of perfusion, SvO_2, and T_2* during reactive hyperemia may help to provide insight into the function of the peripheral microvasculature in patients with PAD.

2.2. Introduction

As discussed in Chapter 1, peripheral artery disease (PAD) causes significant morbidity and mortality in the United States (11-13,118). Baseline blood flow to skeletal muscle is generally maintained through the recruitment of collateral arteries (15,119), however the vasculature is unable to quickly respond to changes in metabolic demand, such as those that occur with exercise or following a period of ischemia. Analogous to cardiac stress testing, the functional integrity of the peripheral vasculature can be interrogated by measuring the dynamic response to a period of induced ischemia. This period of transient ischemia causes buildup of vasodilator metabolites and reduces the vascular resistance in the capillary bed. Upon release of the proximal arterial occlusion reactive hyperemia ensues, and the kinetics of the hyperemic response can provide information on microvascular integrity and endothelial function. The vasculature of healthy subjects is able to rapidly respond to the increase in flow, recovering to baseline more quickly than patients with PAD (52,66,68).

Also as introduced previously, there are several MRI methods that can yield data that are sensitive to the dynamic processes that occur during reactive hyperemia. Independently, perfusion (52), SvO_2 (67), and T_2* (68,69) have been used to evaluate the hyperemic response. Additionally, the measurements of perfusion and the BOLD signal have been combined to simultaneously investigate the relative changes in microvascular flow and capillary bed oxygen saturation (51,120). However, these methods have not been able to also investigate SvO_2 kinetics. On the other hand, measurement of SvO_2 has been combined with the measurement of macrovascular flow (66,88), but not with the spatially localized measurement of perfusion.

The post-ischemia recovery dynamics are altered in each of these parameters in situations of impaired vascular function, as in PAD (52,66-69); therefore there is potentially added benefit to concurrent measurement. Thus, in this work, we developed a method to measure perfusion, SvO_2, and T_2* simultaneously. Such a technique allows for a more complete functional

assessment of the peripheral vasculature during a single scan providing information on the temporal relationships between these various functional parameters.

2.3. Theory

The technical foundations of ASL perfusion quantification, MR susceptometry based oximetry, and the measurement of BOLD signal changes have already been described Chapter 1.

To briefly summarize, perfusion can be measured through ASL by taking the difference between images acquired with and without magnetically labeling the inflowing blood (45,76). These images are known as the label and control images, respectively. Aside from the application of the labeling pulse the label and control images are otherwise identical, thus the difference between them cancels out signal contribution from the static tissue and the leftover signal can be converted into perfusion in absolute physiologic units (34,47,80,81). Specific to this application, a method proposed by Raynaud, et al for the measurement of perfusion in skeletal muscle uses slice-selective and non-selective inversion pulses to achieve the label and control conditions. To reset the magnetization, a saturation pulse follows each image acquisition. This variant of the PASL-FAIR method is known as Saturation Inversion Recovery (SATIR) (34). Essential to all ASL methods is the presence of a delay time between the application of the label and the image acquisition, known as the post-labeling delay (PLD). The PLD is necessary to allow the transit of labeled blood water into the tissue.

In MR susceptometry, venous oxygen saturation is quantified by measuring the local magnetic field offset induced by the presence of an accumulation of paramagnetic deoxyhemoglobin (e.g. large draining vein) (58,87). By modeling the vein as a long paramagnetic cylinder, the field offset, measured as the difference in inter-echo phase accrual between the vein and background tissue, can be directly related to the concentration of deoxyhemoglobin provided that the vein is relatively parallel to the main magnetic field (59,121). Therefore a field mapping

sequence, such as a multi-echo GRE, can be used to quantify SvO_2 in physiologic units (% HbO_2).

The BOLD signal refers to the measurement of relative changes in the effective transverse relaxation time (T_2*), and is related to changes in blood oxygen level in the capillary bed, perfusion, and cellular pH, and is also associated with vessel diameter and vessel orientation (100-103). Quantification of T_2* can be achieved by fitting signal intensity (SI) data from a multi-echo GRE to a monoexponential function.

Thus, a multi-echo GRE sequence can be used to measure both SvO_2 from the evolution of the signal phase, and T_2* from the rate of decay of the signal magnitude. Here, a sequence is introduced, termed Perfusion, Intravascular Venous Oxygen saturation, and T_2* (PIVOT). PIVOT makes use of the PLD dead time inherent to all ASL sequences to acquire multi-echo GRE data at a separate, downstream slice location (**Figure 2.1**). This allows dynamic quantification of perfusion, SvO_2, and T_2* within a single scan.

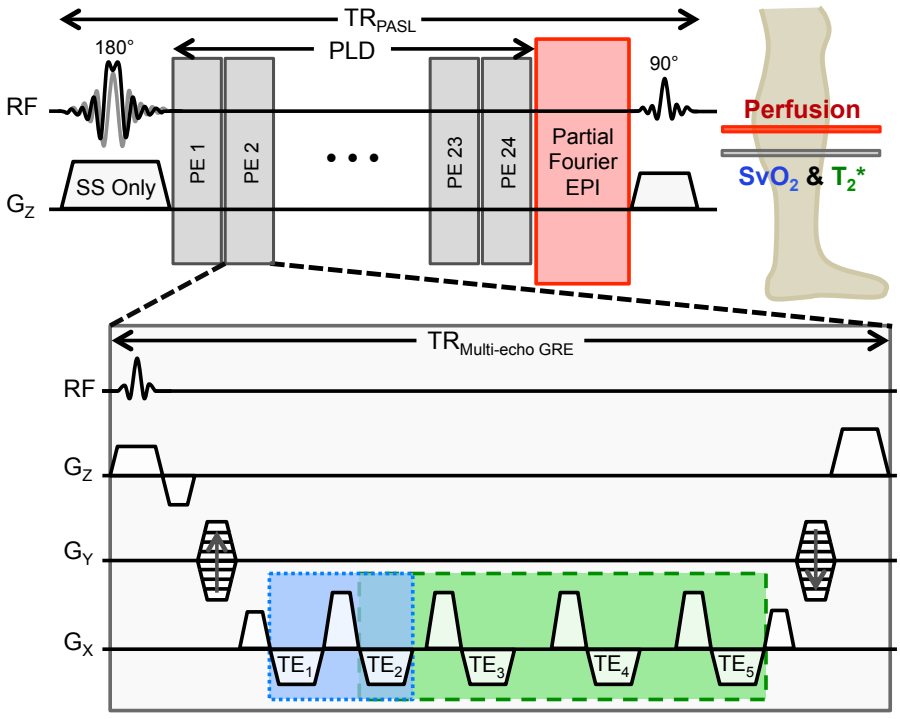

Figure 2.1. Pulse sequence diagram of PIVOT. A slice-selective (shown by SS only gradient) or non-selective adiabatic inversion pulse labels blood for perfusion imaging. During the PLD a keyhole multi-echo GRE acquires data downstream from the perfusion slice location for SvO_2 (blue) and T_2* (green) analysis. An EPI readout at isocenter (red) is used to acquire the images for perfusion quantification.

In PIVOT, as in SATIR, label and control conditions for perfusion imaging are achieved using SS and NS inversion pulses, respectively. During the PLD, a keyhole (122) multi-echo GRE sequence acquires data at a distal slice for SvO_2 and T_2* quantification. The distal location was chosen to ensure that the multi-echo GRE interleave does not impact the signal from previously labeled perfusing blood. Because the NS inversion affects both the PASL and multi-echo GRE slices, only multi-echo GRE data acquired following SS inversion are analyzed, though the interleave is run every PLD to control for magnetization transfer effects. The multi-echo GRE is

immediately followed by a GRE-EPI readout at isocenter to capture data for perfusion quantification.

2.4. Methods

2.4.1. Study Design

The University of Pennsylvania's Institutional Review Board approved all imaging procedures, and each subject provided informed consent prior to his or her participation. To evaluate PIVOT compared to the standard measurement methods, five young healthy male subjects (27±2 years old) were recruited and imaged on two separate occasions (Visit 1 and Visit 2). Four ten-minute scans were run in both sessions, each scan consisting of one minute baseline, three minute arterial occlusion, and six minute recovery. PIVOT, a repeat of the PIVOT scan (PIVOT Repeat), an otherwise identical PASL-only sequence, or otherwise identical multi-echo GRE-only sequence was run in a randomized order. To ensure the PASL interleave did not impact quantification of SvO_2 and T_2*, dynamic SvO_2 and T_2* results obtained with PIVOT were compared to the multi-echo GRE-derived SvO_2 and T_2* results. Similarly, to ensure the multi-echo GRE interleave did not confound perfusion, the perfusion results obtained with PIVOT were compared to the PASL-derived perfusion data. PIVOT was repeated to provide data on the intra-session variability of these parameters.

In addition, five PAD patients (67.2±6.8 years old, ankle-brachial index (ABI) = 0.61±0.14, 3 male) were drawn from an ongoing study and PIVOT imaging was performed during a single ischemia-reperfusion paradigm. For experiments in PAD patients, the total scan time was 12 minutes, with 2 minutes of baseline, 5 minutes of arterial occlusion, and 6 minutes of recovery. Since repeated arterial occlusions were not performed in PAD patients, a longer ischemic duration was used to ensure a maximal hyperemic response.

2.4.2. Imaging

PIVOT, PASL-only, and multi-echo GRE-only sequences were written in SequenceTree (123) and exported for use on a 3T scanner (Siemens Medical Equipment; Erlangen, Germany). Each subject was positioned with the maximum girth of the calf centered in an 8-channel transmit/receive knee coil (InVivo, Inc; Gainesville, FL). For proximal arterial occlusion, a cuff was secured around the thigh and was rapidly inflated to 75 mmHg above the systolic pressure using the Hokanson E20 AG101 Rapid Cuff Inflation System (D. E. Hokanson, Inc; Bellevue, WA). Perfusion images were acquired with a partial Fourier GRE-EPI readout with the following parameters: FOV=250×250 mm^2; acquired matrix=80×50, reconstructed to 80×80; slice thickness=1 cm; slice location=isocenter; TR/TE=1 s/8.05 ms; PLD=952 ms. The keyhole multi-echo GRE used the following parameters: FOV=96×96 mm^2; keyhole acquired matrix=96×24, (for SvO_2 data analysis, reconstructed matrix=96×96 using a fully sampled reference image obtained immediately after the dynamic PIVOT or multi-echo GRE acquisition; only dynamic data were used for T_2* analysis, with acquired matrix = reconstructed matrix=96×24); slice thickness=1 cm; slice location=3 cm inferior from isocenter; $TR/TE_1/TE_2/TE_3/TE_4/TE_5$=38.12/3.78/6.99/12.32/ 19.32/26.32 ms. Perfusion, SvO_2, and T_2* each were quantified with two-second temporal resolution.

2.4.3. Data Analysis

Perfusion: Perfusion was measured in the soleus muscle. High spatial-resolution scout images were used as a reference, and a region of interest (ROI) in the soleus was visually selected on the EPI images. As the GRE-EPI data are inherently T_2*-weighted, SI variation occurred throughout the ischemia-reperfusion paradigm due to the BOLD effect. Direct subtraction between adjacent NS and SS images would yield data with a mixture of perfusion, and ΔT_2*-weighting. To account for this potential confound, NS time-series data were linearly

interpolated to temporally match the SS time-course prior to perfusion quantification (124). Perfusion (f) was calculated as described by (34):

$$f = -\frac{\lambda}{T} \cdot \ln\left[\frac{M_{SS}(t)-M_{NS}(t)}{M_{SS}(t)+M_{NS}(t)} \cdot \left(1-e^{T/T_1}\right) + 1\right] \quad [2.1]$$

where M_{SS} and M_{NS} are the signal intensities (SI) in the image acquired after SS and NS inversion, respectively, λ is the tissue partition coefficient (0.9 mL/g), T is the PLD, defined as the time between the inversion pulse and readout, and T_1 is the longitudinal relaxation time of arterial blood. At 3T, T_{1blood} = 1664 ms (125) and $T_{1tissue}$ = 1420 ms (126). A numerical calculation based on actual values for blood and tissue T_1 shows that for perfusion values up to 100 mL/min/100g, using $T_{1tissue} \approx T_{1blood}$ = 1420 ms, underestimates perfusion by less than 5%. In order to correct for baseline perfusion offset, the average perfusion during the period of arterial occlusion was calculated and subtracted from each time-point as described in (124). Peak hyperemic flow (PHF), time to peak (TTP), hyperemic flow volume (HFV), and hyperemic duration were measured (**Figure 2.2a)**.

Oximetry: Dynamic SvO_2 images were reconstructed to a matrix size of 96×96 using outer k-space data from a fully sampled reference image acquired immediately after the dynamic scan (122). A phase difference image was generated for each of the dynamic time-points and the low spatial-frequency phase modulation was removed as described in (99). An ROI was prescribed in the larger of the peroneal veins, and reference tissue was selected in an ROI immediately surrounding the peroneal vein. The phase accumulation was calculated from echoes at TE_1 and TE_2, with DTE=3.21 ms and the difference between the intravascular and extravascular phase accumulation $\Delta\varphi$ was computed. SvO_2 was calculated as described in (58) as:

$$SvO_2 = \left[1 - \frac{2\,|\Delta\varphi|/\Delta TE}{\gamma\,\Delta\chi_{do}\cdot Hct\cdot B_0\left(\cos^2\theta - 1/3\right)}\right] \times 100 \quad [2.2]$$

where $\Delta\chi_{do}$ represents the susceptibility difference between fully oxygenated and fully deoxygenated blood ($\Delta\chi_{do} = 4\pi \bullet 0.27$ ppm (SI units) (96,97)), B_0 is the main magnetic field strength, and θ is the angle of the vessel with respect to B_0 (58,87). Hematocrit of 0.45 was assumed for the healthy subjects, and the PAD patients' hematocrit was measured by blood draw. Washout time (time at which minimum SvO_2 occurs), upslope, representing the rate of venous resaturation (maximum slope during recovery), and overshoot (peak SvO_2 – baseline SvO_2) were recorded (**Figure 2.2b)**.

T_2*: T_2* analysis was performed on keyhole-only data since high spatial resolution is not necessary (acquired matrix = reconstructed matrix = 96×24). T_2* was calculated by fitting a monoexponential function to magnitude SI from echoes TE_2-TE_5. Even though TE_1 should have highest SNR, TE_1 was not included in the monoexponential fitting because large switching gradients just prior to TE_1 induced significant eddy current effects that would potentially confound T_2* quantification. For BOLD analysis, average SI in an ROI prescribed in the soleus muscle for each of the four echoes was fitted to a mono-exponential function to determine T_2* at each time-point. T_2* values were normalized to the baseline average and relative $T_2^*_{min}$, relative $T_2^*_{max}$, and time to peak (TTP_{T2^*}) were determined (**Figure 2.2c)**.

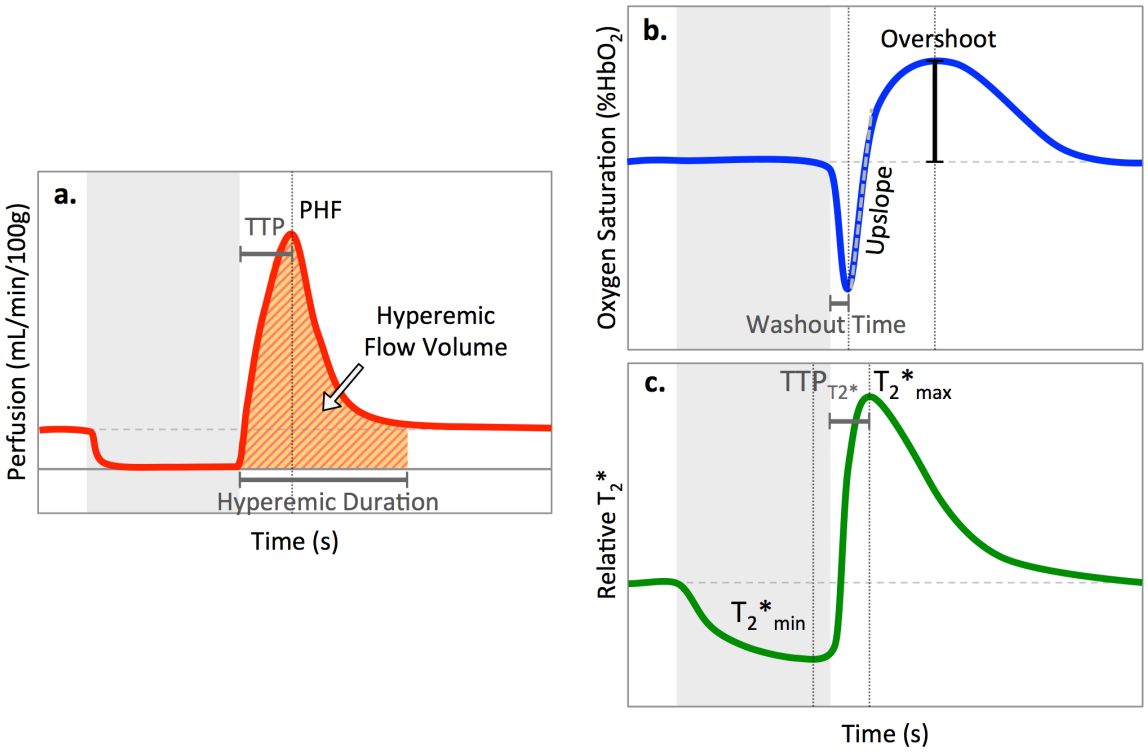

Figure 2.2. Schematic of time-course for perfusion (**a**), SvO_2 (**b**), and T_2* (**c**) illustrating the time-course-derived metrics for each parameter. Grey box indicates the period of proximal arterial occlusion.

2.4.4. Statistical Analysis

The average and standard deviation of every time-point across all subjects and both sessions was calculated for PIVOT, PASL, and multi-echo GRE time-course data. Pearson's correlation coefficient was calculated to compare the time-courses measured with PIVOT and the standard methods.

For each key time-course-derived parameter, Wilcoxon signed-rank tests were used to assess whether statistically significant differences exist between PIVOT and the standard method. Specifically, PIVOT-derived perfusion parameters were compared to results obtained with PASL-only, and PIVOT-derived SvO_2 or T_2* parameters were compared to results from the multi-echo GRE. Wilcoxon signed-rank tests were also used to determine whether significant

differences exist between key parameters measured with PIVOT and PIVOT Repeat. Wilcoxon signed-rank tests were used in lieu of a standard paired Student's t-test as only five subjects were enrolled in the evaluation study and thus it cannot be assumed that the data are normally distributed. Statistical significance was set at $p<0.05$.

To assess both intra-session and inter-session repeatability, the average within-subject coefficient of variation (CV) was calculated. Specifically, to calculate intra-session repeatability, for each parameter the within-subject standard deviation across PIVOT and PIVOT Repeat from Visit 1 was averaged across subjects, then divided by the between-subject mean parameter value from Visit 1. The same analysis was performed for intra-session repeatability on data acquired during Visit 2. Similarly, to calculate inter-session repeatability, the within-subject standard deviation across all PIVOT scans from Visit 1 and Visit 2 (4 measurements per subject) was averaged across all subjects and divided by the between-subject mean parameter value from both visits.

In the PAD patients, all time-course parameters described above were calculated, but no statistical analyses were performed since patients included in this preliminary study have varying disease severity and the ischemia-reperfusion paradigm was slightly different. The purpose of including PAD patient data was for proof of principle and to explore differences that exist between patients and healthy subjects.

2.5. Results

2.5.1. PIVOT evaluation in young healthy subjects

Example images are shown for a representative subject in **Figure 2.3**. High-resolution images corresponding to the PASL (isocenter) and multi-echo GRE slices (30 mm inferior) along with highlighted regions indicating the muscle or vein of interest are included in panels (**a**) and (**b**). Sample baseline and peak hyperemia perfusion maps are shown in (**c**) and (**d**), respectively.

These images highlight the dramatic increase in perfusion that occurs in response to induced ischemia. The green box in (**b**) shows the full FOV of the multi-echo GRE. Because the FOV of the multi-echo GRE was only 96×96 mm, aliasing along the phase-encoding direction occurred in several subjects. In this subject, the tibialis anterior muscle has wrapped posteriorly, and part of the gastrocnemius muscle has wrapped anteriorly. This aliasing did not affect the quantification of SvO_2, and wrapped regions were avoided when selecting the soleus ROI for T_2* measurement. Sample phase images used for SvO_2 quantification at baseline and hyperemia (corresponding to the minimum SvO_2, which occurs at the washout time) are shown in (**e**) and (**f**). Keyhole reconstruction was used for the phase images to achieve higher apparent in-plane spatial resolution (1×1 mm), which is necessary in order to resolve the veins. However, since spatial resolution is less critical for T_2* only data acquired every TR was used for analysis. Thus each image in (**g**) has in-plane resolution of 1×4 mm.

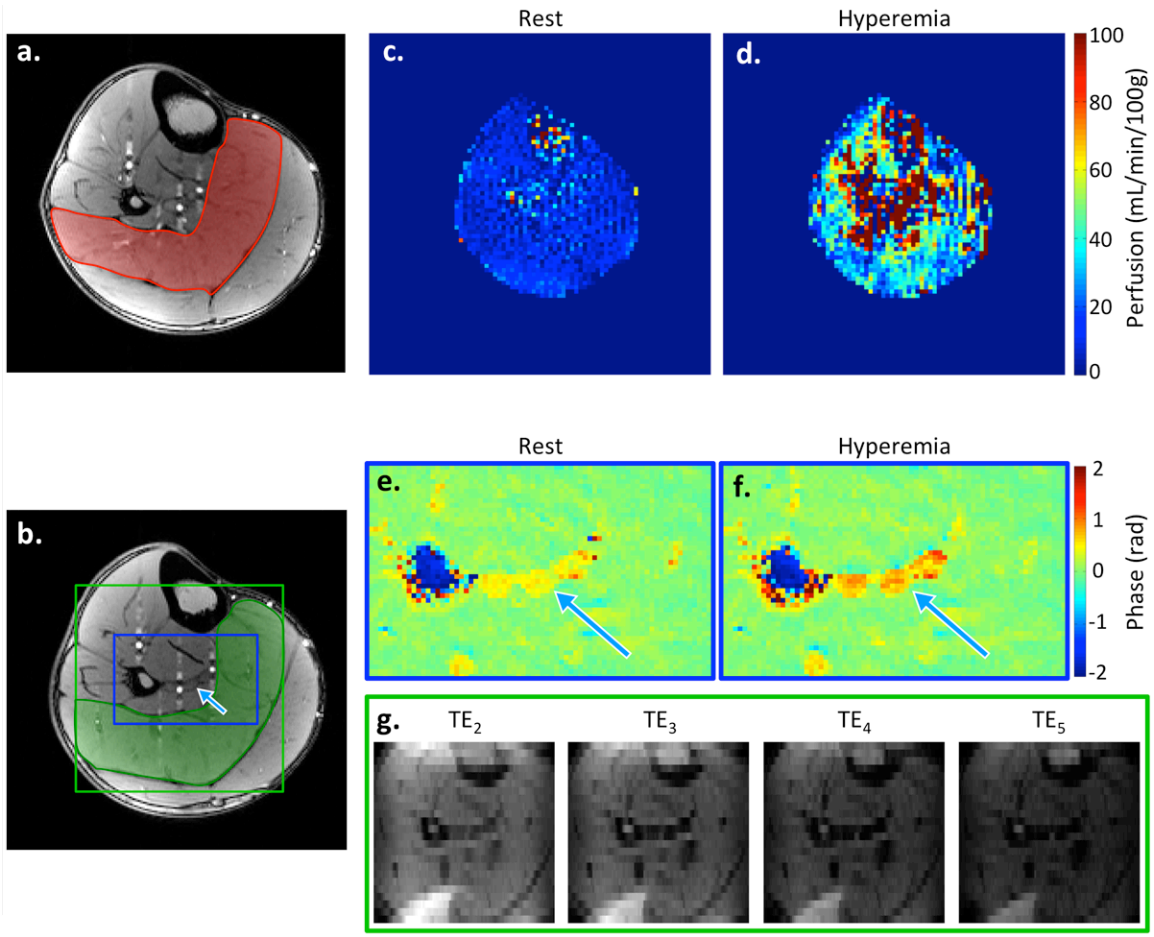

Figure 2.3. Example images from a representative young healthy subject. High-resolution scout images located at isocenter (**a**) and 3 cm inferior (**b**), corresponding to the PASL and multi-echo GRE slice locations, respectively. The soleus is indicated in red (**a**) and green (**b**), and the blue arrow points to the peroneal vein. Perfusion images represent baseline (**c**) and peak hyperemic flow (**d**). Phase images are shown for baseline (**e**) and the washout time (**f**). Note the increased phase accrual in the three veins at washout time, corresponding to a decrease in SvO_2. The blue arrow identifies the peroneal vein that was used for dynamic SvO_2 analysis. Multi-echo GRE magnitude images for each of the echo times used to quantify T_2* are shown in (**g**).

Data for all healthy subjects were averaged to yield an average perfusion, SvO_2, or T_2* time-course in order to investigate the correlation of the results between PIVOT and PASL-only or multi-echo GRE-only methods. For each parameter, average and standard deviation of the time-

courses across all subjects is shown in **Figure 2.4**. Following cessation of arterial occlusion, the typical reactive hyperemia response is seen in each of the measured parameters. The time-course measured with PIVOT is in good agreement with PASL-only or multi-echo GRE-only-measured responses. The correlation coefficient between PIVOT and PASL average perfusion time-course is 0.99, and between PIVOT and multi-echo GRE average SvO_2 and T_2* time-courses are 0.98 and 0.99, respectively.

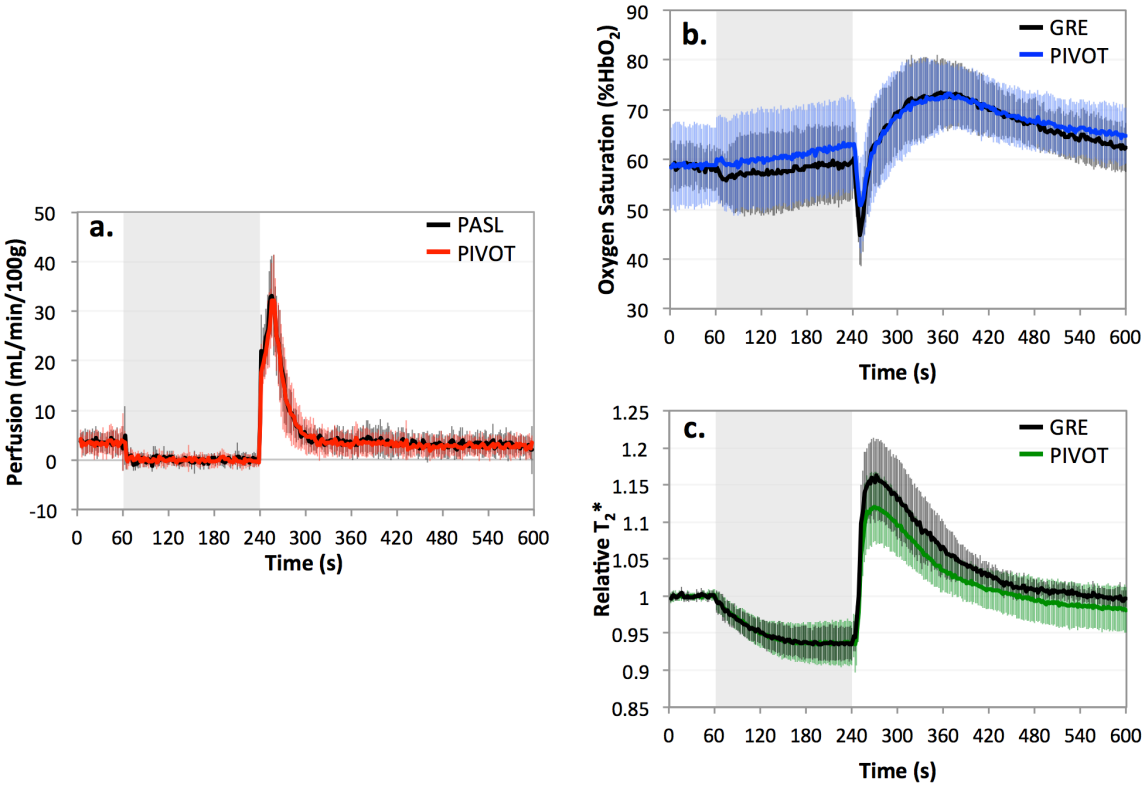

Figure 2.4. Average time-course data measured with PIVOT and standard measurement methods. (**a**) Average perfusion time-course across all young healthy subjects measured with PIVOT (red) and PASL (black). Average SvO_2 (**b**) and T_2* (**c**) time-courses measured with PIVOT (blue, green, respectively) and a multi-echo GRE (black). Error bars indicate standard deviation. Grey box indicates period of arterial occlusion.

Average (standard deviation) of key time-course parameters from PIVOT and the standard measurement methods are shown in **Table 2.1**. The Wilcoxon signed-rank tests did not detect statistically significant differences between PIVOT and PIVOT Repeat, or between PIVOT and the standard measurement method for any of the key time-course parameters ($p > 0.05$). **Table 2.2** summarizes the intra-session and inter-session repeatability measured with PIVOT.

Table 2.1. Means and standard deviations (in parentheses) of key time-course metrics measured with PIVOT and standard measurement methods. In five young healthy subjects, soleus perfusion, peroneal vein SvO_2, and soleus T_2* were measured with PIVOT, PIVOT Repeat, and the standard method (PASL or multi-echo GRE) on two separate occasions (Visits 1 and 2). No statistically significant differences in any measured parameter were detected.

	Visit 1			*Visit 2*		
	PIVOT	**PIVOT Repeat**	**Standard Method**	**PIVOT**	**PIVOT Repeat**	**Standard Method**
Perfusion (Standard Method = PASL)						
PHF (mL/min/100g)	34.8 (7.5)	34.5 (10.2)	37.9 (9.0)	39.2 (4.1)	38.3 (6.0)	37.6 (5.6)
TTP (s)	19.6 (3.6)	18.0 (3.5)	17.2 (2.3)	18.4 (5.7)	17.2 (4.1)	17.6 (5.2)
HFV (mL/100g)	17.0 (5.3)	14.0 (5.0)	16.2 (5.6)	16.7 (5.4)	14.4 (1.9)	16.1 (2.3)
Hyperemic duration (s)	53.6 (15.7)	46.8 (13.8)	53.6 (10.4)	48.8 (14.9)	44.8 (10.3)	49.6 (14.2)
SvO_2 (Standard Method = multi-echo GRE)						
Washout time (s)	11.6 (2.2)	10.0 (2.0)	10.4 (1.7)	12.4 (3.6)	11.2 (4.8)	10.0 (1.4)
Upslope (%HbO_2/s)	0.83 (0.32)	1.08 (0.47)	1.21 (0.54)	1.14 (0.42)	0.91 (0.43)	1.13 (0.48)
Overshoot (%HbO_2)	17.6 (7.5)	17.1 (6.1)	16.8 (7.1)	18.6 (6.5)	16.5 (7.6)	18.3 (5.0)
T_2* (Standard Method = multi-echo GRE)						
Baseline T_2* (ms)	23.4 (1.4)	22.5 (1.5)	23.1 (2.0)	22.0 (1.9)	21.7 (1.6)	22.2 (2.0)
Relative $T_{2\ min}$*	0.90 (0.04)	0.93 (0.03)	0.92 (0.01)	0.92 (0.03)	0.93 (0.04)	0.94 (0.02)
Relative $T_{2\ max}$*	1.09 (0.03)	1.13 (0.04)	1.16 (0.05)	1.14 (0.05)	1.15 (0.05)	1.18 (0.05)
TTP_{T2*} (s)	34.0 (11.6)	29.2 (3.6)	26.8 (5.2)	28.4 (3.6)	24.8 (5.0)	28.4 (4.8)

Table 2.2. Summary of intra-session and inter-session repeatability for all time-course-derived metrics. The within-subject coefficient of variation is shown for PIVOT versus PIVOT Repeat on Visit 1, Visit 2, and for all PIVOT data acquired on Visits 1 versus 2.

	Intra-session Visit 1	Intra-session Visit 2	Inter-session Visit 1 vs. 2
Perfusion			
PHF (mL/min/100g)	6.3%	5.0%	12.4%
TTP (s)	6.0%	11.1%	16.4%
HFV (mL/100g)	18.8%	23.4%	18.9%
Hyperemic duration (s)	15.2%	25.4%	19.9%
SvO_2			
Washout time (s)	15.7%	12.0%	18.9%
Upslope (%HbO_2/s)	26.2%	15.8%	37.3%
Overshoot (%HbO_2)	15.3%	18.3%	6.5%
T_2*			
Baseline T_2* (ms)	3.1%	1.3%	4.6%
Relative $T_{2\ min}^*$	2.4%	0.9%	1.8%
Relative $T_{2\ max}^*$	3.0%	1.1%	3.9%
TTP_{T2^*} (s)	17.9%	9.6%	19.9%

2.5.2. PIVOT in PAD Patients

Figure 2.5 shows the reactive hyperemia time-course for perfusion, SvO_2, and T_2* measured with PIVOT in a single PAD patient and a representative young healthy subject. A summary of key time-course parameters measured in individual PAD patients is presented in **Table 2.3** along with average values for young healthy subjects. The perfusion time-course data show that patients experienced a lower PHF, a delay in TTP, a prolonged hyperemic duration, and a greater HFV. The SvO_2 response was also delayed and blunted; PAD patients exhibited a longer washout time, and reduced upslope and overshoot. T_2* data showed characteristic changes expected in patients with reduced endothelial function. PAD patients had higher $T_2^*{}_{min}$, even though the ischemic duration is 5 minutes instead of 3 minutes as in the healthy subjects. Patients' $T_2^*{}_{max}$ was lower and TTP_{T2^*} was delayed. These results are in agreement with previous findings measuring perfusion (52), SvO_2 (66,67), or T_2* (68,69) individually in PAD patients.

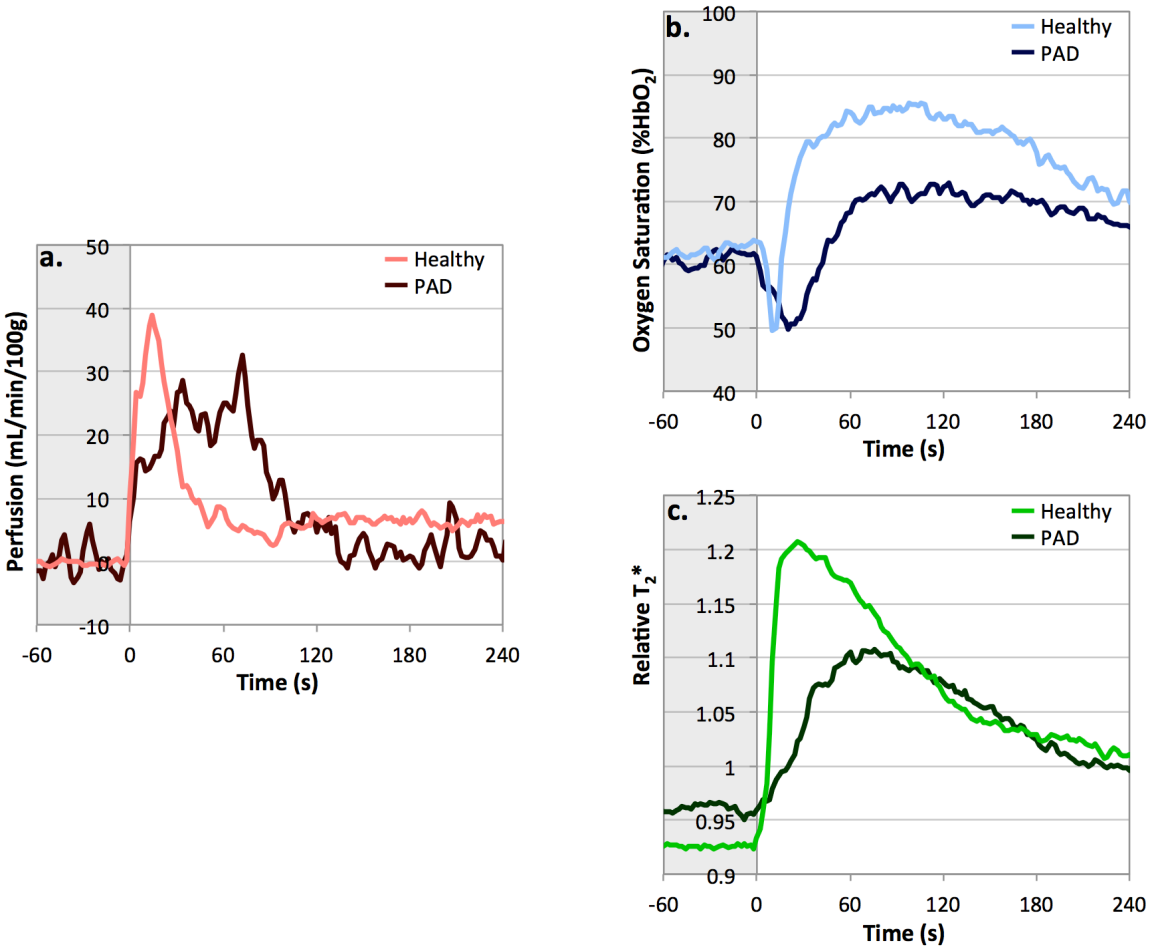

Figure 2.5. Time-courses measured with PIVOT for perfusion (**a**), SvO_2 (**b**), and T_2^* (**c**) in one representative young healthy subject and one PAD patient (PAD #5 in **Table 2.3**). Light colored lines represent healthy subject, and dark colored lines represent PAD patient. Grey box indicates period of arterial occlusion. PAD patient exhibits a blunted and delayed hyperemic response for each of the measured parameters compared to the young healthy subject.

Table 2.3. PIVOT results in individual PAD patients and for the average of all young healthy subjects.

	Healthy	PAD #1	PAD #2	PAD #3	PAD #4	PAD #5
ABI	N/A	0.41	0.52	0.68	0.72	0.74
Perfusion						
PHF (mL/min/100g)	37.0 (6.1)	26.9	22.0	31.3	29.9	37.3
TTP (s)	19.0 (4.5)	110	72	90	52	32
HFV (mL/100g)	16.9 (5.1)	48.2	26.5	78.7	37.7	33.8
Hyperemic duration (s)	51.2 (14.6)	182	124	240	110	108
SvO_2						
Washout time (s)	12.2 (2.2)	48	50	22	36	22
Upslope (%HbO_2/s)	1.0 (0.6)	0.24	0.18	0.45	0.69	0.45
Overshoot (%HbO_2)	18.1 (6.5)	16.4	17.9	13.2	16.7	12.9
T_2*						
Baseline T_2* (ms)	22.6 (1.7)	22.2	22.4	21.6	20.4	20.0
Relative $T_{2\ min}$*	0.91 (0.03)	0.93	0.94	0.92	0.95	0.94
Relative $T_{2\ max}$*	1.11 (0.04)	1.04	1.04	1.11	1.04	1.12
TTP_{T2*} (s)	32.8 (8.8)	120	160	94	56	68

2.6. Discussion

2.6.1. PIVOT Repeatability

The repeatability assessment comparing perfusion, SvO_2, and T_2* metrics derived from the two successive PIVOT scans show some intra-session variability. This variability could be physiologic in nature or could be due to noise in the time-course data. Given the low average baseline signal standard deviation (perfusion: 1.6 mL/min/100g; SvO_2: 1.5 %HbO_2; T_2*: 0.5%) it is likely that intra-session variations of key measured parameters are outweighed by physiologic variability during separate ischemia-reperfusion episodes. In all cases there were no significant differences detected between time-course parameters measured with PIVOT and PIVOT Repeat ($p>0.05$), suggesting that there was no training effect due to multiple periods of ischemia. This finding justifies the comparison of within-session PIVOT to PASL-only or to multi-echo GRE-only sequences, even though the data were acquired separately.

2.6.2. PIVOT Effect on Perfusion Quantification

In comparing perfusion metrics measured with PIVOT to those measured with an otherwise identical PASL-only sequence, it is evident that the two measurements provide similar values of all perfusion time-course-derived metrics. Specifically, there were no significant differences between any of the key parameters measured with PIVOT or with PASL. This suggests that the multi-echo GRE interleave does not impact the quantification of perfusion.

Perfusion time-course metrics had expected results for longitudinal reproducibility. A CV of approximately 20% has been reported in previous studies (47,127). Perfusion varies physiologically with time of day (128), hydration level (129), and hormonal fluctuations (130) among other factors (131). Care was taken to schedule Visits 1 and 2 at the same time, and all subjects were instructed to refrain from caffeine intake and vigorous activity for 12 hours prior. Yet even within a single scan there was variability in the hyperemic response from one ischemia-reperfusion episode to another, suggesting that these physiologic factors cannot be completely controlled. The time-course data averaged over all experiments and all healthy subjects showed good correlation in the shape and magnitude of the reactive hyperemia response, reflected by the high correlation coefficients. Thus not only were the key time-course-derived metrics not significantly different, but that the overall response was highly similar.

Peak hyperemic flow measured with either PIVOT or PASL was somewhat lower than previously reported values, where PHF was measured to be 50±13 mL/min/100g using the same SATIR perfusion preparation, but with a RARE readout (34). PHF in the soleus in our study was lower, reaching only 37.0±6.1 mL/min/100g. This difference in perfusion could be attributed to the fact that Raynaud et al quantified whole-leg perfusion (34), while individual muscle perfusion was calculated here. Additionally, care was taken to exclude vessels from the ROI, as their inclusion would increase measured perfusion. In another study by Proctor and colleagues, perfusion was measured in the calf of 64 men using strain gauge plethysmography (132), a technique

considered to be a standard for limb perfusion measurement. Peak perfusion in the calf was found to be 35.1±1.1 mL/min/100g following a period of 10 minutes of ischemia. Both this work and that by Raynaud (34) and Proctor (132) report much lower PHF than a similar study by Wu et al using continuous arterial spin labeling (CASL). In Wu's study, PHF in the soleus muscle was found to be 116±57 mL/min/100g (47), however the temporal resolution in CASL was limited to 16 seconds. Using an EPI readout, the magnitude signal over the course of an ischemia reperfusion paradigm varies substantially due to the BOLD effect. If the time course is not sampled with high enough temporal resolution, the changing signal intensity due to the BOLD effect may contaminate the quantification of perfusion (84). The higher temporal resolution data acquired with SATIR can track the changes in signal intensity better and thus may be less susceptible to BOLD contamination, allowing more accurate quantification of perfusion.

Time to peak perfusion agreed with Raynaud's values (34), however it was much shorter than the TTP reported by Wu (47). Again, this discrepancy between our work and that of Wu et al could be due to the better temporal resolution of SATIR over CASL. The temporal resolution for PIVOT and SATIR was 2 seconds, while that of the CASL sequence employed in Wu's work was 16 s. The improvement in temporal resolution was in part due to the pulsed labeling scheme used in SATIR, in which arterial labeling takes only 8 ms instead of 2 seconds as in CASL.

Hyperemic flow volume quantified the total blood delivery during hyperemia, and along with the hyperemic duration may provide more qualitative measures of hyperemia. HFV in particular may be less sensitive to time-course noise compared to PHF and TTP. PHF and TTP are determined based on a single data-point, whereas HFV is the total integrated area. The values we reported for HFV and hyperemic duration were lower and shorter than those reported by Wu, et al (47), which is not surprising since our measured PHF and TTP are lower and shorter as well.

2.6.2. PIVOT Effect on SvO_2 Quantification

High spatial resolution is necessary to measure the phase in the vein; therefore the keyhole multi-echo GRE data was supplemented with outer k-space data from a fully-phase-encoded reference scan that was run at the end of the dynamic acquisition. Langham et al have previously shown that keyhole reconstruction provides accurate SvO_2 results with high temporal resolution during reactive hyperemia in the femoral vein (56).

No significant differences were detected between time-course metrics measured with PIVOT or with the multi-echo GRE. While inter-session variability was present, it was comparable to the intra-session variability measured between PIVOT and PIVOT Repeat on the same visit. Average washout time was slightly lower than previously reported in the femoral vein of young healthy subjects (17±7 s), but upslope and overshoot were in agreement with prior results (67). The lower washout time could be explained by the fact that the tourniquet system used in this study deflated much more quickly than that used in (67). The resulting decrease in the resistance to arterial flow could potentially shorten the washout time. Another potential reason that washout time differs is that we investigated SvO_2 in the peroneal vein, as opposed to the more superior femoral vein. Thus not only does the peroneal vein collect from a smaller volume of muscle, but the distance between the capillary bed and peroneal vein was also smaller. Overall, key parameters measured with PIVOT agree with multi-echo GRE-derived data, suggesting that inclusion of the PASL interleave does not impact quantification of SvO_2.

2.6.3. PIVOT Effect on T_2* Quantification

In both PIVOT and multi-echo GRE T_2* data, the signal intensity in the ROI was first averaged then fit to a mono-exponential function. The fitting of average signal intensity was nearly perfect with an overall average R^2 for all T_2* fits of 0.999.

During the period of arterial occlusion, relative T_2* was found to decrease as the deoxyhemoglobin concentration in the capillary bed increases. Following cuff release, hyperemic arterial inflow replenishes blood in the capillary bed, bringing oxygenated arterial blood in and moving desaturated blood into the large draining veins. Relative T_2* increased during reactive hyperemia due to the increase in perfusion and the decrease in deoxyhemoglobin in the capillary bed. Even though perfusion and T_2* were measured at separate slice locations, they both represent changes that occur in the soleus muscle. TTP_{T2*} was longer than perfusion TTP, suggesting that the increase in oxygen concentration at the level of the capillary bed lasted longer than the increase in microvascular flow. This finding is in agreement with a prior study investigating the combined measurement of perfusion and BOLD during reactive hyperemia (51). Duteil et al suggest that because the brief period of arterial occlusion does not cause significant oxygen debt in muscle (as shown by (109)), the muscle's demand for oxygen remains unchanged and thus the increase in perfusion results in a decrease of oxygen extraction, causing the BOLD signal to increase (51). The decrease in oxygen extraction also physiologically manifests as the SvO_2 overshoot.

The measured values are consistent with previous literature reported values for baseline T_2* (65), relative T_2*_{min} (69), T_2*_{max} (68,133), and TTP_{T2*} (68). Comparisons between PIVOT and multi-echo GRE key time-course parameters yielded no significant differences, and the T_2* time-course data measured with PIVOT and multi-echo GRE were highly correlated (Pearson's r=0.99). These results indicate that T_2* quantification in a downstream slice with PIVOT is not affected by the PASL interleave.

2.6.4. Considerations for Applying PIVOT in PAD Patient Studies

Statistical comparisons between PAD patients and young healthy subjects were not made because the ischemic duration differed in the two cohorts. As repeated periods of arterial occlusion were used to compare PIVOT to standard measurement methods in healthy subjects, a

shortened ischemic duration was used, allowing enough time for the four scans to be performed during one hour of scanning. PAD patients included in this preliminary evaluation had varying disease severity, represented by the diverse ABIs. A five-minute period of arterial occlusion was employed in PAD patients to ensure the maximal hyperemic stimulus. The PAD patient data were, however, included to explore the range of values that exist between states of health and disease. In agreement with the results of Wu et al, PAD patients exhibited a decrease in PHF and an increase in TTP (52). SvO_2 data showed a blunted and delayed response, in agreement with Langham et al (66,67). T_2* data showed the characteristic alterations during the period of ischemia (69) and reactive hyperemia (68).

Quantification of multiple parameters may improve diagnosis and enhance power for detection of the response to therapeutic intervention. The traditional marker of disease severity in PAD is the ankle-brachial index (ABI), which is the ratio of systolic blood pressures measured at the level of the ankle and in the brachial artery. The ABI primarily represents occlusions and stenoses on the macrovascular level. Previous studies have shown that physiologic improvements such as increased peak walking time do not correlate with clinically significant changes in ABI (21,22). PIVOT provides a measure of microvascular function, thus may be more sensitive to early treatment effects. By measuring many parameters, PIVOT will provide insight into the relationship between impairments in perfusion, SvO_2, and T_2*.

In this study we showed that no major measurement bias in key time-course parameters was introduced by using PIVOT instead of the standard individual measurement methods. However, it should be noted that the small sample size affects the power to detect such a bias. Even though no measurement bias was detected, the precision and thus statistical power of PIVOT-derived measures was limited by physiologic variability, which cannot be completely controlled. In order to use this method to assess disease presence or monitor a treatment effect,

the study must be well designed, controlling for factors that are known to affect perfusion and the hyperemic response (128,130,131).

The preliminary PAD patient data showed that for many of the key time-course parameters there was a relatively wide range of values that exist between states of health and disease. A recent study performed at 1.5T showed relatively poor repeatability of BOLD measurements with the exception of TTP_{T2*} during reactive hyperemia in both healthy subjects and PAD patients (127). In our study a lower inter-session CV, and hence better repeatability, was found for several key T_2* parameters in healthy subjects. The improvement in repeatability may be due to the higher field strength, which confers increased signal to noise ratio and greater BOLD signal contrast. A longitudinal study will be necessary to determine the repeatability of PIVOT measures in PAD patients. Additionally vascular reactivity decreases with age (66), therefore it will be important to compare PIVOT results obtained for PAD patients to age-matched healthy controls to assess the impact of age on PIVOT-derived measures of microvascular function.

2.7. Conclusions

In summary, we have introduced a quantitative MRI method that measures perfusion, SvO_2, and T_2* simultaneously, thereby allowing a comprehensive assessment of the functional integrity of the peripheral microvasculature during a single ischemia-reperfusion paradigm. The added value of the proposed approach will require rigorous evaluation in cohorts of patients with impaired peripheral circulation in comparison to their healthy peers. In the future PIVOT could possibly serve as a means to monitor disease progression and effectiveness of intervention.

CHAPTER 3: MEASUREMENT OF SKELETAL MUSCLE PERFUSION DYNAMICS WITH ASL: ASSESSMENT OF PCASL LABELING EFFICIENCY IN THE PERIPHERAL VASCULATURE AND COMPARISON OF POST-ISCHEMIA PERFUSION MEASURED WITH PCASL AND PASL

3.1. Abstract

Purpose: To compare calf skeletal muscle perfusion measured with pulsed arterial spin labeling (PASL) and pseudo-continuous arterial spin labeling (pCASL) methods, and to assess the stability of pCASL labeling efficiency in the popliteal artery throughout an ischemia-reperfusion paradigm.

Materials and Methods: At 3T field strength, pCASL labeling efficiency was experimentally assessed in five subjects by measuring the signal intensity of blood in the popliteal artery just distal to the labeling plane immediately following pCASL labeling or control preparation pulses, or without any preparation pulses throughout separate ischemia-reperfusion paradigms. The relative label and control efficiencies were determined during three distinct phases (baseline, hyperemia, and recovery) defined based on average arterial velocity, which was measured with a projection phase-contrast sequence. In a separate cohort of ten subjects, pCASL and PASL sequences were used to measure reactive hyperemia perfusion dynamics.

Results: Calculated pCASL labeling and control efficiencies were unchanged throughout the baseline, hyperemia, and recovery periods. Perfusion dynamics measured with pCASL and PASL did not significantly differ. Average leg muscle peak perfusion was 47±20 mL/min/100g or 50±12 mL/min/100g, and time to peak perfusion was 25±3 s and 25 ±7 s from pCASL and PASL data,

respectively. Further metrics parameterizing the perfusion time course did not significantly differ between pCASL and PASL measurements.

Conclusion: No change in pCASL labeling efficiency was detected despite the almost ten-fold increase in average blood flow velocity in the popliteal artery. pCASL and PASL provide precise and consistent measurement of skeletal muscle reactive hyperemia perfusion dynamics.

3.2. Introduction

As described Chapters 1 and 2, recent studies have shown that the dynamics of skeletal muscle perfusion can provide insight into endothelial function and vascular reactivity in normal physiologic and pathophysiologic states (48,52,134,135). Perfusion is a tightly regulated physiologic process, serving to provide oxygen and nutrients to active tissue, and to remove waste products. Because metabolic demand of resting skeletal muscle is quite low, skeletal muscle perfusion at baseline is generally maintained even in situations of disease such as peripheral artery disease (PAD) or diabetes mellitus. However, these diseases do manifest with an impairment of vascular reactivity.

These functional deficits of the vasculature can be evaluated by monitoring the kinetics of the response to a situation of increased flow demand, akin to cardiac stress testing. In skeletal muscle, this can be accomplished by measuring the response during or following exercise (functional hyperemia) (34,107,136), or following induced ischemia (reactive hyperemia) (34,47,51). Functional vascular impairment manifests as a blunting and delay of reperfusion in response to the stressor (52). Even though it is not physiologically analogous to the demands of daily living, reactive hyperemia provides a more reproducible and subject effort-independent stimulus compared to functional hyperemia, and thus has been purported as the preferred stressor for studying peripheral vascular function (25).

Arterial spin labeling (ASL) permits the measurement of perfusion in physiologic units (45,76). Previous studies have used ASL to measure perfusion in the brain (77,82), kidneys (137), and skeletal muscle (34,47). While several ASL labeling schemes exist, they each work by taking the pair-wise difference of two images – one with magnetically labeled blood (label) and one without (control). Tissue magnetization is measured with and without inversion of arterial blood water and after allowing enough time for the inverted or uninverted spins to perfuse the organ of interest. Subtraction between the label and control images cancels out the contribution from static tissue and yields a signal that is proportional to microvascular perfusion. This signal can be converted into perfusion in units of mL/min/100g through application of various models (34,47,80,81).

Skeletal muscle perfusion during hyperemia has been quantified with PASL (34), which achieves inversion using a single adiabatic inversion pulse (77), continuous ASL (CASL) (47) or, more recently, pCASL (48). Each of these methods has benefits and drawbacks. PASL uses a single RF pulse for nearly instantaneous and complete inversion, therefore perfusion can be measured at a temporal resolution of up to 2 second (34). However, pCASL and CASL utilize a series of pulses to achieve inversion, thereby reducing labeling efficiency (82) and limiting temporal resolution to 6-8 seconds (47,48,52). On the other hand, CASL or pCASL methods do offer an increase in signal-to-noise ratio compared to PASL as the labeled blood water spins accumulate in the tissue throughout the longer labeling duration (83).

Both CASL and pCASL rely on flow-driven adiabatic inversion to label arterial blood (45,82). To achieve efficient flow-driven adiabatic inversion, blood flow velocity (v) must satisfy the adiabatic condition: $\frac{1}{T_2} \ll \frac{Gv}{|B_{eff}|} \ll \gamma|B_{eff}|$, where T_2 is the transverse relaxation time of blood water protons, G is the average gradient amplitude, B_{eff} is the effective magnetic field, and γ is the proton gyromagnetic ratio (85). Flow-driven adiabatic inversion will invert spins that satisfy this condition. However, if blood flow velocity is too slow, transverse relaxation effects dominate, and

blood will not be inverted. On the other hand, if flow is too fast, the effective frequency sweep rate will be too fast the magnetization will not be inverted. Blood flow velocity, therefore must remain in a specific range in order to achieve efficient flow-driven adiabatic inversion (138).

In contrast to the arteries supplying the brain, the peripheral circulation has higher impedance resulting in a distinctive flow waveform (57,139,140). Specifically in the popliteal artery, which supplies muscles in the calf, the blood flow waveform is triphasic at baseline with antegrade flow during systole followed by retrograde then antegrade flow during diastole (139,140). During reactive hyperemia, the flow waveform becomes entirely antegrade due to vasodilation of capillaries to accommodate increased blood flow demand downstream (57). Beyond the changes in the waveform characteristics, average blood flow velocity differs substantially between baseline, ischemia, and reactive hyperemia. This variability may result in blood flow velocity-dependent changes in labeling efficiency for techniques that rely upon flow-driven adiabatic inversion.

Theoretical explorations of the dependence of blood flow velocity on labeling efficiency show that with decreasing peak flow, there is a decrease in labeling efficiency (76,82,138). These simulations have been corroborated by experimental investigations of labeling efficiency performed in the brain (141). However, those results may not apply to muscle perfusion, due to the different characteristics of the blood flow waveform in the peripheral vasculature.

Prior studies investigating muscle perfusion dynamics with PASL and pCASL or CASL have yielded disparate results, wherein peak perfusion measured with pCASL (48) or CASL (52) methods was much higher than that measured by PASL (34,142). However, the precise quantification of perfusion depends both on the acquisition approach, experimental stimulus, as well as the analysis methods, for instance how to deal with outliers, etc., thus true comparison between ASL methods for quantification of skeletal muscle perfusion has not yet been explored. Current hardware limitations make implementation of CASL on clinical imaging systems difficult,

thus the focus of this work was on comparison of perfusion quantified with pCASL and PASL. Furthermore, to our knowledge, there has not been any exploration of the effect of the labeling method on quantification of muscle perfusion and perfusion dynamics in a reactive hyperemia paradigm.

The purpose of this study was to experimentally investigate pCASL label efficiency during an ischemia reperfusion paradigm in the peripheral vasculature, and to compare muscle perfusion dynamics measured using pCASL and PASL.

3.3. Methods

3.3.1. Experimental overview

The Institutional Review Board of the University of Pennsylvania approved all aspects of the study. Fifteen healthy subjects were recruited to participate after providing written, informed consent. Five healthy subjects (33±7 years old, 4 male) participated in the pCASL labeling efficiency experiments, and ten healthy subjects (60±4 years old, 7 females) were scanned with both PASL and pCASL sequences. All subjects were free from overt cardiovascular disease. For each subject, all experiments were performed on the same day, within the same scan session.

Imaging was performed at 3.0 T (Siemens Magnetom Tim Trio, Siemens Medical Equipment; Erlangen, Germany) with an eight-channel transmit/receive knee coil (InVivo, Inc; Gainesville, FL). All experimental imaging sequences were written in SequenceTree (143). Reactive hyperemia was induced for both sets of experiments using an ischemia-reperfusion paradigm consisting of 3-5 minutes of proximal arterial occlusion via a pneumatic cuff secured around the thigh. The cuff was rapidly inflated to 75 mmHg above each subject's systolic blood pressure using the Hokanson E20 AG101 Rapid Cuff Inflation System (D.E. Hokanson, Inc; Bellevue, WA). Data analysis was performed with in-house-written software using MATLAB

(MathWorks, Natick, MA), and statistical analyses were executed with JMP (SAS Institute., Cary, NC, 1989-2007).

3.3.2. pCASL labeling efficiency during reactive hyperemia

First we aimed to assess whether pCASL labeling efficiency varies over the course of an ischemia reperfusion paradigm. By measuring the signal intensity in the artery following pCASL labeling period, the inversion efficiency can be experimentally estimated (144). For the purpose of this study, precise quantification of the inversion efficiency was of less interest than its variation over the course of the reactive hyperemia paradigm.

Relative inversion efficiency was estimated experimentally using a modified pCASL sequence in which the imaging readout, located just distal to the labeling plane, immediately followed the labeling or control period (**Figure 3.1a**). Rather than measuring signal intensity in the muscle tissue, magnitude signal intensity was measured in the blood contained within the popliteal artery to assess the impact of the labeling period. Following the imaging readout, additional time was allotted for signal recovery and inflow of fresh spins in the artery.

The reactive hyperemia response is relatively short-lived, therefore temporal sampling of popliteal artery blood signal was maximized by conducting three separate experiments: with EPI data acquired following pCASL label; following pCASL control; or without label or control preparations (termed M_0) (**Figure 3.1b**). The duration of the label and control preparations were selected to match Wu, et al's prior study using CASL for skeletal muscle perfusion quantification (47). For each scan, data were acquired during 1 min baseline, 3 min ischemia, and 2 min recovery. Five subjects were scanned with this repeated reactive hyperemia paradigm (33±7 years old, 4 male). Each subject received additional time to recover back to his or her relative baseline state between scans.

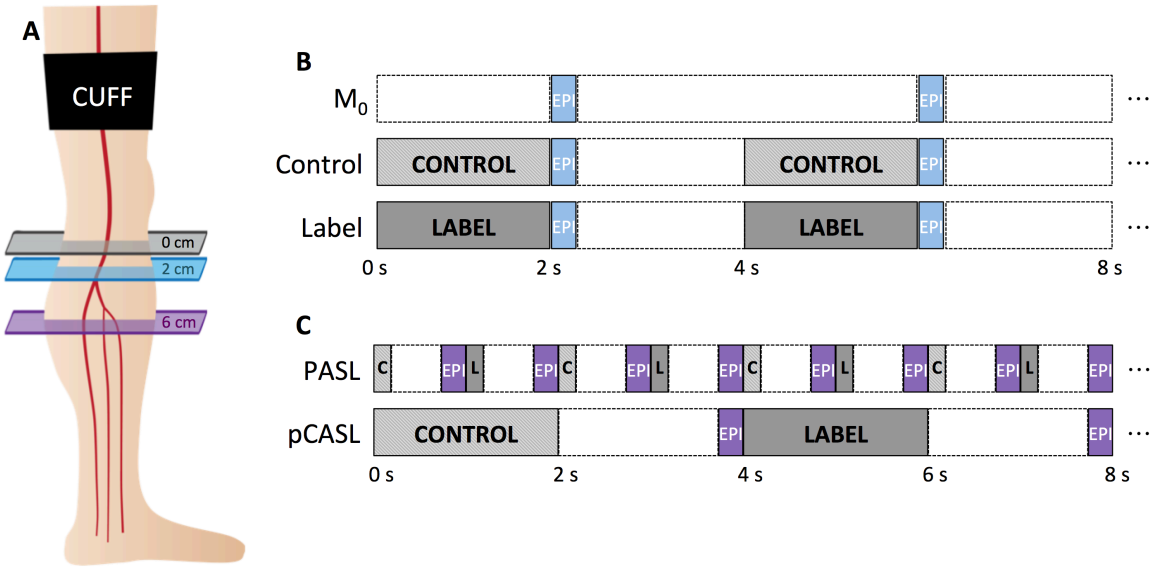

Figure 3.1. (A) Diagram of measurement locations for both the pCASL labeling experiments (blue slice, located 2 cm distal from labeling plane) and perfusion quantification experiments (purple slice, located 6 cm distal from labeling plane). For both experiments, the location of the pCASL labeling plane was approximately at the level of the popliteal artery (grey slice). For PASL, slice selective and non-selective inversion was used for label and control conditions, respectively, but the perfusion measurement slice remained at the same location as in pCASL (purple slice). (**B**) pCASL efficiency data were acquired from repeated ischemia-reperfusion paradigms in which the imaging readout immediately followed the control or label period, and were normalized by an image in which no labeling was conducted (M_0 – shown in the top line of **B**). A fourth scan was conducted to measure blood flow in the popliteal artery during the ischemia-reperfusion paradigm at the level of the labeling plane. (**C**) Timing diagram for PASL and pCASL perfusion quantification sequences. C and L refer to control (non-selective inversion) and label (slice-selective inversion) conditions, respectively for the PASL scan. For both PASL and pCASL measurements, the location of the imaging slice was approximately mid calf (purple slice).

The modified pCASL sequences used the following parameters: for pCASL label or control experiments, labeling duration = 2000 ms (in one subject, labeling duration was 1350 ms), PLD = 1.6 ms, Hanning window-shaped pulses with average B_1 = 1.7 μT, pulse interval = 1 ms, G_{max}/G_{avg} = 9/1 mT/m. The unbalanced control condition utilized average gradient = 0 mT/m and 180° phase shift between adjacent RF pulses. The labeling and control plane was located 20 mm

superior from the EPI readout. The risk of unlabeled blood entering the measurement slice is negligible as flow velocity would have to exceed 1250 cm/s to travel more than 20 mm in the 1.6 ms delay between labeling and image acquisition. The M_0 experiment had identical temporal sampling as the pCASL label and control experiments, but neither pCASL label or control module was applied before the EPI readout. For all scans, an identical velocity-compensated GRE-EPI readout was used for image acquisition with flip angle = 90°, FOV = 20×20 cm^2, slice thickness = 10 mm, acquired matrix = 80×50 (reconstructed to 80×80), TR/TE = 4000/8.1 ms (TR = 3000 ms for one subject).

A fourth scan was conducted during which projection phase-contrast data were continuously acquired in the labeling plane in order to characterize the arterial velocity waveform throughout the ischemia-reperfusion paradigm. Although the beat-to-beat variation in arterial velocity will not match between the scans, average arterial velocity and the velocity range throughout the reactive hyperemia paradigms are repeatable (88). Acquisition parameters for the projection phase-contrast scan were: FOV = 176×176 mm, slice thickness = 5 mm, acquired matrix = 208×1, VENC = 80-120 cm/s, TR/TE = 24/6.5 ms. Fully phase encoded reference images were acquired immediately before and after the projection data with identical imaging parameters and acquired matrix = 208×208 to allow for quantification of velocity as described in (57).

Briefly, to quantify velocity, a static tissue k-space projection was computed by first masking out the artery in the reference image, then taking the inverse Fourier transform and isolating the center k-space line (k_y=0). This static tissue k-space projection was subtracted from every dynamically acquired velocity-encoded projection to isolate blood signal (57). Then the phase difference between adjacent positive and negative velocity-encoded projections was computed and the average velocity across the popliteal artery was quantified with 24 ms temporal resolution. The time-resolved velocity and maximum velocity were recorded. Projection velocity

data were averaged over one cardiac cycle, and downsampled to match the temporal resolution of the pCASL labeling scans.

Knowledge of average arterial velocity data served two purposes. First, the data were used to estimate the transit time between the labeling location and the imaging slice, which will differ between the baseline and hyperemic states. Assuming inversion at the location of the labeling plane, the pCASL label data were then corrected for T_1 recovery that occurs during the transit time. Second, the arterial velocity data were used to divide all reactive hyperemia scans into four periods: baseline, ischemia, hyperemia, and recovery. The hyperemic duration from the projection velocity acquisition was used to define the hyperemia period for pCASL data as the period of time during which the average arterial velocity was more than twice the baseline velocity. Control efficiency was defined as $\frac{M_0+Control}{2M_0}$ where M_0 is the blood signal intensity in the M_0 acquisition (without pCASL labeling), and similarly, Control is that in the pCASL control scan. Label efficiency is defined as $\frac{M_0-Label}{2M_0}$, where Label is the blood signal intensity in the pCASL label acquisition. However, because magnitude images were used for analysis, the experimentally measured label efficiency was defined as $\frac{M_0+Label}{2M_0}$. Wilcoxon signed rank tests were used to test whether the average label or control efficiencies differed between baseline, hyperemia, and recovery.

3.3.3. Perfusion quantification with pCASL and PASL

Next we aimed to compare perfusion dynamics measured during an ischemia-reperfusion paradigm with PASL and pCASL to assess whether significant differences existed between results obtained with the two methods. Perfusion was measured with pCASL and PASL sequences in ten healthy subjects (60±4 years old, 7 females). The reactive hyperemia perfusion data quantified with PASL had been published previously (134). Each subject underwent three ischemia-reperfusion paradigms consisting of 1 minute of baseline, 5 minutes of ischemia

induced via proximal arterial occlusion, and 6 minutes of post-ischemia recovery during a 1-hour scan session. In the first two ischemia-reperfusion scans, perfusion was quantified using a PASL variant and in the third scan, a pCASL sequence was used to measure perfusion (**Figure 3.1c**).

A standard pCASL sequence as described by Alsop, et al (81) was implemented with the following parameters: Single-slice GRE-EPI: acquisition matrix=80×50 (partial Fourier, reconstructed to 80×80), FOV=25×25 cm^2, slice thickness=10 mm, TR/TE = 4000/8.1 ms. Labeling duration and post labeling delay matched values used in Wu, et al's prior CASL muscle perfusion investigation (52), with labeling duration = 2 s, post-labeling delay (PLD) = 1.9 s, Hanning window-shaped pulses with average B_1 =1.7 μT, pulse interval = 1 ms, G_{max}/G_{avg} = 9/1 mT/m. Unbalanced control condition utilized average gradient = 0 mT/m and 180° phase shift between adjacent RF pulses. The labeling plane was located 60 mm superior to the imaging slice. Perfusion was quantified with temporal resolution of 8 seconds.

PASL data were acquired with the Perfusion, Intravascular Venous Oxygen saturation, and T_2* (PIVOT) sequence (142), an interleaved dual-slice PASL and multi-echo GRE sequence. PIVOT employs the saturation inversion recovery PASL variant described by Raynaud, et al (34) for perfusion quantification. Notably, evaluation of PIVOT compared to PASL showed that no error was introduced by interleaving the acquisition of multi-echo GRE data during the PLD, thus quantification of perfusion is unbiased by the use of PIVOT (instead of a standard PASL sequence). Sequence parameters were as follows: Slice-selective or non-selective adiabatic inversion for label and control condition, respectively; single-slice GRE-EPI with acquisition matrix=80×50 (partial Fourier, reconstructed to 80×80) identical to the pCASL imaging readout; FOV = 25×25 cm; slice thickness = 10 mm; TR/TE = 1000/8.1ms. Labeling duration = 8 ms (adiabatic inversion via hyperbolic secant pulse), PLD = 0.94 s. Temporal resolution of perfusion quantified with PASL was 2 seconds.

For both PASL and pCASL datasets, rigid-body motion correction was applied to the time-series of label and control images using National Institutes of Health ImageJ software (developed by Wayne Rasbands; National Institutes of Health, Bethesda, MD). Regions of interest (ROIs) were manually drawn on the EPI images using high-resolution anatomical images as a reference for muscle boundaries (**Figure 3.2a**). After masking out the large arteries, signal intensity was averaged in the gastrocnemius muscle, soleus muscle, peroneus muscle, and anterior compartment, composed of the tibialis anterior and extensor digitorum longus muscles for label and control time series data. These individual muscle ROIs were also combined to determine the average muscle perfusion across the entire cross-section of the calf, referred to as "whole-leg". The EPI readout used for both PASL and pCASL sequences is T_2*-weighted resulting in appreciable change in the signal intensity of the images throughout the ischemia-reperfusion paradigm, thus without any correction for the temporal offset, subtraction between adjacent label and control images yields a difference that is unrelated to perfusion. To account for the temporal offset between the control and label image series, adjacent control data were averaged to yield a temporally matched control series (124). Perfusion was computed from pairs of label and temporally-matched control data according to the appropriate models (Chapter 1, equations 1.6 and 1.7) for each ASL method as described Chapter 1 with *PLD* = 1.9 s in pCASL, 0.94 s in PASL, $T_{1,blood} \approx T_{1,tissue}$ = 1420 ms (126). In the pCASL perfusion model, α is the labeling efficiency (85%) (82), τ is the labeling duration (τ = 2000 ms).

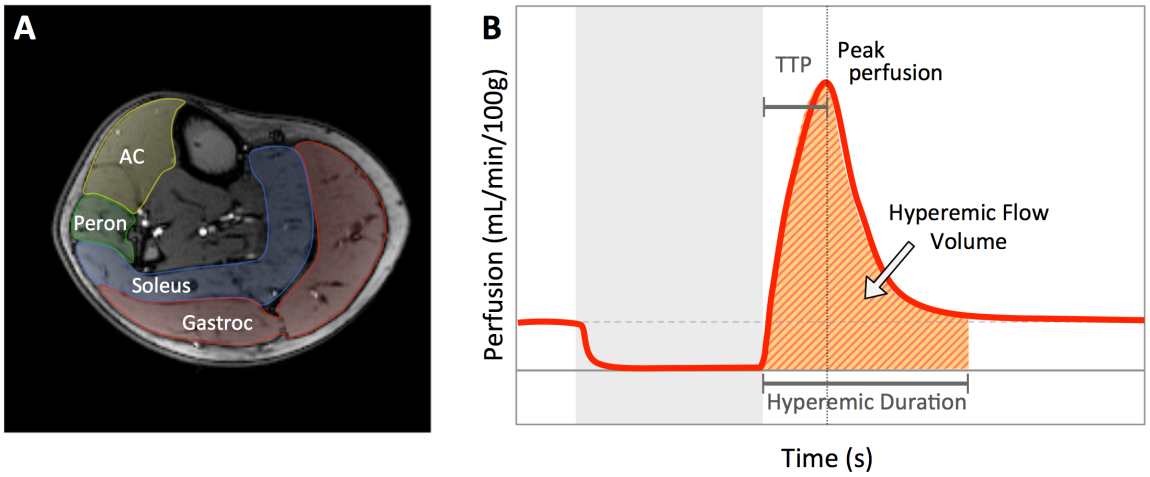

Figure 3.2. High-resolution anatomical images were used to define muscle boundaries for region of interest selection (**A**). Perfusion time courses were generated for each muscle ROI (**B**). Grey box indicates period of ischemia. Reactive hyperemia ensues following deflation of the cuff. Metrics of the dynamic reactive hyperemia response including the peak perfusion, time to peak perfusion (TTP), hyperemic flow volume (HFV), and the hyperemic duration were calculated.

Cuff inflation and deflation resulted in slight motion of the calf, thus the pair of label and control images acquired immediately after inflation or deflation were excluded from the time series. The baseline perfusion offset was calculated by averaging perfusion during the period of cuff ischemia (47), and the offset was then subtracted from each time point. PASL and pCASL perfusion time courses were smoothed to minimize non-physiologic noise using a three-time point sliding-window average. The peak perfusion, time to peak perfusion, hyperemic flow volume, and the hyperemic duration were identified and recorded from the perfusion time courses for each muscle ROI (**Figure 3.2b**). Wilcoxon signed rank tests were performed for repeated measures of perfusion. Holm adjustment for multiple comparisons was applied to all tests to maintain the family-wise error rate of 0.05. Thus, for all tests, $P_{holms}<0.05$ was considered to be significant.

3.4. Results

3.4.1. pCASL labeling efficiency during reactive hyperemia

Figure 3.3a shows the temporally resolved and average velocity in a single representative subject throughout the ischemia reperfusion paradigm as measured in the popliteal artery at the location of the pCASL labeling plane. Velocity during the baseline period (**Figure 3.3b**) exhibited the expected triphasic waveform, with antegrade flow during systole, followed by slight retrograde and antegrade flow during diastole. During the hyperemic period blood flow became monophasic, as it was antegrade during both systole and diastole (**Figure 3.3c**). From baseline to peak hyperemia, the average blood velocity increased by approximately tenfold and the peak velocity during systole roughly doubled. Across all subjects, the average baseline blood flow was 3.9±0.9 cm/s, and the diastolic to systolic range was -13.7±2.1 to 46.3±5.4cm/s. The average peak hyperemic blood flow was 34.1±12.5 cm/s, with a range of 14.0±6.4 to 87.6 ±33.6 cm/s.

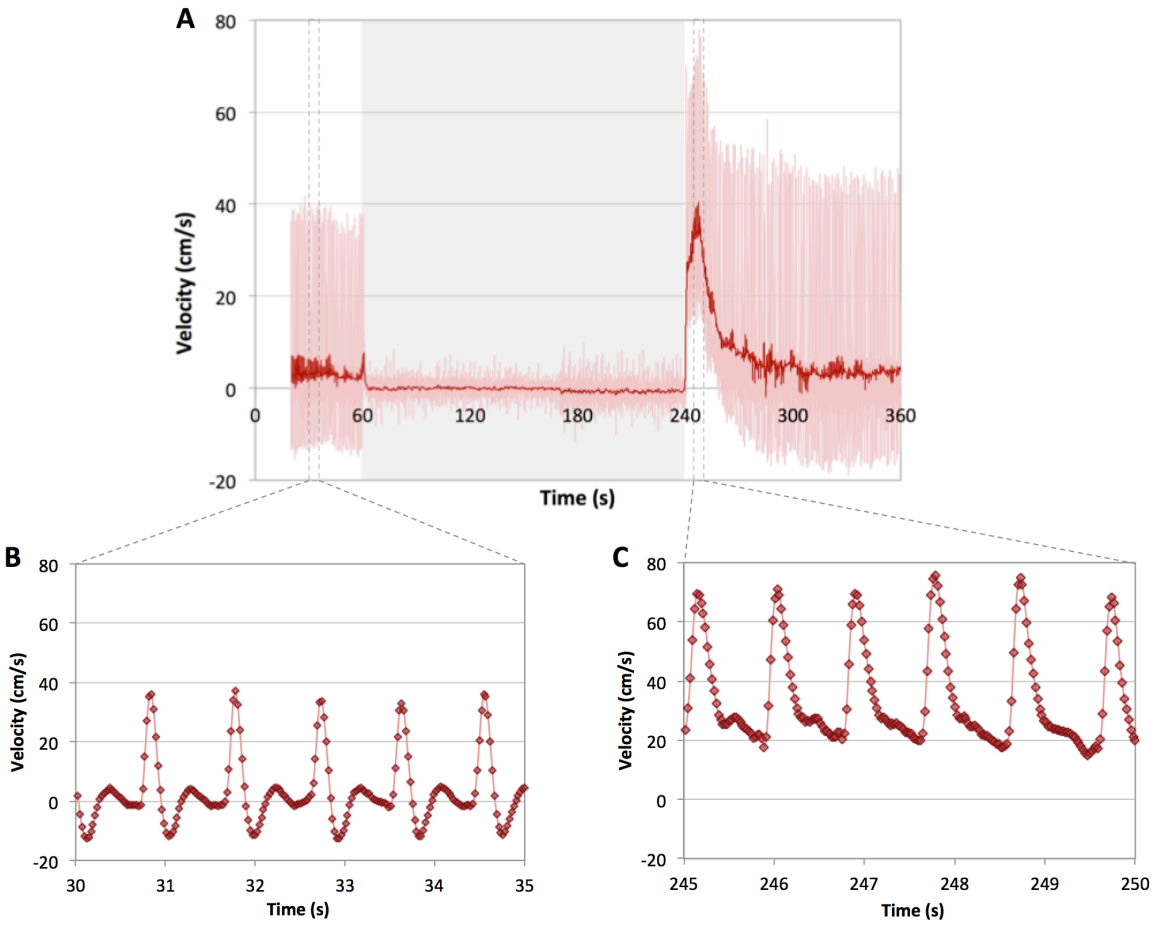

Figure 3.3. (**A**) Temporally resolved (light red) and averaged over 1 second (dark red) blood flow velocity in the popliteal artery in a representative subject. The first 20 seconds of data acquisition were used to acquire the reference image used to generate a tissue k-space projection. Baseline VENC was 80 cm/s and was raised to 120 cm/s at approximately 170 s into the experiment to account for the higher flow velocities during hyperemia. (**B**) Temporally resolved velocity from the baseline period in (**A**) shows the typical and expected triphasic waveform. (**C**) During reactive hyperemia, the blood flow is entirely antegrade, with forward flow throughout the cardiac cycle.

The variability in blood flow velocity throughout the baseline and reactive hyperemia segments was not found to significantly impact labeling efficiency. **Figure 3.4** shows the average label efficiency with and without correction for the T_1 recovery during the transit time between the labeling plane and image slice location and the control efficiency, as well as the average blood flow velocity during the ischemia reperfusion paradigm. T1-corrected label efficiency data were

not calculated during the period of ischemia (grey box) since there is no flow, but through the uncorrected label data, we observe that the label and control conditions had similar signal intensity with respect to M_0. During baseline, hyperemia, and recovery, a significant change in control or T_1 recovery-corrected label efficiencies was not detected (**Table 3.1**).

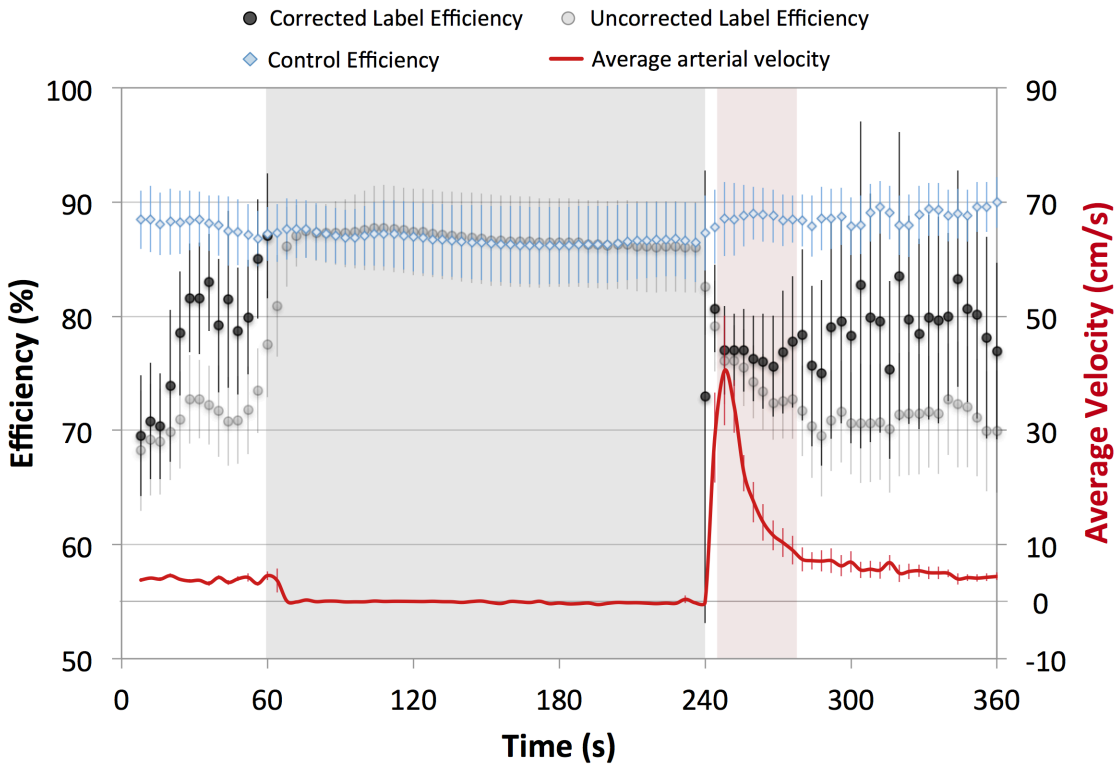

Figure 3.4. Control and label efficiency are plotted over the course of the ischemia reperfusion paradigm (grey box indicates period of arterial occlusion). Label efficiency data are plotted both with (black) and without (grey) correction for T_1 recovery during the transit time between the labeling plane and the imaging slice location. The transit time was calculated as the separation distance (20 mm) divided by the average velocity (shown in red). Data are averaged across all subjects and error bars indicate standard error. Blood velocity was used to define the hyperemic period (indicated by the red box) as the time during which average blood velocity was at least more than double the average baseline velocity. No significant differences were detected between the baseline, hyperemia, and recovery periods for control or label efficiency.

Table 3.1. Average (standard deviation) of control and label efficiencies during the average baseline, hyperemia, and recovery periods.

	Baseline	Hyperemia	Recovery
Control efficiency (%)	88 (5)	89 (5)	89 (4)
Label efficiency (%)	77 (9)	75 (7)	81 (10)

3.4.2. pCASL versus PASL

One subject was excluded from the analyses because the cuff-occlusion paradigm did not result in a reactive hyperemia response in pCASL data. Averaged over the remaining nine subjects, significant differences between the temporal dynamics of perfusion measured with PASL and pCASL were not detected in any muscle groups. **Table 3.2** shows the results of the parameterized time-course data. Significant differences were not observed between PASL and pCASL or between the two PASL acquisitions for any of the perfusion time course metrics. Perfusion time courses were calculated for each scan and were averaged across all subjects (**Figure 3.5**). Similar to the results in **Table 3.2**, the measured whole-leg perfusion dynamics appear to be in agreement between pCASL and PASL despite the differences in labeling method, post-labeling delay, and perfusion quantification model.

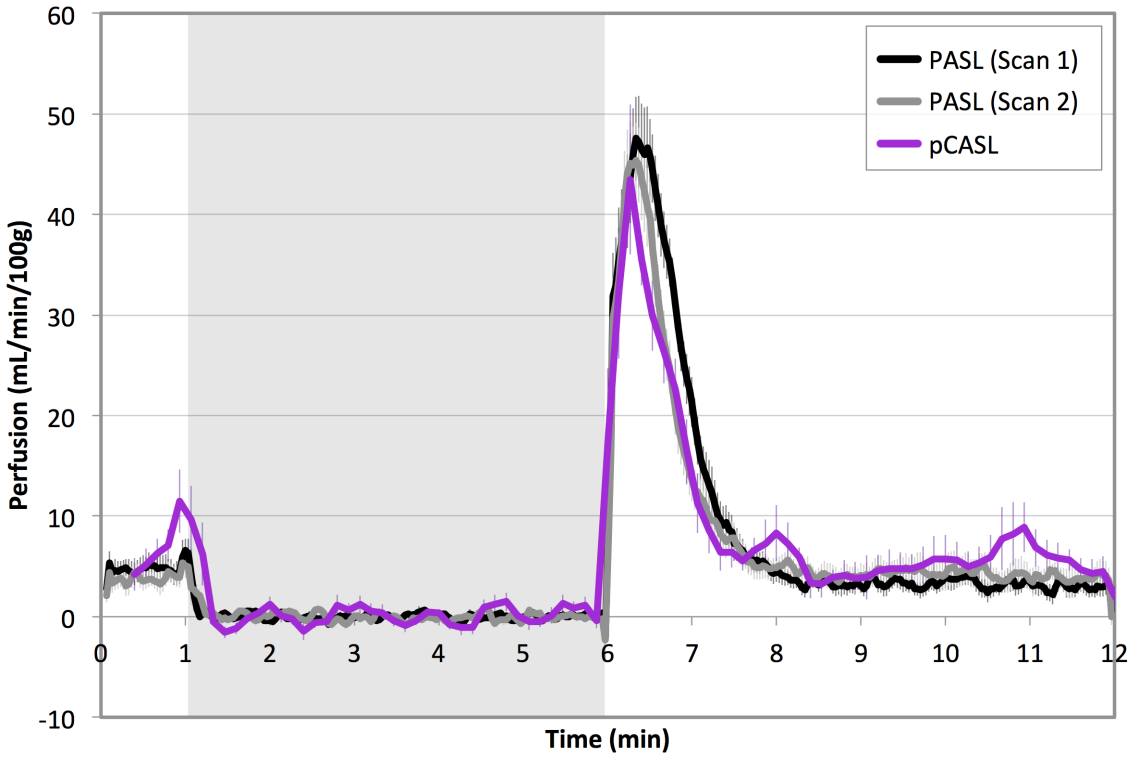

Figure 3.5. Perfusion time course averaged across 9 subjects quantified with pCASL (purple), and two identical PASL scans (grey and black). Grey box indicates period of arterial occlusion. Error bars indicate standard error. The reactive hyperemia perfusion time course did not significantly differ between PASL and pCASL measurements.

Table 3.2. Average perfusion time course metrics measured with pCASL or PASL. Two identical PASL scans were conducted to assess repeatability of the measured hyperemic response. Results shown are average (standard deviation).

	pCASL	***PASL (scan 1)***	***PASL (scan 2)***
Gastroc Peak Perfusion (mL/min/100g)	41 (9)	51 (11)	52 (13)
Soleus Peak Perfusion (mL/min/100g)	50 (26)	78 (33)	69 (28)
Peroneus Peak Perfusion (mL/min/100g)	50 (6)	41 (12)	45 (12)
AC Peak Perfusion (mL/min/100g)	47 (13)	44 (16)	45 (14)
Whole-Leg Peak Perfusion (mL/min/100g)	47 (20)	51 (12)	50 (12)
Gastroc TTP Perfusion (s)	23 (3)	33 (9)	30 (8)
Soleus TTP Perfusion (s)	28(8)	30 (12)	22 (7)
Peroneus TTP Perfusion (s)	26 (5)	27 (10)	24 (7)
AC TTP Perfusion (s)	23 (3)	20 (8)	18 (7)
Leg TTP Perfusion (s)	25 (3)	27 (7)	23 (7)
Gastroc HFV (mL/100g)	33 (10)	42 (13)	37 (14)
Soleus HFV (mL/100g)	39 (23)	70 (35)	52 (24)
Peroneus HFV (mL/100g)	29 (10)	23 (8)	20 (7)
AC HFV (mL/100g)	25 (11)	22 (10)	18 (5)
Leg HFV (mL/100g)	33 (15)	42 (12)	38 (13)
Gastroc HD (s)	82 (21)	88 (14)	90 (21)
Soleus HD (s)	80 (29)	101 (35)	102 (28)
Peroneus HD (s)	73 (22)	68 (17)	65 (26)
AC HD (s)	65 (45)	71 (25)	63 (20)
Whole-Leg HD (s)	77 (19)	99 (22)	105 (29)

Gastroc signifies the gastrocnemius muscle, AC the anterior compartment, TTP the time to peak, HFV the hyperemic flow volume, and HD the hyperemic duration.

3.5. Discussion

3.5.1. pCASL labeling efficiency

Previous studies have investigated the impact of temporal variation of blood velocity on the measured perfusion in the brain (138,141,145,146). In the brain, all blood delivered through the internal carotid and vertebral arteries traverses the brain via capillary microcirculation. A simple method to experimentally measure pCASL labeling efficiency was reported by Aslan, et al (141) in which total cerebral blood flow was measured in both the internal carotid and vertebral arteries using phase contrast MRI and was compared to whole-brain averaged blood flow measured by pCASL. If all other assumptions in the perfusion model are correct, the difference between total cerebral blood flow measured by phase contrast and pCASL can be accounted for by the labeling efficiency.

The approach utilized by Aslan, et al cannot be employed in the peripheral circulation for several reasons. First, blood flow in the popliteal artery is not exclusively delivered to the calf muscles. The popliteal artery branches to supply muscles of the foot, and also delivers blood to the skin, intra-muscular fibrous tissue, bone, and other structures, thus a precise and specific measure of muscle blood flow in a large artery is difficult. Furthermore, even if a distinct measure of total muscle blood flow in the feeding artery were achieved, the PASL and pCASL sequences employed in this study provided single-slice measurements therefore do not yield total muscle blood flow.

The methodology employed herein was not directed to measure absolute labeling efficiency, although a similar approach has been used to measure labeling efficiency in a phantom experiment (144). The more pertinent question was to determine whether the labeling or control efficiency was impacted by the substantial changes in average arterial velocity between rest and reactive hyperemia in skeletal muscle. As expected, the control condition did not

significantly impact signal in the feeding artery, and control efficiency remained relatively constant throughout the paradigm. No significant change was detected in labeling efficiency during the period of hyperemia compared to the baseline and recovery periods.

The correction of the label signal intensity for T_1 recovery is a necessary step as the transit time between the labeling location and the imaging slice location differs substantially between the baseline and hyperemic states. For example, at an average blood flow velocity of approximately 4 cm/s at baseline it would take 0.5 seconds for the blood to traverse the 20 mm separation between the labeling plane and image slice location. If the blood water spins were 100% inverted at the labeling plane, this would account for ~ 26% signal recovery. However, during hyperemia, arterial velocity increases by an order of magnitude, and the blood would traverse the distance between the labeling and imaging locations in only 0.05 seconds, resulting in much less time for T_1 recovery (only about 3% signal recovery). Following correction for this effect, there is no significant difference between the calculated label efficiency during the baseline, hyperemia, and recovery states.

Experimentally derived average labeling efficiency of approximately 75% was lower than the estimated 85% labeling efficiency achieved in the brain (82), or the 94% labeling efficiency used in a previous muscle pCASL study (48). Partial-volume effects due to the low resolution of the EPI readout may have caused underestimation of the calculated labeling efficiency, however this would likely not affect the observed relative constancy of labeling efficiency between baseline and hyperemia.

The finding of relative stability of labeling efficiency is surprising, as studies in the brain have shown a significant decrease in labeling efficiency in response to a stimulus that increases arterial velocity (141). Potentially, the periods of retrograde and low velocity antegrade blood flow during diastole at baseline may not substantially contribute to the downstream delivery of blood, and therefore may not impact the overall labeling efficiency. Rather than blood water

spins traveling forward at a constant velocity of 5 cm/s, blood in the artery spurts forward at speeds approaching 40 cm/s, but only for the short systolic period. This hypothesis is supported by 4D flow measurements of blood flow in the peripheral vasculature (74), which show fast forward flow during systole, and near stagnation during diastole.

3.5.2. Perfusion quantification with pCASL and PASL

A subset of the data included in this study has been published previously. Specifically, the repeated PASL measurements were used to investigate intra-session repeatability of perfusion dynamics and to compare perfusion dynamics between healthy individuals and patients with peripheral artery disease in (134). In the present work, we sought to examine the agreement between skeletal muscle perfusion dynamics measured with PASL and pCASL. One subject was excluded from the present analysis since no hyperemic response was detected with pCASL.

In the nine subjects in whom perfusion was measured with PASL and pCASL, the quantified perfusion time course metrics were not significantly different for any muscle group. The average perfusion time course was very similar in appearance between the two PASL scans, implying that there was little difference between the successive reactive hyperemia responses, and between either PASL and pCASL scans, suggesting that the different methods for measuring perfusion may not impact the measurement precision.

Despite the differences between the employed PASL and pCASL methods in labeling method, labeling duration, post-labeling delay, and perfusion quantification model, the quantified time course metrics were not found to significantly differ between the two sequences for any muscle group. Quantified reactive hyperemia peak perfusion was in approximate agreement with prior studies using the SATIR PASL variant (34,51,142). However compared to Wu, et al's results from a CASL sequence (52), Grozinger et al's results using pCASL (48), or Lopez, et al's results using Q2TIPS PASL (25) peak perfusion in all muscles was lower in the present study. This bias could be attributed to different post-processing methods as we excluded macro-vessels in the

ROI, which would increase apparent perfusion if included. It is important to note that exactly the same muscle ROIs were used for quantification of perfusion in this study.

The present study is the first that we are aware of to directly compare skeletal muscle perfusion dynamics with PASL and pCASL sequences. It is not without limitation, though. The perfusion model used for PASL assumes that T_1 of blood and muscle tissue are equal. This is not the case at 3T, however, the difference between T_1 of muscle and blood would result in an approximate 5 mL/min/100g perfusion offset within the physiologic range of perfusion expected (142).

This study did not investigate the potential impact of the difference in arterial transit time that would occur between baseline and hyperemia. If blood flow velocity in the popliteal artery is only approximately 4-5 cm/s at baseline, and the pCASL labeling plane is 6 cm proximal to the imaging slice, it would take 1.2-1.5 seconds to travel in the large arteries to the imaging slice. Additional time would be required for the blood to perfuse through the muscle tissue, thus a longer post-labeling delay could have resulted in higher baseline perfusion. However, during hyperemia the average flow velocity peaks around 40 cm/s, corresponding to a transit time of 0.15 s. These effects may have masked a true reduction in labeling efficiency between baseline and hyperemia. A follow-up study investigating the effect of arterial transit time would provide insight on this issue. Differences in arterial transit time may be more of an issue in patients with peripheral artery disease, in which a stenosis or occlusion may be present distal to the labeling plane, proximal to the perfusion imaging slice. This would result in an apparent perfusion reduction, but would be due to the increase in arterial transit time due to impaired arterial flow.

The impact of arterial transit time is less of an issue for PASL since a flow-alternating inversion recovery variant is used. Blood only needs to travel a short distance from just outside of the imaging slice to contribute to the measured perfusion. However, for fast flow (greater than 20 cm/s in the microcirculation), there is potential that blood from outside of the coil sensitivity profile

could reduce the effective PASL labeling efficiency, which is assumed to be 100%. Although blood flow velocity in the artery exceeds 20 cm/s during hyperemia, the speed of blood flow in the arterioles and capillaries is much slower. However, this should be taken into consideration when selecting the transmit and receive coil setup.

3.6. Conclusions

The pCASL labeling efficiency was not significantly impacted by the variation between baseline and reactive hyperemia arterial velocity. Time course metrics were similar for both PASL scans, and between either of PASL scans and the pCASL acquisition. The benefit of increased temporal resolution with PASL, particularly during non-linear changes in the T_2*-based EPI time course may outweigh the theoretical benefit of the greater SNR achievable with pCASL. Overall, reactive hyperemia perfusion dynamics were in agreement whether measured with PASL or pCASL sequences.

CHAPTER 4: SIMULTANEOUS QUANTIFICATION OF MACROVASCULAR AND MICROVASCULAR BLOOD FLOW AND OXYGEN SATURATION USING *v*PIVOT

4.1. Abstract

Background: The regulation of blood flow and oxygen consumption in skeletal muscle is a dynamic, tightly controlled process. The purpose of this work is to develop and evaluate a magnetic resonance technique for simultaneous measurement of bulk blood flow, perfusion, draining vein SvO_2, and skeletal muscle T_2*.

Methods: An expanded version of the PIVOT is introduced, termed Velocity and PIVOT (*v*PIVOT). *v*PIVOT comprises a three-slice interleaved structure for the measurement of blood velocity and SvO_2 from the superior slice, perfusion from the central slice, and SvO_2 and T_2* from the inferior slice. In five subjects, vPIVOT was compared to PIVOT and a velocity-encoded dual-echo GRE, termed OxFlow, during separate ischemia-reperfusion paradigms to assess the ability of vPIVOT to accurately measure the reactive hyperemia response. Then in ten subjects, vPIVOT was applied to assess muscle blood flow and oxygen consumption during the transition to rest following dynamic exercise of the calf.

Results: No significant differences between *v*PIVOT-derived data and comparison sequences were observed. Blood flow in the large vessels and in the capillary bed was found to respond quickly to the cessation of induced ischemia, reaching its peak at 6±2 s, and 20±6 s, respectively. Following exercise, macrovascular flow response was similar, reaching its maximum 8±3 s after relaxation, however microvascular perfusion in the gastrocnemius muscle continued to rise for 101±53 s. Oxygen consumption was calculated based on either mass-normalized arterial blood

flow, or perfusion measurements, and the peak was measured as 15.2±6.7 mL O_2/min/100g or 6.0±1.9 mL O_2/min/100g, respectively.

Conclusion: Simultaneous quantification of bulk blood flow, perfusion, SvO_2, and T_2* is possible with *v*PIVOT. Together, the measurement of SvO_2 and blood flow, either perfusion or bulk flow, may be used to quantify the muscle oxygen consumption following exercise.

4.2. Introduction

As described in Chapter 1, peripheral vascular reactivity and the dynamics of muscle metabolism may be better understood by measuring the temporal relationship of blood flow and oxygen saturation in the micro- and macrovasculature. Indeed, through reactive hyperemia studies, it has been shown that patients with peripheral artery disease (PAD) exhibit alterations in recovery dynamics of perfusion (52,134), arterial blood flow (66), venous oxygen saturation (SvO_2) (66,134), and skeletal muscle T_2* (68,69). Furthermore, together the measurement of blood flow and venous oxygen saturation can provide the metabolic rate of oxygen consumption ($\dot{V}O_2$) through the Fick principle:

$$\dot{V}O_2 = C_aO_2 \cdot flow \cdot (SaO_2 - SvO_2) \quad [4.1]$$

where C_aO_2 is the oxygen carrying capacity of blood ($C_aO_2 = C_a \cdot \mathrm{Hgb}$, C_a = 1.34 mL O_2/g hemoglobin (Hgb)), flow is either muscle-mass normalized bulk arterial/venous flow or local tissue perfusion, and SaO_2 and SvO_2 represent the arterial and venous oxygen saturations, respectively. The measurement of time resolved skeletal muscle $\dot{V}O_2$ in humans remains a difficult problem.

Recently, MRI methods to investigate the regulation of skeletal muscle blood flow and oxygen consumption during exercise have been developed. Implementations have focused on either the response to a sustained isometric contraction, or to the dynamics of the transition between exercise and rest, known as the off-kinetics. Specifically, Mathewson, et al proposed a

method to simultaneously measure venous bulk flow and intravascular venous oxygen saturation through a projection phase-contrast and susceptometry-based oximetry approach (113). Resisted knee extension exercise was performed, and the oxygen consumption during the off-kinetics in the quadriceps muscles was dynamically assessed. However, the blood flow dynamics in the large arteries and draining veins may differ from the blood flow delivery to the muscle fibers via the capillary circulation.

An alternate approach measures blood flow and oxygen saturation locally at the level of the capillary bed rather than in the large vessels. Blood flow is measured through ASL-MRI (45,76) and blood oxygenation is quantified based on either empirically derived (49) or theoretical (114) relationships between the RF-reversible transverse relaxation rate (R_2') and $\%HbO_2$. Initially investigated by Zheng and colleagues, the image acquisition suffered from low temporal resolution, thus limiting the acquisition to one measurement at baseline and one during a sustained isometric contraction (115). A more recent method proposed by Buck, et al uses a faster image acquisition strategy for the measurement of R_2', providing temporal resolution of approximately 2.5 seconds. To calculate $\dot{V}O_2$ this was combined with a separate measurement of blood flow through ASL with 4-second temporal resolution (116). Thus, the investigators were able to assess the dynamic changes in oxygen consumption kinetics in the transition period between rest and exercise (on-kinetics), and between exercise and rest (off-kinetics).

However, both of the R_2'/ASL methods described in the previous paragraph required separate contractions for the blood flow or oxygenation measurements. Given the presence of variability in the physiologic response, the true temporal relationship may be slightly different between the two acquisitions. Therefore, a combined and simultaneous method would be desirable. While the work conducted by Mathewson, et al did allow for simultaneous measurement of blood flow and oxygenation the measurement was not spatially localized, and

flow may have increased in other muscles that were not specifically targeted by the exercise paradigm.

Described in chapter 2, an interleaved pulsed ASL (PASL) and multi-echo gradient recalled echo (GRE) sequence, termed Perfusion, Intravascular Venous Oxygen saturation, and T_2* (PIVOT) was introduced that allows for the simultaneous acquisition of perfusion, draining vein SvO_2, and the skeletal muscle BOLD response. However, presently no single technique is capable of also measuring arterial blood flow. Concurrent acquisition of micro- and macrovascular blood flow alongside SvO_2 and T_2* would offer a comprehensive functional assessment of the peripheral vasculature and would perhaps allow investigation of the independent contributions of macrovascular and microvascular reactivity. Furthermore, results from such an approach could be used in aggregate to calculate muscle oxygen consumption.

To address this unmet need, the development of a 3-slice interleaved PASL and velocity-encoded multi-echo GRE sequence is presented, termed Velocity and PIVOT (*v*PIVOT). We hypothesize that *v*PIVOT allows faithful and unbiased measurement of each of the individual parameters, and that through investigation of the off-kinetics of exercise *vPIVOT* will be able to quantify $\dot{V}O_2$ based either on mass-normalized flow or local tissue perfusion. Furthermore, we hypothesize that these results may allow us to address the disparity in results from prior studies. Thus, the purpose of the work described in this Chapter was to develop a technique to dynamically and simultaneously measure flow in the micro and macrovasculature, as well as oxygen saturation, and to apply the technique to measurement of the off-kinetics of exercise in human skeletal muscle.

4.3. Methods

4.3.1. Sequence overview

Simultaneous measurement of perfusion, macrovascular blood flow, SvO_2, and T_2* was achieved with a 3-slice interleaved sequence termed *v*PIVOT shown in **Figure 4.1**. As described in Chapter 2, the original PIVOT sequence comprises a dual-slice acquisition scheme in which a multi-echo GRE sequence acquires data at a downstream slice location from the perfusion slice during the PASL post-labeling delay (PLD) (142). Here, the framework of PIVOT was expanded to include an upstream velocity-encoded dual-echo GRE acquisition following the PASL EPI readout. From the upstream dual-echo GRE data, bulk blood flow in the arteries and veins is quantified through phase contrast, and similarly to the downstream slice, SvO_2 in the vein is quantified via susceptometry-based oximetry. Like in PIVOT, the non-selective (NS) inversion used for the control condition of PASL will impact all tissue within the volume of the coil sensitivity, therefore only GRE data acquired following slice-selective (SS) PASL inversion (i.e. the label condition) are used for analysis.

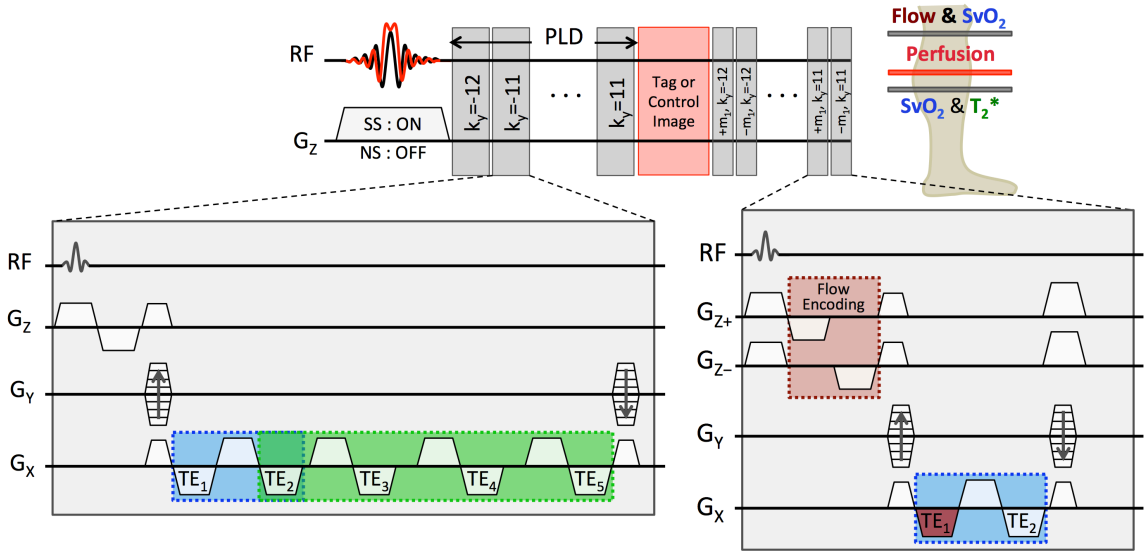

Figure 4.1. vPIVOT pulse sequence diagram. Similar to PIVOT, multi-echo GRE data are acquired downstream from the PASL slice location during the PLD. In *v*PIVOT, velocity-encoded GRE data are also acquired after perfusion EPI acquisition at a location superior to the PASL slice location. Perfusion is quantified through ASL (data used are shown in light red), SvO_2 through susceptometry-based oximetry (data used are shown in blue), blood velocity through phase contrast (data used are shown in dark red), and T_2* by fitting the magnitude signal to a mono-exponential function (data used are shown in green). Temporal resolution for all quantified parameters is 4 seconds.

To maintain high temporal resolution sampling, keyhole reconstruction (122) was used for both the superior and inferior GRE datasets, allowing reconstruction of high-resolution velocity images and field maps from the dynamically acquired data. Thus only the central quarter of k-space is acquired at each time point, and fully phase-encoded reference images with otherwise identical sequence parameters are acquired separately. The outer k-space data from the reference images are then used to fill in k-space of the dynamic data. Keyhole reconstruction requires that the reference images and dynamic data have exact anatomical correspondence (e.g. no movement between the two acquisitions). Due to the extreme motion of dynamic exercise, data cannot be reconstructed during the exercise portion, and since there may be a

difference in the physical location of the leg before and after exercise, the reference images are acquired both before and after the dynamic acquisition and used for reconstruction appropriately.

The combination of MR susceptometry and phase contrast was previously proposed for the measurement of oxidative metabolism in the brain (147,148) and was termed OxFlow. This velocity-encoded dual-echo acquisition provides flow through the phase difference between k-space data from the first echo acquired in adjacent TRs with alternating gradient first moments. The velocity-encoding gradients cause a constant phase offset between the first and second echoes, therefore taking the inter-echo difference in phase accrual removes the velocity-encoded phase. As each k-space line is encoded twice for phase contrast, those data are averaged to reduce the noise in the field map used for SvO_2 quantification.

4.3.2. Experimental protocol

*v*PIVOT-derived time course parameters were compared to independently acquired PIVOT or OxFlow data throughout ischemia-reperfusion paradigms in 5 subjects. These data allowed for the investigation of the presence of significant differences between *v*PIVOT and standard non-interleaved methods. Additionally, the functional hyperemia response following a bout of plantar flexion contractions was assessed with *v*PIVOT in ten healthy subjects. The dynamics of the macro- and microvascular flow responses were compared, and gastrocnemius $\dot{V}O_2$ was calculated.

The Institutional Review Board of the University of Pennsylvania approved all aspects of the study. A total of ten healthy subjects were recruited to participate after providing written, informed consent. All imaging was performed at 3.0 T (Siemens Magnetom Tim Trio (VB17), Siemens Medical Equipment; Erlangen, Germany) with an eight channel transmit/receive knee coil (InVivo, Inc; Gainesville, FL). Subjects were positioned supine and the maximum cross-section of the calf was centered in the knee coil. *v*PIVOT, PIVOT, and OxFlow experimental

imaging sequences were written in SequenceTree (143). Data analysis was performed with in-house-written software using MATLAB, Version 7.12.0 (MathWorks, Natick, MA), and statistical analyses were executed with JMP, Version 11 (SAS Institute., Cary, NC, 1989-2007). In applicable experiments, arterial occlusion was achieved by application of supersystolic pressure (at least 200 mmHg) via a cuff secured around the thigh inflated by a pneumatic tourniquet system (D.E. Hokanson, Inc; Bellevue, WA). Exercise was performed against a custom-built, MRI compatible plantar flexion ergometer.

Sequence parameters. PASL images were acquired with a partial Fourier GRE-EPI readout with the following parameters: FOV = 250 × 250 mm^2; acquired matrix = 80×50, reconstructed to 80 × 80; slice thickness = 1 cm; slice location = isocenter; TR/TE = 2 s/8.05 ms; PLD = 952 ms. The inferior multi-echo GRE had the following parameters: FOV = 96 × 96 mm^2; keyhole acquired matrix = 96 × 24, (for SvO_2 data analysis, reconstructed matrix = 96 × 96 using a fully sampled reference image; only dynamic data were used for T_2* analysis); slice thickness = 1 cm; slice location = 3 cm inferior from isocenter; TR/TE1/TE2/TE3/TE4/TE5 = 38.1/3.8/7.0/12.3/19.3/26.3 ms, α = 15°. The superior velocity-encoded dual-echo GRE had the following parameters: FOV = 96 × 96 mm^2; keyhole acquired matrix = 96 × 24, (for SvO_2 and velocity analyses, reconstructed matrix = 96 × 96 using a fully sampled reference image); VENC = 120 cm/s; slice thickness = 0.5 cm; slice location = 3-4 cm superior from isocenter; TR/TE1/TE2 = 20.0/6.0/9.7 ms, α = 10°. Flip angle was reduced in the superior multi-echo GRE to mitigate the potential error in perfusion due to a reduction in the starting magnetization of the blood water spins prior to NS inversion. Perfusion, bulk flow, SvO_2, and T_2* each were quantified with four-second temporal resolution.

4.3.3. Reactive hyperemia protocol

To assess whether *v*PIVOT is biased in its measurement of each parameter, *v*PIVOT-derived perfusion, SvO_2, and T_2*, or SvO_2 and flow were compared to those obtained with PIVOT

or OxFlow, respectively. In five healthy subjects (4 male, 32.4±6.4 years old), data were acquired with each of the three sequences throughout separate ischemia-reperfusion paradigms, each with 2 minutes of baseline, 3 minutes of ischemia, and 4 minutes of recovery.

Average signal intensity was determined for SS and NS EPI data at each time point in regions of interest (ROIs) in muscles of the calf including: the gastrocnemius muscle, the primary muscle activated by plantar flexion contraction; the soleus muscle, a postural muscle also involved in plantar flexion contraction; the peroneus muscles, a group of muscles that are involved in plantar flexion contraction and eversion of the foot; and the anterior compartment, comprising the tibialis anterior and extensor digitorum longus muscles, which are primarily responsible for dorsiflexion. Additionally, signal intensities in all of the ROIs were averaged together to calculate the average perfusion of the cross-section of the leg. Perfusion was quantified from the label and temporally-matched control data (see chapter 2 and 3 for details) using the model proposed by Raynaud, et al (34). As described previously (124), the perfusion offset was corrected by subtracting the average perfusion during the period of arterial occlusion from each time point. From the perfusion time courses, the time to peak perfusion and peak perfusion were determined.

The superior slice was positioned such that it intersected the tibioperoneal trunk, a short arterial segment distal to the branch point of the anterior tibial artery, before the bifurcation of the posterior tibial and peroneal arteries. Artery and vein velocities were quantified from the superiorly located multi-echo GRE data of *v*PIVOT and were compared to OxFlow-derived measures from the same slice location. Velocity was averaged over the cross-section of the artery or vein, and was multiplied by the vessel's cross-sectional area to derive flow.

Using the susceptometry-based oximetry model (58), SvO_2 was quantified for both the superiorly and inferiorly acquired GRE data in *v*PIVOT and were compared to OxFlow and PIVOT, respectively. Hematocrit was not measured in this study, but instead was assumed to be

0.45 or 0.40 for the male and female subjects, respectively. In the inferior slice, SvO_2 was quantified in the peroneal vein and results were compared to those from PIVOT. In the superior slice, positive and negative VENC acquisitions were averaged and SvO_2 was quantified in the tibioperoneal vein and results were compared to those from OxFlow. In all cases, the average baseline SvO_2 and the washout time (time to minimum SvO_2) was recorded from the dynamic time course.

From the inferior multi-echo GRE data for both *v*PIVOT and PIVOT sequences, T_2^* was quantified in a ROI in the soleus muscle by fitting the magnitude signal intensities from echoes 2-5 to a mono-exponential function. T_2^* was then normalized to the average baseline value, and the maximum relative T_2^* (T_{2max}^*) and time to peak T_2^* were determined.

4.3.4. Exercise protocol

The five subjects involved in the reactive hyperemia evaluation plus another five subjects (7 male, 31.7±5.0 years old) were scanned during a dynamic contraction protocol. *v*PIVOT data were acquired continuously throughout 2 minutes baseline, 2 minutes of resisted dynamic plantar flexion contractions, and 8 minutes recovery. Contractions were performed against the foot pedal of a custom-built, MRI-compatible ergometer. Subjects were coached to perform one full contraction and relaxation cycle every second against a pressure of 10 psi, corresponding to 6 watts.

Data analysis for each parameter was the same as for the reactive hyperemia evaluation. Of note for subjects only involved in the exercise study, vPIVOT data were acquired during a scan consisting of 2 mins baseline and 2 mins of arterial occlusion to determine the baseline perfusion offset as described above. In subjects who participated in both the ischemia and exercise protocols, the baseline offset calculated from the ischemia data were applied. In all subjects, muscle volume was quantified via manual segmentation from a 3D SSFP-echo acquisition. Muscle volume was converted to mass using the density of muscle (1.06 g/mL).

$\dot{V}O_2$ was calculated via the Fick principle (equation [4.1]) using flow measured either from perfusion ($\dot{V}O_{2,perf}$) or muscle mass-normalized arterial flow ($\dot{V}O_{2,flow}$). In both cases, SaO_2 was assumed to be 100% and thus arteriovenous oxygen difference was estimated as (1-SvO_2). Peak $\dot{V}O_2$, time to peak $\dot{V}O_2$, and net $\dot{V}O_2$ (total integrated post-exercise area) were recorded for $\dot{V}O_{2,perf}$ and $\dot{V}O_{2,flow}$.

4.3.5. Statistical analyses

Given the limited sample size, Wilcoxon signed rank tests were used to assess whether significant differences existed between *v*PIVOT-measured responses and PIVOT or OxFlow measures from the reactive hyperemia evaluation. For the exercise evaluation, Wilcoxon-signed rank tests were also used to assess whether significant differences existed between the time to peak perfusion and time to peak arterial and venous blood flow, and whether differences existed between $\dot{V}O_{2,flow}$ and $\dot{V}O_{2,perf}$ peak, time to peak, or net responses.

4.4. Results

4.4.1. Post-ischemia reactive hyperemia evaluation.

Figure 4.2 shows the time courses for the reactive hyperemia experiments from *v*PIVOT and comparison sequences. **Table 4.1** shows the results of the metrics to parameterize the time courses from each sequence. Overall, the reactive hyperemia response was not observed to be significantly different when measured with *v*PIVOT and PIVOT or OxFlow.

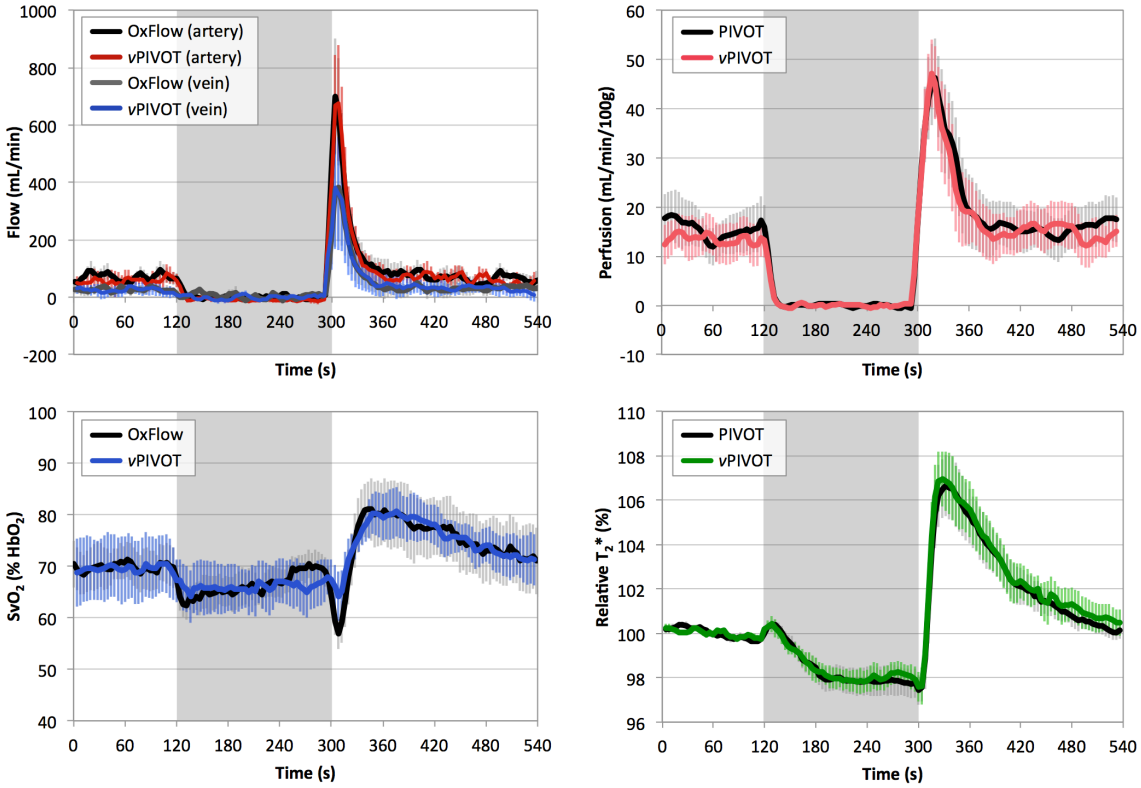

Figure 4.2. Averaged across all five subjects, *v*PIVOT reactive hyperemia data are compared to OxFlow-derived flow and SvO_2, and PIVOT-derived perfusion and T_2*. Grey box indicates period of arterial occlusion and error bars indicate standard error. A significant difference was not observed between *v*PIVOT and OxFlow or PIVOT for any of the quantified time course metrics.

Table 4.1. *v*PIVOT derived time course metrics are compared to those obtained with OxFlow or PIVOT. Significant differences between sequences were not observed for any parameter.

	OxFlow	***v*PIVOT**	**PIVOT**
Max venous flow (mL/min)	213 (21)	191 (47)	
TTP venous flow (s)	6 (3)	6 (4)	
Max arterial flow (mL/min)	513 (172)	527 (220)	
TTP arterial flow (s)	6 (3)	6 (2)	
Gastrocnemius muscle peak perfusion (mL/min/100g)		50 (13)	52 (13)
Gastrocnemius muscle TTP perfusion (s)		20 (6)	18 (9)
Soleus muscle peak perfusion (mL/min/100g)		42 (17)	44 (19)
Soleus muscle TTP perfusion (s)		14 (6)	15 (7)
Whole-leg average peak perfusion (mL/min/100g)		40 (12)	41 (12)
Whole-leg average TTP perfusion (s)		13 (7)	16 (7)
Tibioperoneal trunk baseline SvO_2 (%HbO_2)	70 (8)	70 (14)	
Tibioperoneal trunk SvO_2 washout time (s)	8 (3)	8(0)	
Posterior tibial vein baseline SvO_2 (%HbO_2)		63 (7)	65 (7)
Posterior tibial vein SvO_2 washout time (s)		16 (7)	23 (15)
Soleus muscle relative $T_2^*{}_{max}$ (%)		107 (3)	107 (3)
Soleus muscle TTP T_2^* (s)		30 (7)	30 (8)

Specifically for the arterial velocity time course results, no significant difference was detected between *v*PIVOT and OxFlow. Of note, the OxFlow sequence uses full k-space acquisition for each data point, whereas *v*PIVOT uses keyhole reconstruction for view sharing. The interleaved sequence and the keyhole reconstruction did not appear to impact the quantification of velocity or flow in the artery or the vein. Peak arterial flow was 706±442 mL/min for *v*PIVOT and 701±445 mL/min when quantified from OxFlow data. Of note, one subject had particularly high flow values, which were well represented by both vPIVOT and OxFlow. Removing the outlying subject's data, the average was 527±220 mL/min and 513±172 mL/min for *v*PIVOT and OxFlow, respectively. Time to peak arterial flow was 6±2 s or 6±3 s for *v*PIVOT or

Ox Flow, respectively (P>0.05). Phase contrast data also allows for the quantification of venous blood flow, and again a difference was not observed between *v*PIVOT and OxFlow data.

Perfusion metrics were not found to significantly differ when measured with *v*PIVOT or PIVOT. In the gastrocnemius muscle, the peak perfusion was 50±13 mL/min/100 g when measured with *v*PIVOT, and 52±13 when measured with PIVOT (P>0.05). Time to peak in the gastrocnemius muscle was 20±6 s and 18±9 s with *v*PIVOT and PIVOT, respectively. In the soleus muscle, the peak perfusion was 42±17 mL/min/100g and 44±19 mL/min/100g, and time to peak was 14±6 and 15±7 seconds when measured with *v*PIVOT and PIVOT. Again, the Wilcoxon signed rank test was not significant for differences between *v*PIVOT and PIVOT.

SvO_2 dynamics were not found to differ between *v*PIVOT and PIVOT in the inferior slice location, nor did they differ between *v*PIVOT and OxFlow in the superior slice location. In two subjects, the peroneal veins were too small, thus in the inferior slice SvO_2 could not be measured with either PIVOT or *v*PIVOT. In the remaining three subjects, washout time was 16±7 s and 23±15 s. In one subject, (different than the two mentioned previously) changes in SvO_2 were not measured using either OxFlow or vPIVOT in the superior slice. In the remaining four subjects, the washout time was 8±0 s and 8±3 s for vPIVOT and OxFlow, respectively. A difference was not observed between the baseline SvO_2 for either slice location.

The BOLD response in the soleus muscle was the most delayed in reaching its peak magnitude for both *v*PIVOT and *v*PIVOT (TTP_{T2^*} = 30±7 s or 30±8 s for *v*PIVOT or PIVOT, respectively). Relative T_2^* changes were successfully measured in each of the five subjects, and a significant difference between sequences was not detected (P>0.05). Relative $T_2^*{}_{max}$ was 107±3% in vPIVOT and 107±3% in PIVOT as well.

4.4.2. Post-exercise functional hyperemia investigation

Each subject was coached throughout the two-minute bout of exercise, and plantar flexion contractions were practiced prior to the scan. However, the precise workload of the exercise was not quantified for each subject. Although hyperemia was induced by the exercise in all subjects, two datasets were removed from the final analysis: one because the subject was incapable of maintaining the 1-second contraction rate, and the other due to substantial motion during the recovery period following exercise. The remaining eight subjects are included in subsequent analyses.

Gastrocnemius muscle volume was quantified for each subject from the SSFP-echo images, which provided contrast between muscle tissue and facial planes and blood, allowing conspicuity of muscle boundaries. Average gastrocnemius muscle mass was 349±75 g.

Table 4.2 summarizes the results from the exercise protocol, and **Figure 4.3** shows the time course of each of the measured parameters over the course of the scan. Compared to the response following induced ischemia in which the times to peak perfusion and peak arterial and venous flow were approximately equivalent, there is a substantial delay in the time to peak perfusion following exercise. In fact, both arterial flow and venous flow reached their peaks 8±3 s after cessation of exercise, while gastrocnemius muscle perfusion did not reach its maximum until 101±53 s ($p<0.005$). **Figure 4.4** shows the average perfusion response in each of muscles in the calf.

Table 4.2. Synopsis of *v*PIVOT-measured responses during the dynamic exercise protocol. * indicates presence of a significant difference between flow and perfusion responses.

	***v*PIVOT**
Max venous flow (mL/min)	463 (149)
TTP venous flow (s)	8 (3)
Max arterial flow (mL/min)	624 (223)
TTP arterial flow (s)	8 (3)
Gastrocnemius muscle peak perfusion (mL/min/100g)	88 (33)
Gastrocnemius muscle TTP perfusion (s)	101 (53)*
Peak $\dot{V}O_{2,flow}$ (mL O_2/min/100g)	15.2 (6.7)
TTP $\dot{V}O_{2,flow}$ (s)	12 (7)
Net $\dot{V}O_{2,flow}$ (mL O_2/100g)	20.6 (9.7)
Peak $\dot{V}O_{2,perf}$ (mL O_2/min/100g)	6.0 (1.9)*
TTP $\dot{V}O_{2,perf}$ (s)	102 (37)*
Net $\dot{V}O_{2,perf}$ (mL O_2/100g)	22.3 (13.5)

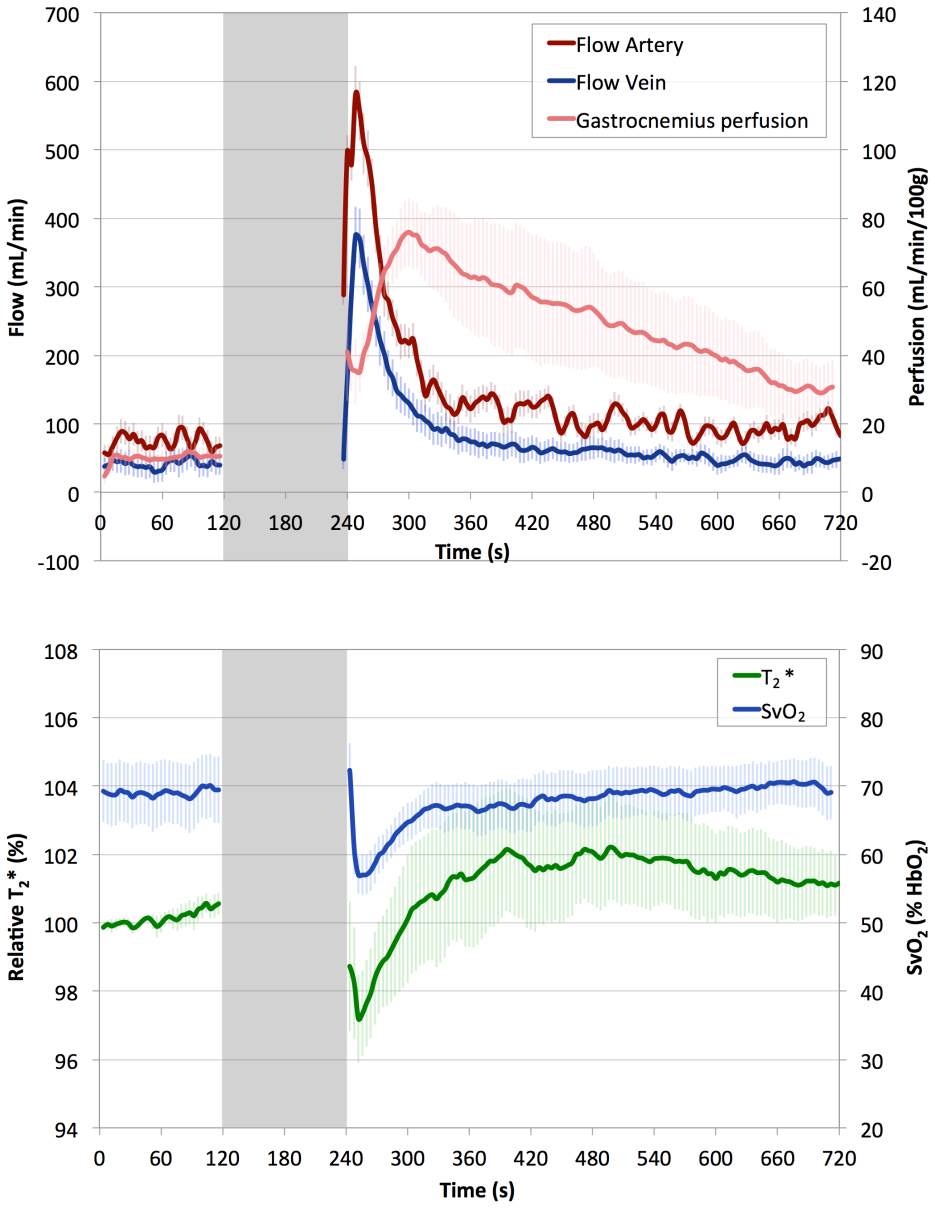

Figure 4.3. *v*PIVOT-measured responses during the dynamic exercise protocol. The quantified time courses were averaged over the eight subjects, and error bars indicate standard error. Flow peaked and recovered rather quickly, while perfusion continued to increase for more than one minute after exercise. The SvO_2 and T_2* responses both drop upon relaxation then begin to recover at a similar rate.

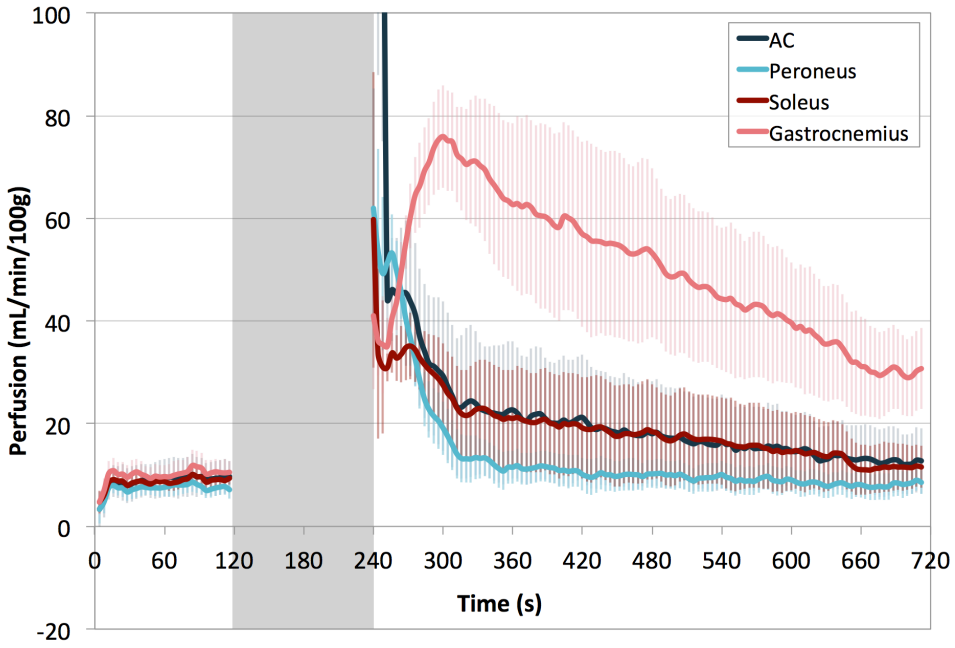

Figure 4.4. Average exercise vPIVOT-derived perfusion data is shown for individual muscles. Hyperperfusion is primarily observed in the gastrocnemius. No substantial response is detected in the soleus or peroneus muscles or in the muscles of the anterior compartment.

SvO_2 was computed for both the superior and inferior slice locations and results were averaged for use for the quantification of muscle oxygen consumption. **Figure 4.5** shows the calculated $\dot{V}O_{2,flow}$ and $\dot{V}O_{2,perf}$ responses. Similar to the relationship between macrovascular flow and perfusion, $\dot{V}O_{2,flow}$ peaks and recovers quickly, while the $\dot{V}O_{2,perf}$ response is more delayed. Peak $\dot{V}O_2$ was significantly different when measured with mass-normalized flow compared to perfusion: $\dot{V}O_{2,flow}$ was 15.2±6.7 mL O_2/min/100g while $\dot{V}O_{2,perf}$ was 6.0±1.9 mL O_2/min/100g ($p<0.005$). The time to peak was also significantly different: time to peak $\dot{V}O_{2,flow}$ was 12±7 s, and time to peak $\dot{V}O_{2,perf}$ was 102±37 s ($p<0.01$). However, the net $\dot{V}O_2$ was not observed to significantly differ. Net $\dot{V}O_{2,flow}$ was 20.6±9.7 mL/100g and net $\dot{V}O_{2,perf}$was 22.3±13.5 mL/100g ($P>0.05$).

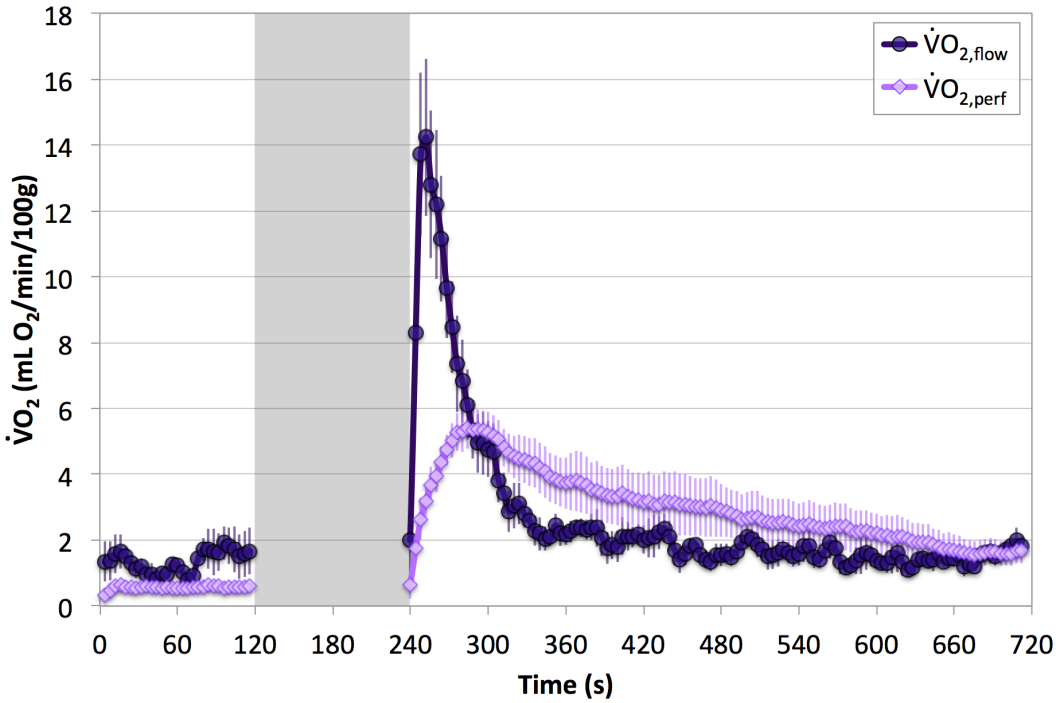

Figure 4.5. $\dot{V}O_2$ was calculated via the Fick principle using perfusion or mass-normalized average arterial flow. The average of eight subjects is shown, with error bars indicating standard error. Exercise occurred during the grey box from 2 minutes to 4 minutes. Although the peak amplitude and time to peak of the $\dot{V}O_{2,flow}$ and $\dot{V}O_{2,perf}$ are significantly different, the total integrated post-exercise response is similar.

4.5. Discussion

Overall, *v*PIVOT was capable of measuring the reactive hyperemia and functional hyperemia responses. *v*PIVOT results quantifying the reactive hyperemia response were not observed to significantly differ from those obtained by the comparison sequences, however the limited sample size exposes this conclusion to the potential of a Type II error. The dynamic measurement of the functional hyperemia response of the off-kinetics using *v*PIVOT may provide insight into the regulation of blood flow and oxygen consumption in skeletal muscle.

The ability to measure blood flow both in the large arteries and capillary bed provides a unique method for the investigation of the regulation of blood flow to skeletal muscle. Following

ischemia, no substantial delay in the perfusion response was detected in these healthy subjects. During the period of transient ischemia, the terminal arterioles are able to vasodilate both due to the accumulation of vasodilator metabolites and the reduction in intra-arterial pressure. Upon cuff release, the return of arterial blood flows to the low-resistance capillary bed resulting in an almost immediate perfusion. On the other hand, during exercise, there is still a buildup of metabolic waste products, and a demand for increased oxygen due to increased oxygen utilization. However, the capillary bed remains a high-resistance structure. Upon relaxation, the intramuscular pressure drops allowing for the increase in blood flow through the large arteries. The microvascular response, however, lags as it takes some finite amount of time for the terminal arterioles to relax due to NO-mediated vasodilation from increases in wall shear stress, as described in previous chapters. The relationship between the microvasuclar and macrovascular flow may differ in patients with primary microvascular impairment, such as diabetics.

4.5.1. Post-ischemia reactive hyperemia evaluation

In the present study, vPIVOT was compared to two sequences: OxFlow and PIVOT. PIVOT was previously evaluated compared to independent PASL and multi-echo GRE measurements during reactive hyperemia, and no bias was detected between any of these scans. OxFlow has been proposed as a method for the simultaneous quantification of blood flow and oxygen saturation and has been applied in both the brain (147-149) and in the peripheral circulation (88).

The temporal resolution of sampling for both PIVOT and OxFlow were adapted to match that of vPIVOT, and overall this resulted in a reduction of the sampling rate. PIVOT in its original implementation had a temporal resolution of 2-seconds for each measurement, compared to the 4-second temporal resolution of vPIVOT. OxFlow's temporal resolution can be varied, depending on the specific application. For example, the temporal sampling rate can exceed 2 s through the application of view-sharing techniques, useful for the measurement of dynamic events (148). Or,

full images can be acquired when assessing the baseline state, with a temporal resolution of 8-30 s (147,149). In the present study, keyhole reconstruction was used as a view-sharing technique (122), permitting high apparent spatial resolution from the dynamically acquired data. Each of the dynamic GRE acquisitions took approximately 1 second.

Of note, none of the acquired GRE data following the non-selective inversion are used in the analysis, as the inversion impacts all signal within the coil sensitivity. However, it is important to maintain identical tissue contrast between the label and control conditions for perfusion quantification, thus the GRE data are still acquired.

To evaluate the combined sequence to the standard measures, post-ischemic reactive hyperemia was selected as the functional paradigm since relatively good repeatability of the results has been reported within the same scan session (142). Furthermore, the protocol is subject-effort independent, and the response is shorter-lived than in the post-exercise active hyperemia protocol. A recent report from Lopez, et al suggests that post-ischemia reactive hyperemia is the method of choice for the measurement of vascular reactivity (25). However, $\dot{V}O_2$ was not quantified from the reactive hyperemia paradigm due to the fact that the measured temporal dynamics of oxygen saturation do not reflect the true underlying physiologic response at the level of the tissue. Rather, the response measured is the aggregate affect from the prior period of induced ischemia. This can be seen as the T_2* continues to drop throughout the period of proximal arterial occlusion, but SvO_2 remains relatively constant during this time.

In the distal peripheral circulation, SvO_2 is the most challenging of the PIVOT parameters to measure due to the size of the vessels in the calf and the potential for compression from the weight of the calf resting on the coil (134). The measurement of SvO_2 at two different slice locations may improve the chances of acquiring suitable data, especially because veins widen as they become more proximal to the heart. However, the presence of differences between SvO_2 measured at the two different slice locations will require further investigation.

The most likely error in *v*PIVOT would be a reduction in the measured perfusion. During the superior multi-echo GRE sequence, application of RF excitation pulses proximal to the PASL measurement site will result in a reduction in the magnetization of blood water spins. Because of this, the superior GRE data are acquired outside of the PASL sequence so that the label remains undisturbed. However, the OxFlow interleave will cause a reduction in the magnetization prior to non-selective (control) inversion, reducing the labeling efficiency, thus resulting in an underestimation of the measured perfusion. Furthermore, this impact will depend upon the arterial blood flow velocity, since the number of excitation pulses, and hence the degree of excitation that each spin will experience is related to the slice thickness and velocity. In *v*PIVOT, the excitation flip angle and slice thickness were reduced for the superior GRE acquisition to reduce the potential error.

It did not appear that the superiorly located excitation pulses substantially impacted the perfusion quantification, as significant differences between vPIVOT and PIVOT measures were not detected. Furthermore, reactive hyperemia results are in relative agreement with prior studies. In comparison to prior investigations, the peak perfusion in the soleus is approximately equal: 42 ± 17 mL/min/100g in the present study compared to the results from Chapter 2 where peak perfusion was found to be 37.0 ± 6.1 mL/min/100g (142). With the pseudo-continuous ASL technique described in Chapter 3, peak perfusion values of approximately the same magnitude as those presented herein were measured as well. However, all of these results are much lower than the peak perfusion in the soleus muscle of 80 ± 31 mL/min/100g reported by Wu, et al using a continuous ASL technique (47). Comparing whole-leg perfusion to another study, there is approximate agreement: 40 ± 12 mL/min/100g in the present study compared to Raynaud, et al's measurement with the same PASL sequence of 50 ± 13 mL/min/100g (34). In general, the results presented in this study are also in relative agreement with prior reports of arterial blood flow in the peripheral circulation (66,88), SvO_2 dynamics (66,75,142), and the relative response of T_2* (68,142).

4.5.2. Post-exercise functional hyperemia evaluation

In all subjects, a functional hyperemic response was stimulated from the bout of resisted plantar flexion contractions. Subjects reported that the exercise load was moderate; therefore it is assumed that muscle pH did not substantially change (although this was not measured). The average perfusion response was greatest in the gastrocnemius muscle, although some subjects also had an increase in perfusion in the soleus muscle, another muscle involved in plantar flexion contraction. The anterior compartment (involved in dorsiflexion) had almost no hyperemic response for all subjects.

The SvO_2 and T_2* time courses were not parameterized for the exercise study as they were for the reactive hyperemia evaluation. The SvO_2 washout time may have less physiologic relevance as the deoxygenated blood during the exercise period is constantly flowing out into the large draining veins though the rhythmic muscle contractions. There is, however, a slight dip in the average SvO_2 time course upon relaxation. The relative T_2* response may help to inform on the relationship between the oxygen saturation in the draining vein and that in the capillary bed. As mentioned previously, T_2* depends on blood oxygen saturation in the capillary bed as well as perfusion, vessel orientation, pH, and other factors. The only two of those factors that are expected to change in this study are oxygen saturation and perfusion. Looking at the relationship between these three parameters, it is noted that SvO_2 and T_2* both continue to rise as perfusion is beginning to drop, perhaps providing evidence that the draining vein SvO_2 response may be used as a surrogate for the capillary bed oxygen saturation for the post-exercise response. This, however, requires additional investigation.

The discrepancy between the maximum $\dot{V}O_{2,flow}$ and $\dot{V}O_{2,perf}$ is partially explained by the fact that bulk flow was normalized only to the gastrocnemius muscle mass, yet the blood flow in the tibioperoneal trunk supplies other muscles of the calf and foot in addition to other structures. Based on the perfusion measurements, the hyperemia response seems to be primarily localized

to the gastrocnemius muscle, however there is an early increase in flow in all of the muscles around the same time as the macrovascular flow peak. Another reason that $\dot{V}O_{2,flow}$ may be overestimating the true oxygen consumption is due to the presence of non-nutritive flow. Given that the macrovascular blood flow in the arteries and veins peak simultaneously, this suggests that there may be substantial non-nutritive flow shunted from the arteries to the veins upon relaxation.

It is difficult to compare these results to the prior studies mentioned in the introduction for several reasons. Each study has employed different methods, have varied in their measurement locations, and have used different exercise protocols including type of exercise and workload. Compared to Mathewson, et al's study investigating the off-kinetics in the quadriceps muscles, the measured peak $\dot{V}O_2$ was slightly lower, 9.6±1.8 mL/min/100g, however similar to this study, the response appears to have occurred immediately after cessation of exercise (113). Zheng, et al reported a $\dot{V}O_2$ of 3.8±2.5 mL/min/100g and 6.1±2.9 mL/min/100g during two separate sustained isometric plantar flexion contrations in the calf (115). Even though this result is similar to the findings of the present study, a direct comparison cannot be made between these two investigations due to the difference in exercise protocols. Finally, Buck et al's study, investigating the off-kinetics used an isometric dorsiflexion contraction for their exercise protocol but only relative changes in $\dot{V}O_2$ were quantified (116).

In addition to those explored in the present study, an advantage that *v*PIVOT provides is the potential to account for changes in vascular volume during the recovery period following exercise. As long as there is no change in vascular volume, the arterial inflow and venous outflow will match, however if there is a change in the vascular volume (e.g. vascular filling), this could result in an error when quantifying $\dot{V}O_2$. With *v*PIVOT, the arterial inflow and venous outflow are directly measured, thus the aggregate flow volumes can be quantified and could be used to adapt

the calculation of $\dot{V}O_2$. This was, however, not pursued for the present study, as the goal was to explore the fidelity and potential of *v*PIVOT.

4.5.3. Study limitations

There are several limitations to the present study. First, the sample size was limited, thus although a significant difference between vPIVOT and PIVOT or OxFlow was not detected, there is potential that a significant difference does exist, but that this study was underpowered to detect the significant difference.

Additionally, blood flow in the tibioperoneal trunk does not exclusively supply the gastrocnemius muscle. Blood supply to the soleus and peroneus muscles also stems from the tibioperoneal trunk. Both of these muscles are also involved in plantar flexion contraction, and the peroneus muscle also plays a role in eversion of the foot. In addition, the tibioperoneal trunk provides the vascular supply to some muscles of the foot, and skin, tendons, and other connective tissue of the calf and foot. Therefore, $\dot{V}O_{2,flow}$ will be overestimated since it was normalized to only the mass of the gastrocnemius muscle. So while the absolute magnitude of the response may be in error, the temporal response dynamics would not change.

Oxygen saturation was quantified in the large draining veins rather than locally in the capillary bed. As mentioned earlier in the discussion, there is potential that the relative T_2* response will allow for the investigation of this relationship, however this was not undertaken as a part of this study. The comparison between $\dot{V}O_2$ measured with either macrovascular flow or microvascular perfusion, and with either draining vein SvO_2 or R_2'-based capillary bed oxygen saturation would be of great interest.

4.6. Conclusions

In summary, the feasibility of quantification of arterial and venous bulk flow, perfusion, draining vein SvO_2, and skeletal muscle T_2* has been demonstrated in healthy volunteers. The

relationship between macro- and microvascular blood flow was explored following induced ischemia and dynamic exercise, demonstrating the disparity in primarily the microvascular response to the two paradigms. The measurement of the relationship between macro- and microvascular blood flows may be of important clinical significance in patient populations such as diabetics, or patients with peripheral artery disease. Finally, oxygen consumption was calculated based on the aggregate measures of perfusion or bulk arterial flow and draining vein SvO_2, allowing for the dynamic measurement of the muscle's metabolic response following exercise.

CHAPTER 5: MULTIPARAMETRIC ASSESSMENT OF VASCULAR FUNCTION IN PERIPHERAL ARTERY DISEASE: DYNAMIC MEASUREMENT OF SKELETAL MUSCLE PERFUSION, BLOOD-OXYGEN-LEVEL DEPENDENT SIGNAL, AND VENOUS OXYGEN SATURATION

5.1. Abstract

Background – Endothelial dysfunction present in patients with peripheral artery disease (PAD) may be better understood by measuring the temporal dynamics of blood flow and oxygen saturation during reactive hyperemia than by conventional static measurements.

Methods and Results – Perfusion, Intravascular Venous Oxygen saturation, and T_2* (PIVOT), a recently developed MRI technique, was used to measure the response to an ischemia-reperfusion paradigm in ninety-six patients with PAD of varying severity, and ten healthy controls. Perfusion, venous oxygen saturation (SvO_2), and T_2* were each quantified in the calf at two second temporal resolution, yielding a dynamic time course for each variable. Compared to healthy controls, patients had a blunted and delayed hyperemic response. Moreover, patients with lower ankle-brachial index had: 1) a more delayed reactive hyperemia response time, manifesting as an increase in time to peak perfusion in the gastrocnemius, soleus, and peroneus muscles, and in the anterior compartment; 2) an increase in the time to peak T_2* measured in the soleus muscle; and 3) a prolongation of the posterior tibial vein SvO_2 washout time. Intra- and inter-session repeatability was also assessed. Results indicated that time to peak perfusion and time to peak T_2* were the most reliable extracted time course metrics.

Conclusions – Perfusion, dynamic SvO_2, and T_2* response times following induced ischemia are highly correlated with PAD disease severity. Combined imaging of peripheral microvascular blood flow and dynamics of oxygen saturation with PIVOT may be a useful tool to investigate the pathophysiology of PAD.

5.2. Introduction

Peripheral artery disease (PAD) is most commonly a manifestation of atherosclerosis in vessels supplying the lower limbs, and causes significant morbidity and mortality in the United States (11-13,150). In PAD, atherosclerotic plaque encroaches on the peripheral artery lumen, decreasing blood flow and vascular reactivity of the large arteries (15,151). Collateral arteries vasodilate in order to meet the baseline metabolic demand of skeletal muscle; however as described in the preceding chapters, the collateral vasculature may be inadequate to quickly and adaptively accommodate increases in blood flow demand, such as those that occur during exercise (16). This effect can result in an oxygen supply-demand mismatch, causing patients to experience claudication (150).

The presence of flow-limiting stenoses can be quickly and non-invasively detected by measuring the ankle-brachial index (ABI), the ratio of systolic blood pressures in the ankle and brachial artery (150,152). An ABI of less than 0.9 confirms the diagnosis of PAD, and an ABI of less than 0.4 is suggestive of critical limb ischemia (150,153). Interventions such as cilostazol (22) or exercise rehabilitation (21) lessen claudication symptomatology, however are not necessarily associated with a clinically significant improvement in the ABI. Additionally, the ABI is not sensitive to primary microvascular impairment, endothelial dysfunction, or alterations in vascular reactivity that may coexist with the macrovascular lesions (15,154). Thus, there is a compelling need for the development of diagnostic tools that would allow for the interrogation of the contribution of vascular dysfunction to PAD.

As detailed in prior chapters, peripheral vascular function can be interrogated by monitoring the dynamics of blood flow and oxygenation in response to a stressor, analogous to cardiac stress testing. Several magnetic resonance imaging (MRI) techniques can non-invasively evaluate the dynamic changes that occur in blood flow and oxygenation during the hyperemic response. Specifically, prior studies have investigated perfusion using arterial spin labeling (ASL) (34,47,155), dynamics of SvO_2 using MR susceptometry-based oximetry (58,67), and changes in the T_2* signal (commonly known as blood-oxygen-level dependent (BOLD) response) (68,69,156), which provides a relative measure of muscle capillary bed oxygenation (62,63). In response to induced ischemia, an alteration in the response dynamics of each of these variables is associated with the presence of PAD. Compared to healthy controls, patients exhibit a blunted and delayed reperfusion (52), and a reduced rate of recovery of tissue oxygenation, as evidenced by both direct measurement of SvO_2 (66,67), and of relative changes in T_2* (68).

In Chapter 2, we developed a technique termed Perfusion, Intravascular Venous Oxygen saturation, and T_2* (PIVOT) which allows for dynamic and simultaneous quantification of perfusion, SvO_2, and skeletal muscle T_2* (142). The purpose of this work was to evaluate the hyperemic response in patients with PAD and healthy controls using PIVOT. We hypothesize that PIVOT will be able to detect PAD severity-dependent changes in macro- and microvascular function, and that the relationship between these impairments will help us to better understand the pathophysiologic processes that underlie the disease.

5.3. Methods

5.3.1. Subjects

Ninety-six patients with intermittent claudication and a diagnosis of PAD and ten healthy controls were recruited to participate in the study. Upon enrollment, each subject was classified into a disease severity group based on ABI, where healthy subjects had an ABI > 0.90 (10

subjects; 3 males), mild disease corresponded to an ABI range of 0.7 – 0.89 (28 patients; 18 males); moderate disease to an ABI range of 0.50 – 0.69 (45 patients; 28 males); and severe disease to an ABI of less than 0.50 (17 patients; 13 males). Additional characteristics of the study participants are shown in **Table 5.1**.

Table 5.1. Characteristics of study participants.

	Healthy ABI>0.9	**Mild** ABI 0.7 to 0.89	**Moderate** ABI 0.5 to 0.69	**Severe** ABI<0.5	**All patients** ABI<0.9
Total	10	28	49	19	96
Repeat visit	9	11	23	8	42
Gender (M/F)	3/7 *	18/10	29/20	15/4	62/34
Age	59.5 (3.9) *	66.8 (6.3)	69.4 (8.1)	71.3 (8.6)	69.0 (7.8)
BMI	26.2 (4.9)	27/6 (3.9)	27.4 (4.0)	27.5 (4.0)	27.5 (3.9)
Systolic BP	123 (21) *	142 (18)	141 (19)	137 (17)	141 (18)
Diabetes	0 *	10	15	6	31
Smoking status (Never/Past/ Current)	5/5/0 *	2/19/7	4/32/13	2/7/10	8/58/30

Mean (standard deviation) or counts are shown. * Indicates a significant difference between healthy subjects and all PAD patients.

5.3.2. Experimental Protocol

Prior to participation in the study, each subject provided written informed consent. The Institutional Review Board of the University of Pennsylvania approved all aspects of this study.

PAD patient protocol: Each patient reported to the testing center for two separate visits no more than one month apart. Some subjects were selected to return for a third visit, approximately three months after the second. On the first visit, screening and medical history questionnaires were completed, and the ABI was measured bilaterally using Doppler sonography according to the current standards (157). Patients were instructed to refrain from strenuous exercise for 3 days prior to the second visit, and to avoid alcohol and caffeine for 24 hours prior. Upon reporting for the second visit, patients underwent a vascular function MRI scanning session. The MRI protocol

consisted of dynamic imaging of blood flow and oxygenation of the mid-calf using PIVOT throughout an ischemia-reperfusion paradigm. If selected to return, the third visit was identical to the second.

Healthy subject protocol: Healthy subjects reported to the testing center for two identical visits, separated by 1 day to 1 week. Each MRI session included two identical PIVOT scans throughout periods of ischemia-reperfusion.

5.3.3. MRI Scan Protocol

All imaging was performed on a 3T MR imaging system (Siemens, Erlangen, Germany). For every patient, the leg with the lower ABI was scanned, and for each healthy control, the right leg was scanned. The maximum girth of the calf was centered in an 8-channel transmit-receive knee coil (In vivo, Inc. Gainesville, FL). PIVOT data were continuously collected throughout one minute of baseline, five minutes of proximal arterial occlusion, and six minutes following cuff deflation. Proximal arterial occlusion was achieved using a pneumatic tourniquet system (Hokanson, Inc., Bellevue, WA) with a cuff placed on the mid-thigh. After one minute of baseline scanning, the cuff was rapidly inflated to 75 mmHg above the measured systolic blood pressure, or 250 mmHg, whichever was lower. For all healthy subjects, the ischemia-reperfusion paradigm was repeated within the same scan session to assess intra-session repeatability.

As described previously (142), PIVOT allows for continuous, simultaneous measurement of perfusion, intravascular SvO_2, and skeletal muscle T_2* using an interleaved dual-slice pulsed ASL (PASL) and multi-echo GRE sequence. Briefly, perfusion quantification is accomplished using SATuration Inversion-Recovery (SATIR) (34), a Flow-Alternating Inversion Recovery (FAIR) ASL variant, in which slice-selective and non-selective adiabatic inversion pulses are used to achieve label and control conditions, respectively. Image acquisition follows the post-labeling delay (PLD), which is immediately followed by a slice-selective saturation pulse to reset the magnetization. In PIVOT, a keyhole (122) RF-spoiled multi-echo GRE sequence acquires data at

a slice located downstream from the PASL slice during the PLD. Only multi-echo GRE data acquired during the PLD following the slice-selective inversion are used for SvO_2 and T_2* analysis, however the multi-echo GRE interleave was run during every PLD to control for potential magnetization transfer effects. From these data, SvO_2 is derived using susceptometry-based oximetry (58,67), and T_2* is calculated by fitting the signal magnitude to a monoexponential function.

For the PASL interleave, images were acquired with the following parameters: partial-Fourier GRE-EPI readout; field of view (FOV) = 250 × 250 mm^2; acquired matrix = 80 × 50, reconstructed to 80 × 80; slice thickness = 1 cm; slice location = isocenter; TR/TE = 1 s/8.05 ms; PLD = 952 ms. For the multi-echo GRE interleave, images were acquired with: FOV = 96 × 96 mm^2; keyhole acquired matrix = 96 × 24, slice thickness = 1 cm; slice location = 3 cm distal from isocenter; $TR/TE_1/TE_2/TE_3/TE_4/TE_5$ = 38.12/3.78/6.99/12.32/19.32/26.32 ms. For SvO_2 data analysis, the acquired matrix was keyhole (122) reconstructed to 96 × 96 pixels using outer k-space data from a fully sampled reference image obtained immediately after the dynamic PIVOT acquisition; only dynamic data were used for T_2* analysis. Each variable was quantified at 2-second temporal resolution.

5.3.4. Image Analysis

Image analysis was performed using MATLAB (The MathWorks, Inc., Natick, MA). Prior to data processing, the time series of images were motion corrected with rigid-body transformations using NIH ImageJ software (developed by Wayne Rasbands, National Institutes of Health, Bethesda, MD). Perfusion was quantified in regions of interest (ROIs) in the gastrocnemius, soleus, and peroneus muscles, as well as in the anterior compartment (AC) – which includes the tibialis anterior and extensor digitorum longus muscles (**Figure 5.1a**). For the assessment of repeatability, a whole-leg ROI was used, which comprised of all four muscle groups. As described previously (142), an ROI was delineated in the muscle of interest using a

high-resolution scout image as a reference for muscle boundaries. The average signal-intensity in the defined ROI following slice-selective (M_{SS}) or non-selective (M_{NS}) inversion was determined. Using the model described by Raynaud, et al, (34) perfusion (f, in mL/min/100g) was quantified for each label-control pair as:

$$f = -\frac{\lambda}{T} \cdot \ln\left[\frac{M_{SS}-M_{NS}}{M_{SS}+M_{NS}} \cdot \left(1 - e^{T/T_1}\right) + 1\right] \qquad [5.1]$$

where λ is the tissue-partition coefficient (λ=0.9 mL/g), T is the post-labeling delay, T_1 is the longitudinal relaxation time of blood, which in this model is assumed to be equivalent to that of tissue ($T_1 = T_{1muscle}$ = 1420 ms (126) ≈ T_{1blood}). The perfusion offset was corrected by subtracting the average perfusion during the period of cuff occlusion from each time point, as perfusion is assumed to be zero during the period of proximal arterial occlusion (124). For each muscle, the peak perfusion and time to peak perfusion (TTP_{Perf}) were recorded from the dynamic time course data (**Figure 5.1c**).

Using the first two echoes of the multi-echo GRE, SvO_2 was quantified in the larger posterior tibial vein (**Figure 5.1b**). As described previously (67), SvO_2 was calculated by measuring the difference in phase accrual ($\Delta\phi$) between echoes spaced apart by ΔTE in the blood versus surrounding reference tissue as:

$$\%SvO_2 = \left[1 - \frac{2\cdot\Delta\phi/\Delta TE}{\gamma\Delta\chi_{do}\cdot Hct\cdot B_0\left(\cos^2\theta - 1/3\right)}\right]\times 100 \qquad [5.2]$$

where γ is the proton gyromagnetic ratio, $\Delta\chi_{do}$ the susceptibility difference between fully oxygenated and deoxygenated blood ($\Delta\chi_{do}$ = 4p·0.27 ppm (96,97)), Hct the hematocrit measured by venipuncture, B_0 the main magnetic field strength, and *q* the angle of the vessel with respect to B_0 (measured from axial scout images). The washout time, equal to the time between cuff release and the minimum SvO_2, and the upslope, calculated as the maximum slope during recovery, were recorded (**Figure 5.1d**).

T_2* was measured within an ROI in the soleus muscle (**Figure 5.1b**) by fitting multi-echo GRE data from echoes 2-5 to a monoexponential function. Signal intensity in the ROI was first averaged for each echo, then the data were fit to a monoexponential function and T_2* was computed at each time point. The T_2* time course data were normalized to the average baseline value, and relative $T_2^*{}_{max}$, and time to peak T_2* (TTP_{T2*}) were recorded from the time course (**Figure 5.1e**).

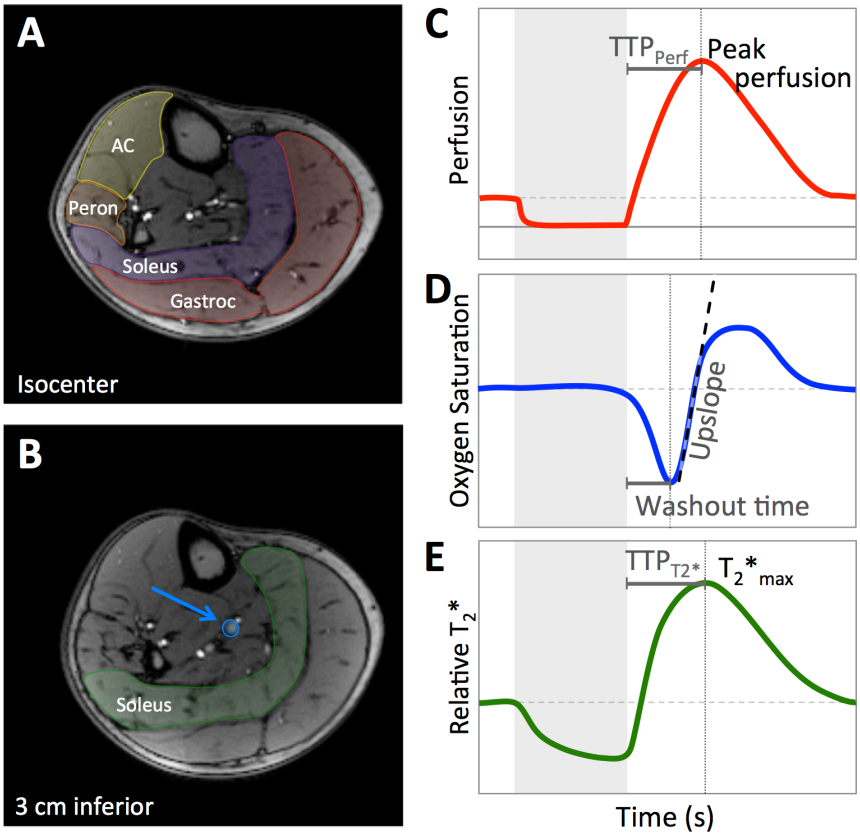

Figure 5.1. Anatomic images corresponding to PASL (**a**) and multi-echo GRE (**b**) slice locations. As shown in (**a**), perfusion is quantified in regions of interest in the gastrocnemius (red), soleus (purple), peroneus (orange), and anterior compartment (AC) (yellow). From the multi-echo GRE data, SvO_2 is quantified in the larger posterior tibial vein (blue arrow), and T_2* is calculated from a region of interest in the soleus (green) shown in (**b**). Each variable is quantified every two seconds, yielding a dynamic time course. Schematics of the perfusion (**c**), SvO_2 (**d**), and T_2* (**e**) time courses are shown, with the extracted metrics indicated. The grey box in c-e indicates the period of proximal arterial occlusion.

5.3.4. Statistical Analysis

All statistical analyses were performed with JMP software (JMP®, Version 11. SAS Institute Inc., Cary, NC). Data normality was evaluated using the Shapiro-Wilk test. For data from the normal or log-normal distribution, two-sample Student's t-tests with equal variance were used to determine whether differences existed between healthy subjects (ABI ≥ 0.9) and patients with PAD (ABI < 0.9). Non-parametric Wilcoxon rank tests were used to assess differences of non-normally distributed variables. In patients with PAD, correlations between the ABI and each time course metric and between pairs of time course metrics were calculated using Pearson's correlation coefficient (if data were normally distributed) or Spearman's rank correlation coefficient (if data were not normally distributed). Holm's adjustment for multiple comparisons was applied to all tests and correlations to maintain the family-wise error rate of 0.05. Thus, for all tests, $p_{holms} < 0.05$ was considered to be significant.

In healthy controls, intra-session and inter-session (1 day to 1 week between scans) repeatability was assessed. Inter-session repeatability was also assessed in a subset of patients with PAD (approximately 3 months between scans). In all cases, the intraclass correlation coefficients (ICC) and mean within-subject coefficients of variation (CV_W) were calculated to assess measurement repeatability.

5.4. Results

5.4.1. Subject Demographics

In six subjects, a cuff pressure of 75 mmHg above systolic blood pressure did not result in a full occlusion, likely due to calcification of the feeding arteries. Insufficient occlusion was determined based on appearance of venous pooling in the EPI images and T_2* time course. In the remaining 100 subjects, several subjects' MRI images were unanalyzable due to motion

contamination, partial volume effects, low SNR, or insufficient vein size. **Table 5.2** shows the number of patients for each variable that were of sufficient quality for analysis. Notably, for all subjects in whom a full occlusion was achieved, at least one variable was fit for analysis.

Table 5.2. Synopsis of number of subjects with analyzable images for each measured variable.

	Healthy ABI>0.9	**Mild** ABI 0.7 to 0.89	**Moderate** ABI 0.5 to 0.69	**Severe** ABI<0.5	**All patients** ABI<0.9
Total	10	27	45	18	100
Gastrocnemius Perfusion	10	26	40	15	91
Soleus Perfusion	10	26	41	14	91
Peroneus Perfusion	10	25	40	9	84
AC Perfusion	10	23	36	13	82
SvO_2	10	20	34	13	77
Relative T_2*	10	27	44	18	99

5.4.2. Visualization of MRI time courses

For visualization purposes, average time courses were generated for all healthy subjects and patients with mild, moderate, and severe PAD disease burden for perfusion in the gastrocnemius muscle (**Figure 5.2a**), posterior tibial vein SvO_2 (**Figure 5.2b**), and relative T_2* in the soleus muscle (**Figure 5.2c**). The typical ischemia-hyperemia response is seen in each variable's time course. During the period of arterial occlusion, T_2* decreases as the stagnant blood in the capillary bed becomes increasingly desaturated. After cuff release, SvO_2 initially drops as the deoxygenated blood from the capillary bed advances into the large draining veins in the measurement slice. Concurrently, perfusion increases in order to repay the oxygen debt incurred during the ischemic period. This hyperperfusion of oxygenated blood causes T_2* and SvO_2 to recover and surpass their baseline values. As blood flow and venous oxygen saturation normalize, so too does T_2*. From the average time courses a striking difference is seen between healthy subjects and patients with PAD, and furthermore, TTP_{Perf}, washout time, and TTP_{T2*} are increasingly prolonged as disease severity worsens.

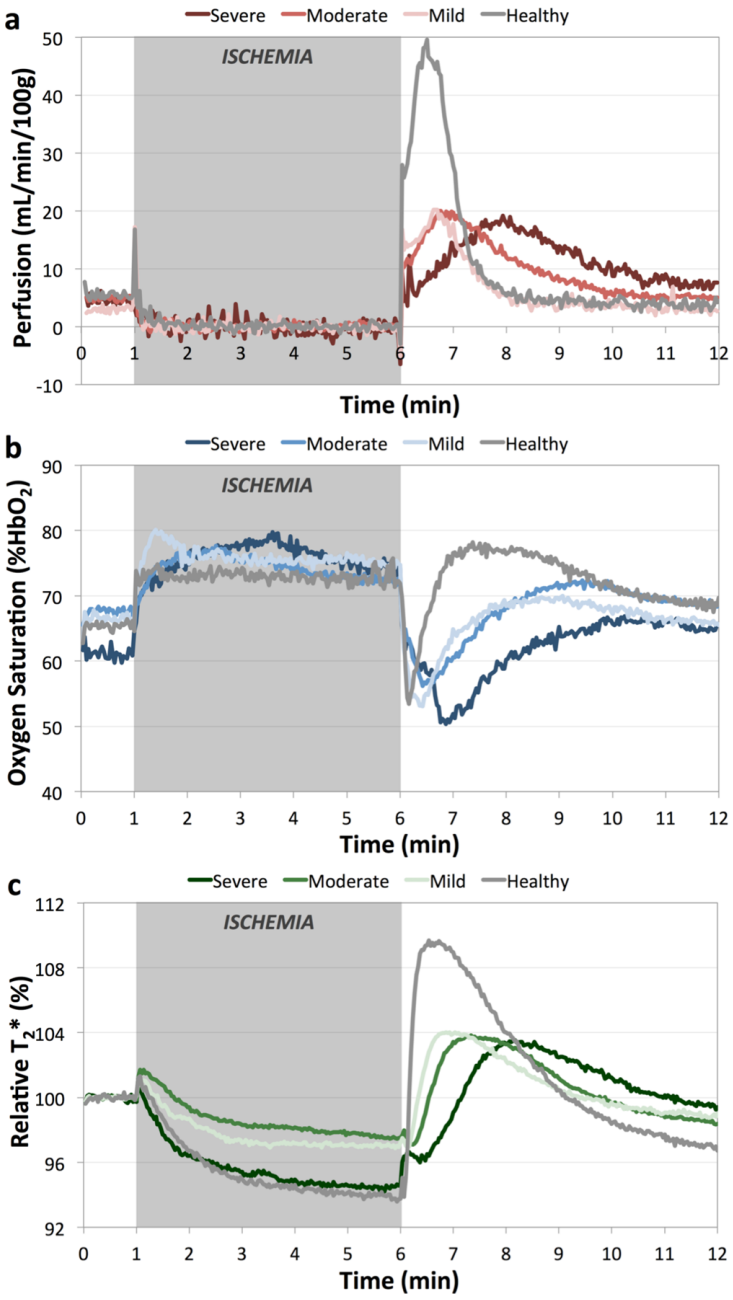

Figure 5.2. Group-average time courses for healthy subjects (grey), and patients with mild (light colored), moderate (medium colored), and severe (dark colored) PAD for gastrocnemius muscle perfusion (**a**), posterior tibial vein SvO_2 (**b**), and relative T_2* in the soleus muscle (**c**). Grey box indicates the period of proximal arterial occlusion. With increasing disease severity, there is a delay in the reactive hyperemia response evident in each variable that was measured.

5.4.3. Comparison between healthy subjects and patients with PAD

The group-wise average (standard deviation) of each time course metric for the measured variables are summarized in **Table 5.3**. TTP_{Perf} in the peroneus, T_2*_{max}, and TTP_{T2*} were not from the normal distribution, all other variables were from the log-normal distribution. Each variable, with the exception of SvO_2 upslope, was significantly different between healthy controls and patients with PAD. With the presence of PAD, there was a significant prolongation of the hyperemic response time, and a reduction in the magnitude of the hyperemic response. SvO_2 washout time increased from 11 s in healthy subjects to 39 s in PAD patients. TTP_{Perf} was delayed as well – averaged over all muscle groups it increased from 24 s to 72 s in patients with disease. Peak perfusion decreased from 52.6 mL/min/100g to 25.6 mL/min/100g with disease. TTP_{T2*} in the soleus muscle increased from 33 s to 91 s between healthy subjects and PAD patients, and relative T_2*_{max} decreased from 110% to 106%. Averaged (standard deviation) over all subjects, baseline T_2* was 19 (2) ms, and averaged across all muscle groups the perfusion offset during ischemia was 7.6 (2.7) mL/min/100g.

Table 5.3. Associations of the presence of PAD with PIVOT time course metrics.

	Healthy ABI > 0.9 (n = 10)	**Patients with PAD** ABI <0.9 (n = 90)
ABI	1.11 (0.10)	0.60 (0.14) *
Gastrocnemius Peak Perfusion (mL/min/100g)	54.0 (14.5)	28.3 (12.9) *
Gastrocnemius TTP_{Perf} (s)	29 (10)	77 (53) *
Soleus Peak Perfusion (mL/min/100g)	74.9 (33.0)	28.9 (13.9) *
Soleus TTP_{Perf} (s)	25 (13)	72 (49) *
Peroneus Peak Perfusion (mL/min/100g)	41.2 (11.3)	20.8 (12.4) *
Peroneus TTP_{Perf} (s)	24 (9)	74 (47) *
AC Peak Perfusion (mL/min/100g)	43.4 (16.0)	24.5 (14.1) †
AC TTP_{Perf} (s)	16 (5)	64 (50) *
Washout time (s)	11 (4)	39 (23) *
Upslope (%HbO_2/s)	0.91 (0.40)	0.51 (0.22)
T_2*_{max} (%)	111 (4)	106 (3) ‡
TTP_{T2*} (s)	35 (12)	91 (55) *

*p_{holms} <0.001; †p_{holms} <0.01; ‡p_{holms} <0.05;

5.4.4. Inter-variable correlations in patients with PAD

Inter-variable correlations were assessed in PAD patients only. The correlations between ABI and time course metrics reinforce some of the findings from the group-wise analysis. A significant correlation was found between the ABI and response time following cuff release (**Figure 5.3 a, c, e**). As the ABI decreases, an increase in the time to peak perfusion in all muscles (gastrocnemius r = -0.60, p_{holms}<0.0001; soleus r = -0.66, p_{holms}<0.0001; peroneus r = -0.43, p_{holms}<0.0001; TA r = -0.55, p_{holms}<0.0001), an increase in the time to peak T_2* (r = -0.55, p_{holms}<0.0001), and an increase in the washout time (r = -0.59, p_{holms}<0.0001) were observed. However, no statistically significant correlation was detected between ABI and peak perfusion (r = 0.08), SvO_2 upslope (r = 0.14), or $T_2^*{}_{max}$ (r = -0.04) (**Figure 5.3 b, d, f**).

In addition to the negative correlation between the hyperemic response time and ABI, significant positive correlations were detected between most pairs of timing metrics. For example, as TTP_{Perf} in the gastrocnemius muscle increased, so too did TTP_{Perf} in the other muscles (averaged over all muscle ROIs, r = 0.71, p_{holms}<0.0001), TTP_{T2*} in the soleus (r = 0.57; p_{holms}<0.0001), and SvO_2 washout time (r = 0.53; p_{holms}<0.0001). The single exception was the lack of a correlation between the peroneus TTP_{Perf} and SvO_2 washout time (r = 0.26). Positive correlations were also detected between peak perfusion measured in the gastrocnemius and soleus (r = 0.53; p_{holms}<0.0001) or anterior compartment (r = 0.40; p_{holms}<0.02). The other significant correlation detected was between relative $T_2^*{}_{max}$ and TTP_{Perf} in the peroneus (r=0.43; p_{holms}<0.005).

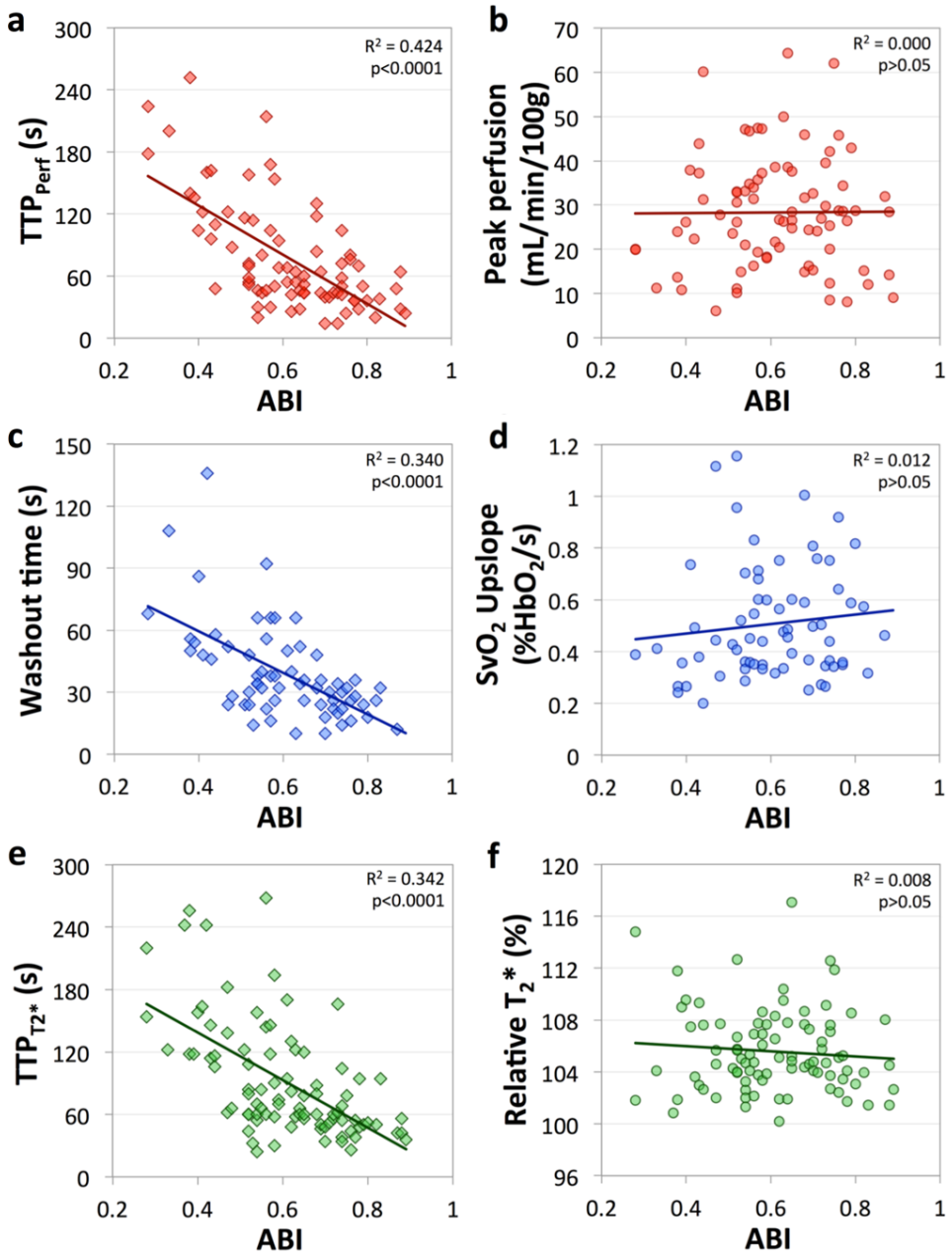

Figure 5.3. Correlation plots for ABI versus gastrocnemius muscle time to peak perfusion (**a**) and peak perfusion (**b**), SvO_2 washout time (**c**) and upslope (**d**), and time to peak T_2* (**e**) and relative T_2*_{max} (**f**) measured in the soleus. As disease severity worsens, the reactive hyperemia response time is progressively prolonged. However, no correlation was observed between the magnitude of the hyperemic response and the ABI.

5.4.5. Repeatability of reactive hyperemia response

In healthy subjects, both intra-session and inter-session repeatability were assessed (**Tables 5.4 and 5.5**). The intra-session ICC was greater than 0.7 for all measured variables, with the exception of TTP_{T2^*} (r = 0.61). One healthy subject was lost to follow-up, thus the number of healthy subjects in whom inter-session repeatability was assessed was 9. Though lower than intra-session repeatability, the inter-session repeatability in the healthy subjects was still high for peak perfusion (r = 0.84) and time to peak perfusion (r = 0.74). The ICC, however, was lower for SvO_2 upslope and washout time, $T_2{}^*_{max}$, and TTP_{T2^*}. In all cases, the mean within-subject CV in healthy subjects was less than 25%. In patients with PAD, the ICCs of the perfusion time course metrics and TTP_{T2^*} were approximately equal to or better than the ICC of the ABI measurement (r = 0.53). The ICC for the SvO_2 washout time and upslope, and $T_2{}^*_{max}$, however, was low (r < 0.35). The mean within-subject CV in patients with PAD was approximately 10% greater than in healthy subjects for all measured variables.

Table 5.4. Assessment of intrasession repeatability in healthy subjects.

	Scan A	Scan B	ICC	CV_w
Healthy subjects				
Leg Peak Perfusion (mL/min/100g)	51.5 (13.5)	51.6 (14.3)	0.95	4.1%
Leg TTP_{Perf} (s)	23 (8)	21 (7)	0.76	11.0%
Washout time (s)	11 (4)	11 (5)	0.90	8.8%
Upslope (%HbO_2/s)	0.9 (0.4)	0.9 (0.5)	0.79	18.5%
$T_2{}^*_{max}$ (%)	111 (4)	112 (4)	0.78	1.1%
TTP_{T2^*}	35 (12)	35 (11)	0.61	15.3%

TTP indicates time to peak.

Table 5.5. Assessment of intersession repeatability in healthy subjects and patients with PAD.

	Session 1	Session 2	ICC	CV_w
Healthy subjects				
Leg Peak Perfusion (mL/min/100g)	52.1 (14.2)	50.3 (17.1)	0.78	11.8%
Leg TTP_{Perf} (s)	23 (8)	21 (7)	0.71	10.9%
Washout time (s)	12 (4)	14 (9)	0.61	23.4%
Upslope (%HbO_2/s)	0.9 (0.5)	0.8 (0.4)	0.57	24.4%
$T_2{}^*_{max}$ (%)	111 (4)	110 (3)	0.58	2.0%
TTP_{T2*}	37 (12)	36 (12)	0.58	16.5%
Patients with PAD				
ABI	0.59 (0.15)	0.59 (0.17)	0.53	11.8%
Leg Peak Perfusion (mL/min/100g)	23.3 (8.9)	35.5 (9.5)	0.52	20.3%
Leg TTP_{Perf} (s)	68 (42)	72 (44)	0.78	22.0%
Washout time (s)	34 (17)	30 (16)	0.13	31.9%
Upslope (%HbO_2/s)	0.5 (0.2)	0.7 (0.4)	0.08	36.7%
$T_2{}^*_{max}$ (%)	106 (3)	106 (3)	0.33	1.9%
TTP_{T2*}	90 (49)	84 (39)	0.57	23.4%

ABI indicates ankle-brachial index; PAD, peripheral artery disease; and TTP, time to peak.

5.5. Discussion

5.5.1. Synopsis of Results

In this study, peripheral vascular function was investigated in patients with PAD and healthy controls using PIVOT, a recently developed MRI technique, allowing for simultaneous measurement of the dynamics of blood flow and oxygen saturation throughout an ischemia-reperfusion paradigm. Compared to healthy controls, PAD patients exhibited a blunted and delayed hyperemic response, as measured by perfusion, SvO_2, and T_2*. Moreover, the results showed a significant correlation between PAD disease severity and the temporal dynamics of recovery of blood flow and oxygenation following induced ischemia. With decreasing ABI, the

time required to accommodate the hyperperfusion of oxygen-rich blood to the ischemic muscle was prolonged; there was an increase in the time needed for desaturated blood to flow out of the capillary bed into the large draining veins; and a delay in the time to peak T_2*, indicating a decrease in the rate of recovery of oxygen saturation in the capillary bed. These data are thus suggestive of disease-severity-dependent impairment of vascular function in PAD.

5.5.2. Comparison to prior studies of muscle perfusion in PAD

Previous studies have used an ischemia-reperfusion model to investigate peripheral vascular function in patients with PAD compared to healthy controls, however these studies were limited to the measurement of a single variable – perfusion(52) or T_2* (68), or two variables – SvO_2 and bulk arterial blood flow (66,67). Separately measuring all of the variables in a single study would require multiple scans. However, with PIVOT, perfusion, SvO_2, and T_2* are measured simultaneously, allowing for the direct investigation of the temporal relationships between perfusion, oxygen saturation, and T_2* at no additional scan time or patient discomfort. PIVOT was previously evaluated by comparing results from PIVOT to those obtained with the traditional PASL or multi-echo GRE sequences in a cohort of young healthy subjects. No bias was detected between PIVOT and the individual measurement methods, suggesting that the simultaneous measurement of perfusion, SvO_2, and T_2* at high temporal resolution is possible with PIVOT (142).

Data in the present study show that the temporal dynamics during reactive hyperemia are associated with the presence of PAD and are tightly correlated with disease severity, thus high temporal resolution sampling of the response is extremely important. PIVOT provides 2-second temporal resolution of each of the measured variables, higher sampling rate than prior studies investigating perfusion alone (16-second temporal resolution) (47,52), or SvO_2 and bulk arterial flow (5-second temporal resolution of SvO_2) (66). Temporal resolution of 1-second was used in previous studies investigating only T_2* in skeletal muscle (68,127).

Unlike perfusion and SvO_2, the origin of the BOLD signal is less physiologically straightforward. BOLD signal depends upon blood oxygenation in the capillary bed, as well as microvascular flow, blood volume, cellular pH, and vessel diameter and orientation (63). So, while relative T_2* can be quickly acquired, and in this study was the easiest variable to measure (relative T_2* was analyzable in 99/100 subjects), the multifactorial contrast mechanism and the fact that the measured response is relative, rather than in physiologic units, makes the interpretation of the BOLD signal more complicated. To reduce potential confounds due to blood volume on the measured T_2*, care was taken to ensure that the patient's leg was at heart height, and each patient was supine for approximately 15 minutes prior to the onset of ischemia (51). Additionally, arterial occlusion was induced using a pneumatic tourniquet system capable of fully inflating in approximately 0.3 second, thus occluding venous and arterial flow nearly simultaneously.

Hyperemia can also be induced via exercise rather than induced ischemia. Exercise is more physiologically relevant to PAD, however muscles may be stressed to varying degrees, depending on which muscle group is activated (e.g. plantar flexion vs. dorsiflexion), and total work is subject-effort dependent. Conversely, tourniquet-induced ischemia is a global stimulus, more uniformly affecting all muscle groups downstream from the site of inflation, and more consistent between subjects.

A prior study by Wu, et al measured post-ischemic skeletal muscle perfusion with a continuous ASL (CASL) technique in patients with PAD and healthy controls (52). Compared to the results from this study, there is good agreement in the trend of timing of the hyperemic response and disease severity – with the presence of PAD, and with increasing disease severity, the time to peak perfusion is progressively prolonged (52). Wu, et al also found an association between the peak perfusion and disease severity (52), whereas in this study an association between peak perfusion and disease presence, but not severity was detected. CASL provides

higher signal-to-noise ratio of the perfusion signal at the cost of lower temporal resolution (16 seconds with CASL (52) compared to 2 seconds in this study). As such, relative to this study much higher peak perfusions were observed in Wu, et al's investigation for all disease severity subgroups. For instance, in the gastrocnemius muscle, peak perfusion of approximately 60 mL/min/100g was reported in patients with PAD, compared to 28.3 mL/min/100g reported in the present study. Using an invasive, but highly precise method, Lassen, et al investigated the clearance rate of radioactive xenon-133 to determine perfusion in patients and healthy controls (35). In that study, the reported peak perfusion and time to peak perfusion are in agreement with the results of the present study – 51.8 mL/min/100g versus 17.1 mL/min/100g, and 22 s versus 138 s for healthy subjects versus patients, respectively. Prior studies investigating perfusion in young healthy subjects using the same PASL variant, either SATIR alone (34,51) or using the combined PIVOT technique (142), found peak perfusion during reactive hyperemia to be similar to those values reported in the present work.

5.5.3. Comparison to prior studies of dynamic oximetry in PAD

Results of intravascular SvO_2 measured in the posterior tibial vein are in relative agreement with Langham, et al's work investigating SvO_2 in the femoral vein of PAD patients compared to young healthy subjects and age-matched healthy controls (66). As in the results of this study, Langham, et al reported a prolonged washout time in patients with PAD compared to their healthy peers. In the present study, a correlation between the ABI and washout time in the posterior tibial vein was additionally detected. Langham, et al also observed a reduction in upslope in patients compared to controls, which was not observed in this study. This deviation could be attributed to the different vessels investigated by the two studies – posterior tibial vein in this study, compared to the larger and more superior femoral vein in the work by Langham, et al A larger vein would result in higher signal-to-noise ratio of the measured SvO_2, thereby increasing measurement precision. In this study, it was necessary to acquire SvO_2 data downstream from

the perfusion measurement location so as to not disturb the magnetization of inflowing blood.

5.5.4. Comparison to prior studies of muscle BOLD in PAD

Finally, the present results are in general agreement with previous BOLD studies in the leg (68,127). The average $T_2^*_{max}$ of patients with PAD of 106% is slightly lower than the relative $T_2^*_{max}$ of 110.5% reported by Ledermann, et al (68). However, these authors normalized T_2^* to the average T_2^* value of the first 3 seconds following cuff release, whereas for the present study, T_2^* was normalized to the baseline average T_2^*. T_2^* decreases during the ischemic period, therefore normalizing the data to the post-ischemic period would increase the T_2^* range and thus increase the relative $T_2^*_{max}$. In agreement with Ledermann et al's study, the current study showed that with decreasing ABI there is an increase in TTP_{T2^*}.

5.5.5. Inter-variable correlations

The inter-variable correlations were investigated to better understand the relationship between blood flow and oxygenation in the capillary bed and large draining veins. Strong positive correlations were detected between the various timing metrics, however, no significant correlations were observed between the response time and response magnitude (e.g. peak perfusion in the gastrocnemius muscle was not significantly correlated with its time to peak perfusion).

In addition to the benefit of assessing inter-variable relationships, the acquisition of simultaneous perfusion, SvO_2, and T_2^* measurements with PIVOT increases the likelihood that at least one of the variables is of sufficient quality for analysis. For example, if a patient has a very small posterior tibial vein, the measure of SvO_2 would not be possible. However, perfusion and T_2^* data could still be used to investigate the hyperemic response. Alternatively, in some patients perfusion was very noisy due to partial-volume effects from unperfused intramuscular fibrous inclusions. Yet the T_2^* and SvO_2 data were still able to provide insight into vascular function. In

the present study, though only 71 subjects had analyzable images for all three variables, in all 100 subjects in whom a complete cuff occlusion was achieved, at least one of the variables was fit for analysis.

The dynamics of the hyperemic response are a function of upstream arterial occlusions, diffuse atherosclerosis, and endothelium-mediated vascular reactivity. Thus, the assessment of the response with several variables provides complementary, rather than independent information. The combination of results from perfusion and SvO_2 could, for example, be used to investigate the relative metabolic response. Furthermore, by modeling the combined PIVOT data, there may be added sensitivity to detect a response to a therapeutic intervention.

5.5.6. Short-term and long-term repeatability of the reactive hyperemia response

The intra-session repeatability in healthy subjects shows that the measured time course metrics have excellent precision in the short term. The hyperemic response measured for relative T_2* had a broad peak, unlike the sharp peak of the perfusion measurement (as shown in **Figure 5.2**). The TTP_{T2*} was, therefore, more sensitive to time course noise than TTP perfusion, resulting in a reduction in repeatability. This pattern was observed for both intra- and inter-session repeatability. Compared to intra-session repeatability, inter-session repeatability was slightly lower. However, it is likely that there are true differences in the reactive hyperemia response due to normal physiologic variation. Care was taken to minimize known factors that impact vascular reactivity - all subjects were instructed to refrain from caffeine intake and vigorous exercise prior to scanning, and scans were conducted at the same time of day. The measured differences are, therefore, a combination of true physiologic variation, measurement error (as is present for intra-session repeatability), and due to the potential impact of slight changes in slice location. Generally, the within-subject CV was still quite small, and similar to the reported results in a previous investigation of inter- and intra-session repeatability of PIVOT-derived time course metrics in young healthy subjects (142).

The inter-session repeatability in patients with PAD was acceptable for some variables, and poor for others (SvO_2 washout time and upslope, and $T_2^*_{max}$). Overall, the variables were similarly repeatable in healthy subjects and patients with PAD. Given that the ABI measurement differed between the two scan sessions, there may be true pathophysiologic progression or regression of disease in some patients. The ICCs of peak perfusion, TTP perfusion and TTP_{T2^*} were on the order of the ICC of the ABI measurement. The relatively low within-subject coefficient of variation suggests that although the measured response may differ between subjects, the span over which they differ is small compared to the range of values expected in healthy subjects versus patients with PAD. Time to peak perfusion and time to peak T_2^* both had relatively good repeatability, and were sensitive to disease presence and severity, making these metrics the most reliable for detection of alterations in vascular function.

5.5.5. Study limitations

There are several limitations to this study. Some variables have inter-session ICCs of <0.6, suggesting that the measurement of vascular function by PIVOT during reactive hyperemia is not suitable for clinical monitoring of a single patient. However, the present method could be well suited to investigate the response to therapy in a cohort of patients with PAD.

The moderate disease severity group was much larger than either the mild or severe disease severity groups, though this is less of a limitation when using correlations to investigate the relationship between disease severity and the MRI-measured variables. Additionally, patients recruited for this study were not restricted to either aortoiliac or femoropopliteal artery PAD. Angiographic data were not available for these patients, thus the site of obstruction is not known.

Furthermore, all correlations of the MRI data to disease severity were based on the ABI. Even though the ABI is the clinical standard for diagnosis of PAD, it is not without limitation. The ABI may be falsely elevated in patients with severely calcified arteries (158), or in situations of undiagnosed brachial or subclavian artery stenosis (14). Direct measurement of a patient's

functional capacity via exercise testing, including the 100 foot walking time or the claudication onset time and peak walking time of the Gardner protocol (159), may provide more physiologically relevant information than the measurement of the ABI alone. However, these physiologic measures are subjective, based upon an individual's pain tolerance or effort. There have been mixed results in prior studies as to whether the physiologic measures of disease severity correlate with the ABI. McDermott, et al showed that maximum treadmill walking time did correlate with the ABI (160); however, Szuba, et al found no correlation (161). Assessment of the correlation between the MRI time course metrics and physiologic testing results would be of great interest.

The variables measured indicate impaired vascular function, related to both macrovascular lesions as well as microvascular dysfunction. Additional measurement of bulk arterial blood flow during the ischemia-reperfusion paradigm would allow for assessment of temporal dynamics of blood flow in the macrovasculature and microvasculature. Comparison of the temporal dynamics in the large artery and capillary bed could help to separate the macrovascular and microvascular responses. This can be accomplished by velocity-encoding the multi-echo GRE interleave of PIVOT, though the temporal resolution of the sequence must be decreased to accommodate double the number of phase encoding segments of the multi-echo GRE (162). Additionally, the MRI data may be complemented with the measurement of hemoglobin oxygen saturation using continuous-wave near infrared spectroscopy (NIRS) (163,164).

5.6. Conclusions

In conclusion, earlier studies investigating peripheral vascular function in patients with PAD were limited to the investigation of only one or two variables. Using PIVOT, simultaneous measurement of perfusion, SvO_2, and T_2^* can be achieved. Results indicate that increasing PAD disease severity is associated with a prolongation of response time following induced ischemia.

Time to peak perfusion and time to peak T_2* were both highly repeatable measures and were sensitive to the presence and severity of PAD. In the future, PIVOT could be used as a means to monitor disease progression and evaluate treatment response in patients with PAD.

CHAPTER 6: CONCLUSIONS AND FUTURE WORK

6.1. Conclusions

The regulation of blood flow to skeletal muscle remains an active area of research, despite the fact that early work was conducted almost 100 years ago. Work progressed from the assessment of blood flow in individual capillaries through the quantitative measurement of flow and oxygenation in vivo. Applications assessing vascular reactivity and the regulation of blood flow in healthy individual enhanced the knowledge of normal physiology, and investigations in states of disease have provided insight into the consequences of endothelial dysfunction.

To that end, the work in this thesis has focused on the development, evaluation, expansion, and clinical application of an MRI method to assess vascular function in humans. In Chapter 2, the PIVOT method was introduced for the measurement of temporally-resolved perfusion, SvO_2, and T_2*. PIVOT was initially evaluated in comparison to the individual components of the sequence: a PASL interleave for the quantification of perfusion; and a multi-echo GRE sequence for the measurement of SvO_2 from the evolution of the signal phase and for the measurement of T_2* from the measured magnitude signal decay rate. In healthy subjects, PIVOT and comparison sequences were used to measure the reactive hyperemia response, and results showed that no bias existed between the combined and individual measurements. Neither the magnitude nor the timing of the reactive hyperemia response was found to significantly differ between PIVOT and the individual methods. However, the maximum post-ischemia perfusion was lower than previous reports, which led us to the pursuit of Chapter 3.

In Chapter 3, internal consistency of the reactive hyperemia perfusion response was assessed between PASL and pCASL. pCASL is a more recently developed technique that has been purported as the preferred method for investigation of perfusion in the brain. Similar to

CASL, pCASL inverts inflowing spins using flow-driven adiabatic inversion, which has not been specifically evaluated in the peripheral circulation. Given the difference in the flow waveform characteristics between the central and peripheral circulation, and given the wide range of blood flow velocities experienced in the peripheral circulation during a reactive hyperemia paradigm, this merited specific investigation. pCASL labeling efficiency was experimentally measured in the popliteal artery throughout an ischemia-reperfusion paradigm. Results suggest that despite the variation in average flow velocity throughout the paradigm, labeling efficiency may not change. Reactive hyperemia perfusion was then quantified with PASL and pCASL sequences and results were not found to significantly differ despite the differences in labeling method, perfusion quantification model, and temporal resolution.

In Chapter 4, the original PIVOT sequence was expanded to include an OxFlow interleave after the PASL acquisition. This third interleaved slice provides a proximal measure of arterial and venous bulk blood flow as well as an additional measurement of SvO_2 in a larger draining vein. The new sequence was termed *v*PIVOT and was applied to the measurement of transient changes of blood flow and oxygen saturation both in the post-ischemia reactive hyperemia and post-exercise functional hyperemia states. Reactive hyperemia results were again compared between the adapted *v*PIVOT sequence and independent measures using either PIVOT or OxFlow. The reactive hyperemia dynamics were not found to differ depending on the acquisition sequence. The measurement of *v*PIVOT during the post-exercise period of functional hyperemia allowed for the investigation of muscle oxygen consumption ($\dot{V}O_2$). With *v*PIVOT, $\dot{V}O_2$ was measured as the product of draining vein SvO_2 and either muscle mass-normalized bulk arterial blood flow or local tissue perfusion. Although the total oxygen consumption was not different between the two measures, the response dynamics including the timing of the maximum and the peak magnitude were significantly different.

Finally, in Chapter 5, we applied the original PIVOT sequence described in Chapter 2 in a

cohort of patients with PAD and healthy controls. Results, in agreement with prior independent studies of perfusion, SvO_2, and skeletal muscle T_2*, showed that compared to healthy controls, patients had a blunted and delayed hyperemic response. Furthermore, correlations between the clinical measurement of disease severity, the ABI, and the timing of the reactive hyperemia response were detected. Specifically, patients with a lower ABI had: 1) a more delayed reactive hyperemia response time, manifesting as an increase in time to peak perfusion in the gastrocnemius, soleus, and peroneus muscles, and in the anterior compartment; 2) an increase in the time to peak T_2* measured in the soleus muscle; and 3) a prolongation of the posterior tibial vein SvO_2 washout time. These results suggest that PIVOT may be a useful tool to investigate the pathophysiology of PAD and potentially response to therapy.

6.2. Future Directions

If I've learned anything in my time as a graduate student, it's that answering one question leaves you asking more. Based on the results presented in this dissertation, several issues could benefit from further investigation:

6.2.1. Technical Development

Dual acquisition for ASL and BOLD measurement: Presently in PIVOT, T_2* is quantified at the downstream slice location, generally located at the distal extent of the gastrocnemius muscle. Thus, T_2* was quantified in the soleus muscle, whose central location and larger cross-sectional area provided better data. However, as described in the introduction there have been several recent studies using a dual echo EPI acquisition to measure the combined ASL and BOLD responses: the first echo with short echo time is used for perfusion quantification, and the second echo with longer echo time is sensitive to BOLD signal changes. PIVOT could be adapted to include a dual-echo readout, which would allow the measurement of the BOLD response in all muscles of the calf and furthermore would provide direct spatial correspondence between the perfusion and BOLD data.

Improved temporal/spatial resolution of MR susceptometry-based oximetry: Given the limited time of the ASL post-labeling delay, a view sharing technique was required to allow the limited data acquired during the dynamic acquisition to be reconstructed at high enough spatial resolution. However, for keyhole acquisition and reconstruction, exact anatomic correspondence must be maintained between the dynamically acquired data and the reference image acquisitions. Cuff-induced motion notwithstanding, it can be very difficult for clinical patients to remain still for a 13 minute scan. The use of more advanced view sharing techniques would allow for more tolerance to patient motion. These include BRISK, in which a slightly smaller segment of the central portion of k-space is acquired dynamically and outer k-space is periodically acquired. Rodgers, et al employed BRISK sampling in OxFlow showed improved motion sensitivity compared to keyhole acquisition (165). Alternatively, the use of parallel imaging methods could increase the speed of acquisition, thus reducing the number of missing k-space lines.

6.2.2. Technical investigations

Comparison between T_2'-based oximetry and susceptometry-based oximetry: As discussed in Chapter 4, draining vein venous oxygen saturation is not synchronized with the tissue oxygen saturation in post-ischemia evaluations, but rather the measured washout of deoxygenated blood is the aggregate from the previous period of ischemia. This is one of the reasons why $\dot{V}O_2$ was not calculated for any of the reactive hyperemia experiments. There is no physical barrier between the capillary bed and the draining vein in exercise, and in fact the rhythmic contractions help to drive the venous flow, thus in the post-exercise functional hyperemia state, we assumed that the draining vein SvO_2 was equivalent to the local capillary bed oxygen saturation. However, given the discrepancy between the macrovascular and microvascular flow responses during the post-exercise functional hyperemic period, there may also be differences between the macro- and microvascular oxygen saturation. The combined assessment with BOLD may help to elucidate this issue, however the direct comparison to a T_2'-

based method would help to directly answer the question. This could be investigated by comparing post-exercise SvO_2 dynamics in the draining vein measured via susceptometry-based oximetry to the capillary bed oxygen saturation measured via the SAGE technique used by Buck, et al (116).

6.2.3. Additional Clinical Translation

Presently, measurement of ABI and physiologic testing via standardized treadmill walking tests are used to assess response to intervention and disease progression. ABI, however, may not change due to exercise intervention despite improvements in patient symptomatology. Therefore, the development and investigation of a non-invasive, subject effort-independent method to assess vascular function is highly desirable. In the future, reactive hyperemia response dynamics measured with PIVOT could potentially be used as a biomarker for disease progression and response to therapeutic intervention. In fact, progress is already being made toward investigating the potential of PIVOT to detect a treatment response. Building upon the study described in Chapter 5, 136 patients with PAD were scanned at baseline, randomized into either a supervised exercise rehabilitation (SER) program or standard medical care (SMC), and then returned for an identical follow-up visit after three months of intervention (**Figure 6.1**). The patients randomized to SMC continued their medical management as prescribed by their primary care physician or cardiologist, and those randomized to SER additionally met with a personal trainer and exercised three times per week for a period of approximately three months.

The baseline and follow-up visits both consisted of a physiologic testing session as well as a reactive hyperemia MRI scan. Physiologic testing involved a treadmill-walking test using the Gardner protocol, which requires patients to walk on a treadmill at 2 mph initially with 0% incline and the incline is increased by 2% every 2 minutes. Patients indicate to study coordinators when they first experience pain (claudication onset time, COT), and when the pain limits their ability to

walk (peak walking time, PWT). For the reactive hyperemia scan, PIVOT was used to investigate the vascular function as described in Chapters 2 and 5.

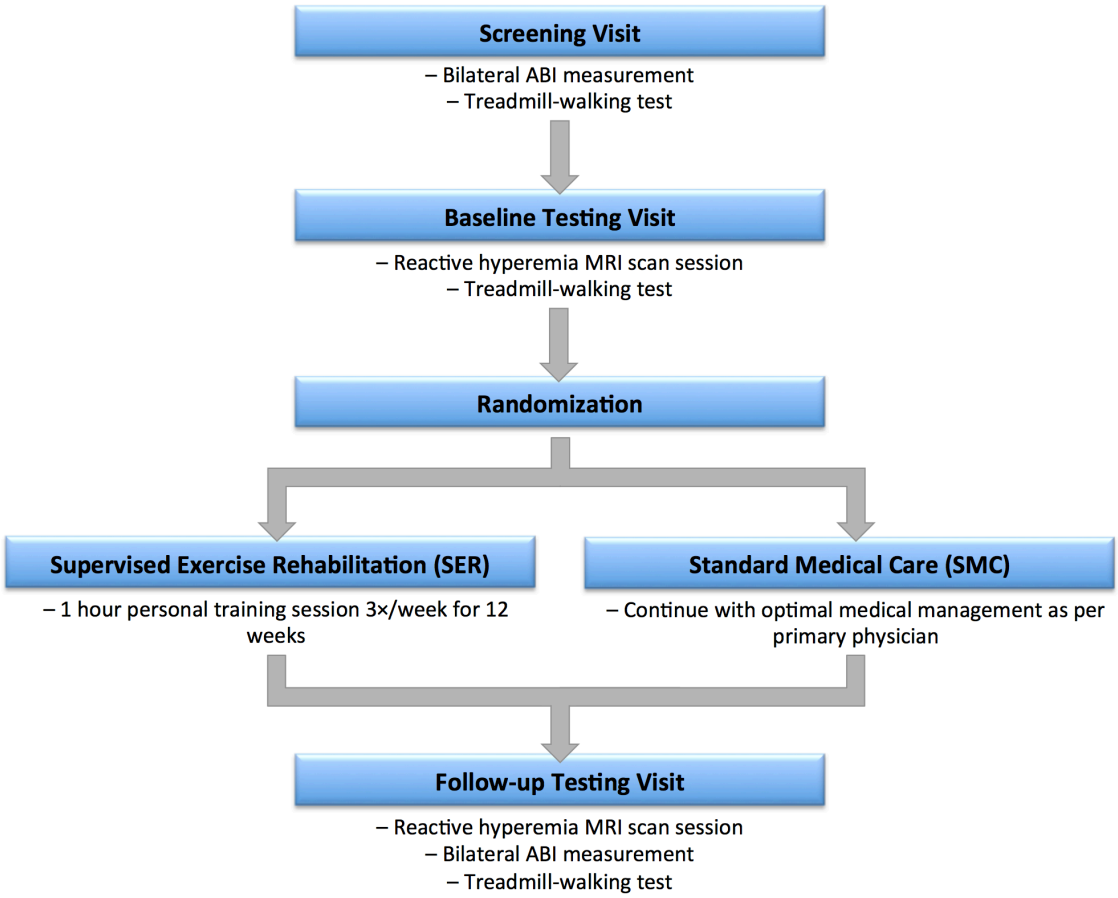

Figure 6.1. Study design for patients recruited to participate. Following screening and baseline testing visits, each patient was randomized into either supervised exercise rehabilitation or standard medical care. All patients returned for a follow-up testing visit approximately 3-4 months after his or her baseline testing visit.

112/136 patients returned for their follow-up visit 119±28 days after the baseline visit (19 lost to follow-up, 5 presently enrolled). From the initial testing visit, significant correlations were

detected between ABI and reactive hyperemia response time across all patients, however no correlation was observed between ABI and reactive hyperemia response magnitude or between ABI and indices of functional disease impairment measured by treadmill-walking test (**Figure 6.2**). From baseline to follow-up, COT and PWT significantly increased in the SER group (paired *t*-test, $p<0.0001$ for both). COT significantly increased in the SMC group as well (paired t-test, $p<0.01$). From the MRI data, no significant differences were detected between the SER and SMC groups at baseline or follow-up for any metric. In the SER group, the change in peak perfusion between baseline and follow-up significantly increased in the peroneus ($p<0.05$) and when averaged across the whole leg ($p<0.05$) (**Figure 6.3**).

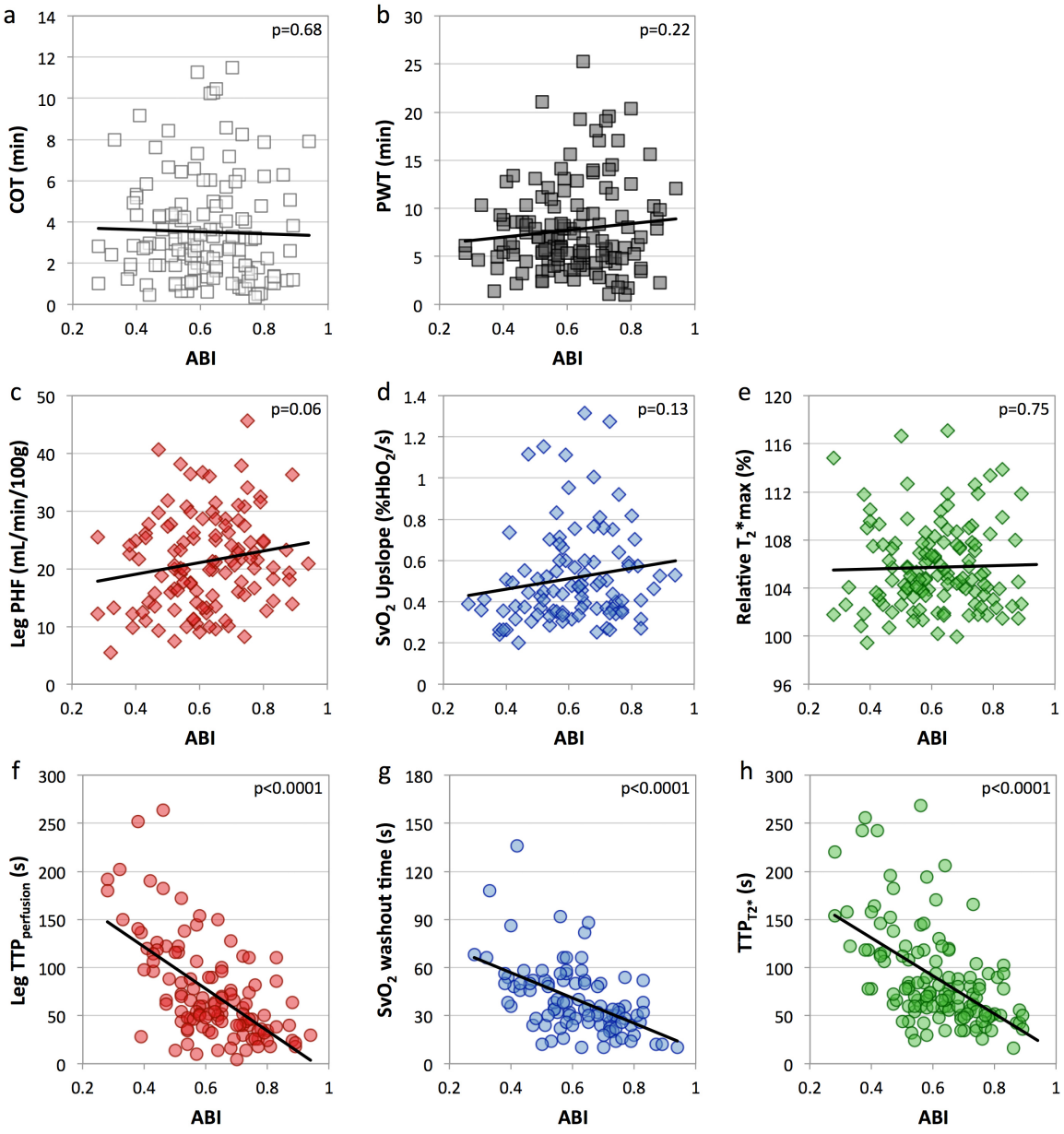

Figure 6.2. Correlation plots between treadmill-walking test and disease severity as assessed by ABI (a-b) and MRI-measured reactive hyperemia response metrics and ABI (c-h). Significant correlations exist between ABI and reactive hyperemia response time (e.g. time to peak perfusion, SvO_2 washout time, and time to peak T_2*).

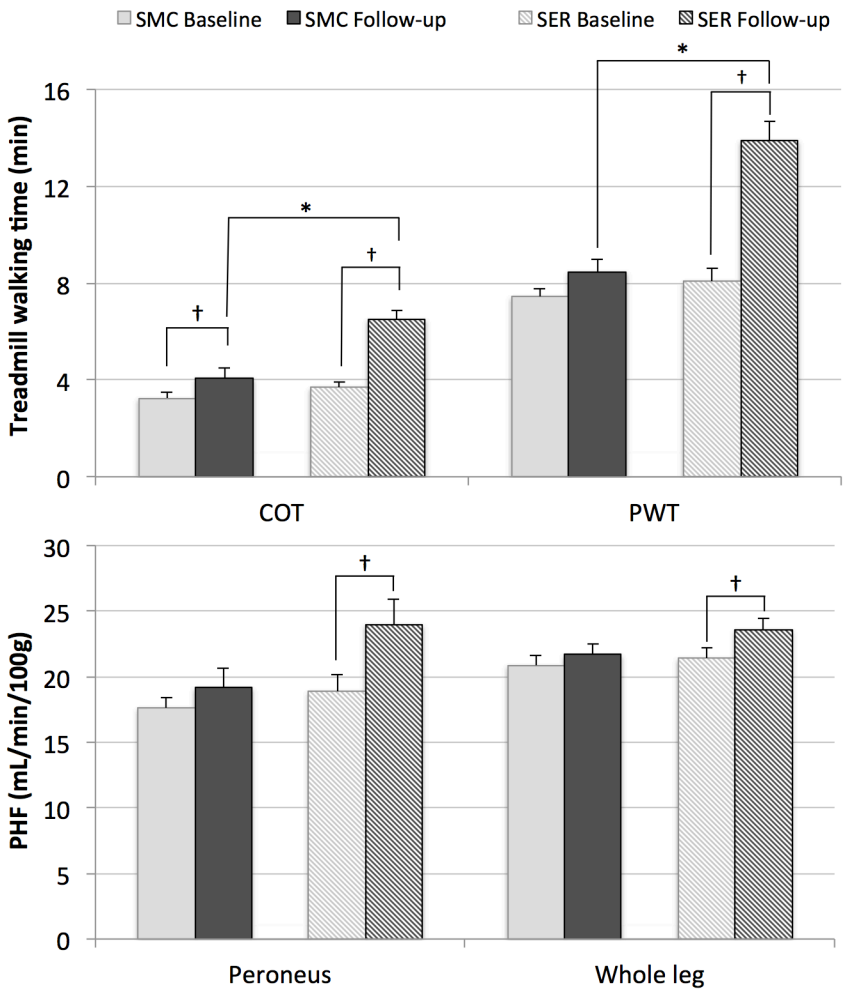

Figure 6.3. Average measurements at baseline and follow-up for SMC (solid) and SER (striped). Error bars represent standard error. * indicates significant difference between SMC and SER groups (unpaired *t*-test), † significant within-group difference between baseline and follow-up (paired *t*-test). All of the significant differences observed are displayed.

This preliminary analysis showed that patients enrolled in a supervised exercise intervention had a significant increase in peak perfusion in the peroneus and across the entire cross-section of the leg. This response may be attributed to increased angiogenesis induced by exercise, however additional studies are needed to investigate that hypothesis. Moreover, since

the reactive hyperemia response time is highly correlated with ABI as seen in **Figure 6.2** (which is primarily a marker of macrovascular disease), it may make sense that changes in response time are not observed since the stenoses, which are responsible for reducing the ABI, are relatively fixed. Future analyses will explore whether changes in the MRI-measures of vascular function are correlated with changes in physiologic response as measured by the treadmill-walking tests, blood markers of angiogenesis, and patient quality of life questionnaires.

BIBLIOGRAPHY

1. Freitas RA. *Nanomedicine*. Austin, Landes Bioscience, 1999.

2. Furchgott RF, Zawadzki JV. The obligatory role of endothelial cells in the relaxation of arterial smooth muscle by acetylcholine. Nature 1980;288:373–376.

3. Luscher TF, Barton M. Biology of the endothelium. Clin Cardiol 1997;20:3–10.

4. Blausen.com. Blausen gallery 2014. Wiver J Med 2014. doi: 10.15347/wjm/2014.010.

5. Palmer RMJ, Ferrige AG, Moncada S. Nitric oxide release accounts for the biological activity of endothelium-derived relaxing factor. Nature 1987;327:524–526. doi: 10.1038/327524a0.

6. Deanfield JE, Halcox JP, Rabelink TJ. Endothelial function and dysfunction: testing and clinical relevance. Circulation 2007;115:1285–1295. doi: 10.1161/CIRCULATIONAHA.106.652859.

7. Davignon J, Ganz P. Role of endothelial dysfunction in atherosclerosis. Circulation 2004;109:III27–32. doi: 10.1161/01.CIR.0000131515.03336.f8.

8. Yamauchi T, Ohnaka K, Takayanagi R, Umeda F, Nawata H. Enhanced Secretion of Endothelin-1 by Elevated Glucose-Levels From Cultured Bovine Aortic Endothelial-Cells. FEBS Lett. 1990;267:16–18.

9. Harrison DG, Freiman PC, Armstrong ML, Marcus ML, Heistad DD. Alterations of Vascular Reactivity in Atherosclerosis. Circulation Research 1987;61:74–80.

10. Zeiher AM, Drexler H, Saurbier B, Just H. Endothelium-Mediated Coronary Blood-Flow Modulation in Humans - Effects of Age, Atherosclerosis, Hypercholesterolemia, and Hypertension. J. Clin. Invest. 1993;92:652–662. doi: 10.1172/JCI116634.

11. Criqui MH, Fronek A, Barrett-Connor E, Klauber MR, Gabriel S, Goodman D. The prevalence of peripheral arterial disease in a defined population. Circulation 1985;71:510–515. doi: 10.1161/01.CIR.71.3.510.

12. Meijer WT, Hoes AW, Rutgers D, Bots ML, Hofman A, Grobbee DE. Peripheral arterial disease in the elderly: The Rotterdam study. Atheroscler Thromb Vasc Biol 1998;18:185–192. doi: 10.1161/01.ATV.18.2.185.

13. Hirsch AT, Criqui MH, Treat-Jacobson D, et al. Peripheral arterial disease detection, awareness, and treatment in primary care. JAMA 2001;286:1317–1324. doi: 10.1001/jama.286.11.1317.

14. Mohler ER III. Peripheral arterial disease: Identification and implications. Arch Intern Med 2003;163:2306–2314. doi: 10.1001/archinte.163.19.2306.

15. Faxon DP, Fuster V, Libby P, et al. Atherosclerotic vascular disease conference: Writing Group III: Pathophysiology. Circulation 2004;109:2617–2625. doi: 10.1161/01.CIR.0000128520.37674.EF.

16. Weitz JI, Byrne J, Clagett GP, Farkouh ME, Porter JM, Sackett DL, Strandness DE, Taylor LM. Diagnosis and treatment of chronic arterial insufficiency of the lower extremities: a critical review. Circulation 1996;94:3026–3049.

17. Rose GA. The diagnosis of ischaemic heart pain and intermittent claudication in field surveys. Bull. World Health Organ. 1962;27:645–658. doi: 10.2471/blt.05.029181.

18. Kannel WB, Skinner JJ, Schwartz MJ, Shurtleff D. Intermittent claudication: Incidence in the Framingham Study. Circulation 1970;41:875–883.

19. Peripheral artery disease. NHLBI

20. Boger RH, Bode-Boger SM, Thiele W, Junker W, Alexander K, Frolich JC. Biochemical evidence for impaired nitric oxide synthesis in patients with peripheral arterial occlusive disease. Circulation 1997;95:2068–2074. doi: 10.1161/01.CIR.95.8.2068.

21. Murphy TP, Cutlip DE, Regensteiner JG, et al. Supervised exercise versus primary stenting for claudication resulting from aortoiliac peripheral artery disease: six-month outcomes from the claudication: exercise versus endoluminal revascularization (CLEVER) study. Circulation 2012;125:130–139. doi: 10.1161/CIRCULATIONAHA.111.075770.

22. Mohler ER III, Beebe HG, Salles-Cuhna S, Zimet R, Zhang P, Heckman J, Forbes WP. Effects of cilostazol on resting ankle pressures and exercise-induced ischemia in patients with intermittent claudication. Vasc Med 2001;6:151–156. doi: 10.1177/1358836X0100600305.

23. Widlansky ME, Gokce N, Keaney JF Jr, Vita JA. The clinical implications of endothelial dysfunction. JACC 2003;42:1149–1160. doi: 10.1016/S0735-1097(03)00994-X.

24. Flammer AJ, Anderson T, Celermajer DS, et al. The assessment of endothelial function: From research into clinical practice. Circulation 2012;126:753–767. doi: 10.1161/CIRCULATIONAHA.112.093245.

25. Lopez D, Pollak AW, Meyer CH, et al. Arterial spin labeling perfusion cardiovascular magnetic resonance of the calf in peripheral arterial disease: cuff occlusion hyperemia vs exercise. Journal of Cardiovascular Magnetic Resonance 2015;17:23. doi: 10.1186/s12968-015-0128-y.

26. Krogh A. The supply of oxygen to the tissues and the regulation of the capillary circulation. The Journal of Physiology 1919;52:457–474. doi:

10.1113/jphysiol.1919.sp001844.

27. Krogh A. The number and distribution of capillaries in muscles with calculations of the oxygen pressure head necessary for supplying the tissue. The Journal of Physiology 1919;52:409–415. doi: 10.1111/(ISSN)1469-7793.

28. Burton KS, Johnson PC. Reactive hyperemia in individual capillaries of skeletal muscle. Am. J. Physiol. 1972;223:517–524. doi: 10.1161/01.res.31.6.953.

29. Klitzman B, Damon DN, Gorczynski RJ, Duling BR. Augmented tissue oxygen supply during striated muscle contraction in the hamster. Relative contributions of capillary recruitment, functional dilation, and reduced tissue PO2. Circulation Research 1982;51:711–721.

30. Delashaw JB, Duling BR. A study of the functional elements regulating capillary perfusion in striated muscle. Microvascular Research 1988;36:162–171.

31. Berg BR, Cohen KD, Sarelius IH. Direct coupling between blood flow and metabolism at the capillary level in striated muscle. Am. J. Physiol. 1997;272:H2693–700.

32. Fry BC, Roy TK, Secomb TW. Capillary recruitment in a theoretical model for blood flow regulation in heterogeneous microvessel networks. Physiol Rep 2013;1:1–13. doi: 10.1002/phy2.50.

33. Hewlett AW, van Zwaluwenburg JG. Method for estimating the blood flow in the arm. Arch Intern Med 1909;III:254–256. doi: 10.1001/archinte.1909.00050140084007.

34. Raynaud JS, Duteil S, Vaughan JT, Hennel F, Wary C, Leroy-Willig A, Carlier PG. Determination of skeletal muscle perfusion using arterial spin labeling NMRI: validation by comparison with venous occlusion plethysmography. Magn. Reson. Med. 2001;46:305–311. doi: 10.1002/mrm.1192.

35. Lassen NA, Lindbjerg J, Munck O. Measurement of blood-flow through skeletal muscle by intramuscular injection of Xenon-133. Lancet 1964;1:686–689.

36. Brevetti G, Silvestro A, Schiano V, Chiariello M. Endothelial dysfunction and cardiovascular risk prediction in peripheral arterial disease: additive value of flow-mediated dilation to ankle-brachial pressure index. Circulation 2003;108:2093–2098. doi: 10.1161/01.CIR.0000095273.92468.D9.

37. Kety SS, Schmidt CF. The nitrous oxide method for the quantitative determination of cerebral blood flow in man: Theory, procedure and normal values. J. Clin. Invest. 1948;27:476–483. doi: 10.1172/JCI101994.

38. Burchert W, Schellong S, van den Hoff J, Meyer G-J, Alexander K, Hundeshagen H. Oxygen-15-water PET assessment of muscular blood flow in peripheral vascular

disease. J Nuc Med 1997;38:93–98.

39. Scremin OU, Cuevas-Trisan RL, Scremin AME, Brown CV, Mandelkern MA. Functional electrical stimulation effect on skeletal muscle blood flow measured with H 2 15 O positron emission tomography. Arch Phys Med Rehabil 1998;79:641–646. doi: 10.1016/S0003-9993(98)90037-5.

40. Scremin OU, Figoni SF, Norman K, Scremin AME, Kunkel CF, Opava-Rutter D, Schmitter ED, Bert A, Mandelkern M. Preamputation Evaluation of Lower-Limb Skeletal Muscle Perfusion with H2 15O Positron Emission Tomography. American Journal of Physical Medicine & Rehabilitation 2010;89:473–486. doi: 10.1097/PHM.0b013e3181d89b08.

41. Selberg O, Müller MJ, van den Hoff J, Burchert W. Use of positron emission tomography for the assessment of skeletal muscle glucose metabolism. Nutrition 2002;18:323–328.

42. Schmidt MA, Chakrabarti A, Shamim-Uzzaman Q, Kaciroti N, Koeppe RA, Rajagopalan S. Calf flow reserve with H(2)(15)O PET as a quantifiable index of lower extremity flow. J Nuc Med 2003;44:915–919.

43. Yu G, Durduran T, Lech G, Zhou C, Chance B, Mohler ER III, Yodh AG. Time-dependent blood flow and oxygenation in human skeletal muscles measured with noninvasive near-infrared diffuse optical spectroscopies. J. Biomed. Opt. 2005;10:024027. doi: 10.1117/1.1884603.

44. Yu G, Floyd TF, Durduran T, Zhou C, Wang DJ, Detre JA, Yodh AG. Validation of diffuse correlation spectroscopy for muscle blood flow with concurrent arterial spin labeled perfusion MRI. Opt. Express [Internet] 2007;15:1064–1075. doi: 10.1364/oe.15.001064.

45. Detre JA, Leigh JS, Williams DS, Koretsky AP. Perfusion imaging. Magn. Reson. Med. 1992;23:37–45. doi: 10.1002/mrm.1910230106.

46. Toussaint J-F, Kwong KK, M'Kparu F, Weisskoff RM, LaRaia PJ, Kantor HL. Perfusion changes in human skeletal muscle during reactive hyperemia measured by echo-planar imaging. Magn. Reson. Med. 1996;35:62–69.

47. Wu W-C, Wang DJ, Detre JA, Wehrli FW, Mohler E, Ratcliffe SJ, Floyd TF. Hyperemic flow heterogeneity within the calf, foot, and forearm measured with continuous arterial spin labeling MRI. AJP: Heart and Circulatory Physiology 2008;294:H2129–H2136. doi: 10.1152/ajpheart.01399.2007.

48. Grözinger G, Pohmann R, Schick F, Grosse U, Syha R, Brechtel K, Rittig K, Martirosian P. Perfusion measurements of the calf in patients with peripheral arterial occlusive disease before and after percutaneous transluminal angioplasty using Mr arterial spin labeling. J. Magn. Reson. Imaging 2013;40:980–987. doi:

10.1002/jmri.24463.

49. Elder CP, Cook RN, Chance MA, Copenhaver EA, Damon BM. Image-based calculation of perfusion and oxyhemoglobin saturation in skeletal muscle during submaximal isometric contractions. Magn. Reson. Med. 2010;64:852–861. doi: 10.1002/mrm.22475.

50. Decorte N, Buehler T, Caldas de Almeida Araujo E, Vignaud A, Carlier PG. Noninvasive Estimation of Oxygen Consumption in Human Calf Muscle through Combined NMR Measurements of ASL Perfusion and T2 Oxymetry. J Vasc Res 2014;51:360–368. doi: 10.1159/000368194.

51. Duteil S, Wary C, Raynaud JS, Lebon V, Lesage D, Leroy-Willig A, Carlier PG. Influence of vascular filling and perfusion on BOLD contrast during reactive hyperemia in human skeletal muscle. Magn. Reson. Med. 2006;55:450–454. doi: 10.1002/mrm.20760.

52. Wu W-C, Mohler E, Ratcliffe SJ, Wehrli FW, Detre JA, Floyd TF. Skeletal muscle microvascular flow in progressive peripheral artery disease: Assessment with continuous arterial spin-labeling perfusion magnetic resonance imaging. JACC 2009;53:2372–2377. doi: 10.1016/j.jacc.2009.03.033.

53. Moran PR. A flow velocity zeugmatographic interlace for NMR imaging in humans. Magnetic Resonance Imaging 1982;1:197–203. doi: 10.1016/0730-725X(82)90170-9.

54. Bryant DJ, Payne JA, Firmin DN, Longmore DB. Measurement of flow with NMR imaging using a gradient pulse and phase difference technique. J Comput Assist Tomogr 1984;8:588–593. doi: 10.1097/00004728-198408000-00002.

55. Moran PR, Moran RA, Karstaedt N. Verification and Evaluation of Internal Flow and Motion - True Magnetic-Resonance Imaging by the Phase Gradient Modulation Method. Radiology 1985;154:433–441. doi: 10.1148/radiology.154.2.3966130.

56. Thompson RB, McVeigh ER. Real-time volumetric flow measurements with complex-difference MRI. Magn. Reson. Med. 2003;50:1248–1255. doi: 10.1002/mrm.10637.

57. Langham MC, Jain V, Magland JF, Wehrli FW. Time-resolved absolute velocity quantification with projections. Magn. Reson. Med. 2010;64:1599–1606. doi: 10.1002/mrm.22559.

58. Fernández-Seara MA, Techawiboonwong A, Detre JA, Wehrli FW. MR susceptometry for measuring global brain oxygen extraction. Magn. Reson. Med. 2006;55:967–973. doi: 10.1002/mrm.20892.

59. Langham MC, Magland JF, Epstein CL, Floyd TF, Wehrli FW. Accuracy and precision of MR blood oximetry based on the long paramagnetic cylinder approximation of large vessels. Magn. Reson. Med. 2009;62:333–340. doi: 10.1002/mrm.21981.

60. Ogawa S, Lee TM, Kay AR, Tank DW. Brain magnetic resonance imaging with contrast dependent on blood oxygenation. Proceedings of the National Academy of Sciences 1990;87:9868–9872.

61. Ogawa S, Menon RS, Tank DW, Kim S-G, Merkle H, Ellermann JM, Uğurbil K. Functional brain mapping by blood oxygenation level-dependent contrast magnetic resonance imaging: A comparison of signal characteristics with a biophysical model. Biophysical Journal 1993;64:803–812. doi: 10.1007/springerreference_182837.

62. Noseworthy MD, Bulte DP, Alfonsi J. BOLD magnetic resonance imaging of skeletal muscle. Seminars in Musculoskeletal Radiology 2003;7:307–315. doi: 10.1055/s-2004-815678.

63. Damon BM, Gore JC. Physiological basis of muscle functional MRI: Predictions using a computer model. Journal of Applied Physiology 2004;98:264–273. doi: 10.1152/japplphysiol.00369.2004.

64. Partovi S, Karimi S, Jacobi B, et al. Clinical implications of skeletal muscle blood-oxygenation-level-dependent (BOLD) MRI. Magn Reson Mater Phy 2012;25:251–261. doi: 10.1007/s10334-012-0306-y.

65. Partovi S, Schulte A-C, Jacobi B, et al. Blood oxygenation level-dependent (BOLD) MRI of human skeletal muscle at 1.5 and 3 T. J. Magn. Reson. Imaging 2012;35:1227–1232. doi: 10.1002/jmri.23583.

66. Langham MC, Englund EK, Mohler ER III, Li C, Rodgers ZB, Floyd TF, Wehrli FW. Quantitative CMR markers of impaired vascular reactivity associated with age and peripheral artery disease. Journal of Cardiovascular Magnetic Resonance 2013;15:1–10. doi: 10.1186/1532-429X-15-17.

67. Langham MC, Floyd TF, Mohler ER III, Magland JF, Wehrli FW. Evaluation of Cuff-Induced Ischemia in the Lower Extremity by Magnetic Resonance Oximetry. JACC 2010;55:598–606. doi: 10.1016/j.jacc.2009.08.068.

68. Ledermann H-P, Schulte A-C, Heidecker H-G, Aschwanden M, Jager KA, Scheffler K, Steinbrich W, Bilecen D. Blood oxygenation level-dependent magnetic resonance imaging of the skeletal muscle in patients with peripheral arterial occlusive disease. Circulation 2006;113:2929–2935. doi: 10.1161/CIRCULATIONAHA.105.605717.

69. Potthast S, Schulte A, Kos S, Aschwanden M, Bilecen D. Blood oxygenation level-dependent MRI of the skeletal muscle during ischemia in patients with peripheral arterial occlusive disease. Fortschr Röntgenstr 2009;181:1157–1161. doi: 10.1055/s-0028-1109786.

70. Bernstein EF, Murphy AE, Shea MA, Housman LB. Experimental and clinical experience with transcutaneous Doppler ultrasonic flowmeters. Arch Surg 1970;101:21–25.

71. Hahn EL. Detection of sea-water motion by nuclear precession. Journal of Geophysical Research 1960;65:776–777. doi: 10.1029/JZ065i002p00776.

72. Nayler GL, Firmin DN, Longmore DB. Blood flow imaging by cine magnetic resonance. J Comput Assist Tomogr 1986;10:715–722.

73. Buonocore MH. Visualizing blood flow patterns using streamlines, arrows, and particle paths. Magn. Reson. Med. 1998;40:210–226.

74. Frydrychowicz A, Winterer JT, Zaitsev M, Jung B, Hennig J, Langer M, Markl M. Visualization of iliac and proximal femoral artery hemodynamics using time-resolved 3D phase contrast MRI at 3T. J. Magn. Reson. Imaging 2007;25:1085–1092. doi: 10.1002/jmri.20900.

75. Langham MC, Zhou Y, Chirico EN, Magland JF, Sehgal CM, Englund EK, Mohler ER III, Guo W, Barhoum S, Wehrli FW. Effects of age and smoking on endothelial function assessed by quantitative cardiovascular magnetic resonance in the peripheral and central vasculature. Journal of Cardiovascular Magnetic Resonance 2015;17:19. doi: 10.1186/s12968-015-0110-8.

76. Williams DS, Detre JA, Leigh JS, Koretsky AP. Magnetic resonance imaging of perfusion using spin inversion of arterial water. Proceedings of the National Academy of Sciences 1992;89:212–216.

77. Kim S-G. Quantification of relative cerebral blood-flow change by Flow-Sensitive Alternating Inversion-Recovery (FAIR) technique: Application to functional mapping. Magn. Reson. Med. 1995;34:293–301. doi: 10.1002/mrm.v34:1.

78. Kim S-G, Tsekos NV. Perfusion Imaging by a Flow-sensitive Alternating Inversion Recovery (FAIR) Technique: Application to Functional Brain Imaging. Magn. Reson. Med. 2005;37:425–435. doi: 10.1002/mrm.1910370321.

79. Wong EC, Buxton RB, Frank LR. Implementation of quantitative perfusion imaging techniques for functional brain mapping using pulsed arterial spin labeling. NMR Biomed. 1997;10:237–249. doi: 10.1002/(sici)1099-1492(199706/08)10:4/5<237::aid-nbm475>3.0.co;2-x.

80. Buxton RB, Frank LR, Wong EC, Siewert B, Warach S, Edelman RR. A general kinetic model for quantitative perfusion imaging with arterial spin labeling. MRM 1998. doi: 10.1002/mrm.1910400308.

81. Alsop DC, Detre JA, Golay X, et al. Recommended implementation of arterial spin-labeled perfusion MRI for clinical applications: A consensus of the ISMRM perfusion study group and the European consortium for ASL in dementia. Magn. Reson. Med. 2014;73:102–116. doi: 10.1002/mrm.25197.

82. Dai W, Garcia D, de Bazelaire C, Alsop DC. Continuous flow-driven inversion for

arterial spin labeling using pulsed radio frequency and gradient fields. Magn. Reson. Med. 2008;60:1488–1497. doi: 10.1002/mrm.21790.

83. Wong EC, Buxton RB, Frank LR. A theoretical and experimental comparison of continuous and pulsed arterial spin labeling techniques for quantitative perfusion imaging. Magn. Reson. Med. 1998;40:348–355.

84. Langham MC, Englund EK, Li C, Floyd TF, Mohler ER III, Wehrli FW. Balanced tissue magnetization reduces confounding BOLD effect in post-ischemic muscle perfusion quantification. Proceedings of the International Society for Magnetic Resonance in Medicine 2012:2027. doi: 10.5296/ijl.v6i3.5332.s856.

85. Dixon WT, Du LN, Faul DD, Gado M, Rossnick S. Projection Angiograms of Blood Labeled by Adiabatic Fast Passage. Magn. Reson. Med. 1986;3:454–462.

86. Edelman RR, Siewert B, Darby DG, Thangaraj V, Nobre AC, Mesulam MM, Warach S. Qualitative Mapping of Cerebral Blood-Flow and Functional Localization with Echo-Planar Mr-Imaging and Signal Targeting with Alternating Radio-Frequency. Radiology 1994;192:513–520. doi: 10.1148/radiology.192.2.8029425.

87. Haacke EM, Lai S, Reichenbach JR, Kuppusamy K, Hoogenraad F, Takeichi H, Lin WL. In vivo measurement of blood oxygen saturation using magnetic resonance imaging: A direct validation of the blood oxygen level-dependent concept in functional brain imaging. Hum Brain Mapp 1997;5:341–346. doi: 10.1002/(SICI)1097-0193(1997)5:5<341::AID-HBM2>3.0.CO;2-3.

88. Langham MC, Wehrli FW. Simultaneous mapping of temporally-resolved blood flow velocity and oxygenation in femoral artery and vein during reactive hyperemia. Journal of Cardiovascular Magnetic Resonance 2011;13:66. doi: 10.1186/1532-429X-13-66.

89. Wright GA, Hu BS, Macovski A. Estimating oxygen saturation of blood in vivo with MR imaging at 1.5 T. J. Magn. Reson. Imaging 1991;1:275–283. doi: 10.1002/jmri.1880010303.

90. Lu H, Ge Y. Quantitative evaluation of oxygenation in venous vessels using T2-Relaxation-Under-Spin-Tagging MRI. Magn. Reson. Med. 2008;60:357–363. doi: 10.1002/mrm.21627.

91. Jain V, Magland J, Langham M, Wehrli FW. High temporal resolution in vivo blood oximetry via projection-based T2measurement. Magn. Reson. Med. 2012;70:785–790. doi: 10.1002/mrm.24519.

92. Lu H, Xu F, Grgac K, Liu P, Qin Q, van Zijl P. Calibration and validation of TRUST MRI for the estimation of cerebral blood oxygenation. Magn. Reson. Med. 2011;67:42–49. doi: 10.1002/mrm.22970.

93. Rodgers ZB, Englund EK, Langham MC, Magland JF, Wehrli FW. Rapid T2- and

susceptometry-based CMRO2 quantification with interleaved TRUST (iTRUST). NeuroImage 2015;106:441–450. doi: 10.1016/j.neuroimage.2014.10.061.

94. Langham MC, Wehrli FW. Improved temporal resolution of dynamic oximetry via keyhole acquisition for quantifying reactive hyperemia. Proceedings of the International Society for Magnetic Resonance in Medicine 2012:1147. doi: 10.5296/ijl.v6i3.5332.s856.

95. Pauling L, Coryell CD. The magnetic properties and structure of hemoglobin, oxyhemoglobin and carbonmonoxyhemoglobin. Proceedings of the National Academy of Sciences 1936;22:210–216.

96. Spees WM, Yablonskiy DA, Oswood MC, Ackerman JJ. Water proton MR properties of human blood at 1.5 Tesla: Magnetic susceptibility, T1, T2, T2* and non-Lorentzian signal behavior. Magn. Reson. Med. 2001;45:533–542. doi: 10.1002/mrm.1072.

97. Jain V, Abdulmalik O, Propert KJ, Wehrli FW. Investigating the magnetic susceptibility properties of fresh human blood for noninvasive oxygen saturation quantification. Magn. Reson. Med. 2011;68:863–867. doi: 10.1002/mrm.23282.

98. Li C, Langham MC, Epstein CL, Magland JF, Wu J, Gee J, Wehrli FW. Accuracy of the cylinder approximation for susceptometric measurement of intravascular oxygen saturation. Magn. Reson. Med. 2011;67:808–813. doi: 10.1002/mrm.23034.

99. Langham MC, Magland JF, Floyd TF, Wehrli FW. Retrospective correction for induced magnetic field inhomogeneity in measurements of large-vessel hemoglobin oxygen saturation by MR susceptometry. Magn. Reson. Med. 2009;61:626–633. doi: 10.1002/mrm.21499.

100. Damon BM, Hornberger JL, Wadington MC, Lansdown DA, Kent-Braun JA. Dual gradient-echo MRI of post-contraction changes in skeletal muscle blood volume and oxygenation. Magn. Reson. Med. 2007;57:670–679. doi: 10.1002/mrm.21191.

101. Lebon V, Brillault-Salvat C, Bloch G, Leroy-Willig A, Carlier PG. Evidence of muscle BOLD effect revealed by simultaneous interleaved gradient-echo NMRI and myoglobin NMRS during leg ischemia. Magn. Reson. Med. 1998;40:551–558. doi: 10.1016/j.jelekin.2015.04.002.

102. Sanchez OA, Copenhaver EA, Elder CP, Damon BM. Absence of a significant extravascular contribution to the skeletal muscle BOLD effect at 3 T. Magn. Reson. Med. 2010;64:527-535. doi: 10.1002/mrm.22449.

103. Partovi S, Karimi S, Jacobi B, et al. Clinical implications of skeletal muscle blood-oxygenation-level-dependent (BOLD) MRI. Magn Reson Mater Phy 2012;25:251–261. doi: 10.1007/s10334-012-0306-y.

104. Ledermann H-P, Heidecker H-G, Schulte A-C, Thalhammer C, Aschwanden M, Jaeger KA, Scheffler K, Bilecen D. Calf muscles imaged at BOLD MR: Correlation with

TcP o2 and flowmetry measurements during ischemia and reactive hyperemia—initial experience. Radiology 2006;241:477–484. doi: 10.1148/radiol.2412050701.

105. Slade JM, Towse TF, Gossain VV, Meyer RA. Peripheral microvascular response to muscle contraction is unaltered by early diabetes but decreases with age. Journal of Applied Physiology 2011;111:1361–1371. doi: 10.1152/japplphysiol.00009.2011.

106. Towse TF, Slade JM, Ambrose JA, DeLano MC, Meyer RA. Quantitative analysis of the postcontractile blood-oxygenation-level-dependent (BOLD) effect in skeletal muscle. Journal of Applied Physiology 2011;111:27–39. doi: 10.1152/japplphysiol.01054.2009.

107. Elder CP, Cook RN, Wilkens KL, Chance MA, Sanchez OA, Damon BM. A method for detecting the temporal sequence of muscle activation during cycling using MRI. Journal of Applied Physiology 2011;110:826–833. doi: 10.1152/japplphysiol.00185.2010.

108. Richardson RS, Haseler LJ, Nygren AT, Bluml S, Frank LR. Local perfusion and metabolic demand during exercise: a noninvasive MRI method of assessment. Journal of Applied Physiology 2001;91:1845–1853.

109. Brillault-Salvat C, Giacomini E, Jouvensal L, Wary C, Bloch G, Carlier PG. Simultaneous determination of muscle perfusion and oxygenation by interleaved NMR plethysmography and deoxymyoglobin spectroscopy. NMR Biomed. 1997;10:315–323.

110. Walvick RP, Lim RP, Lee VS. Simultaneous acquisition of quantitative ASL and T2* (SQUAB) for characterization of skeletal muscle hemodynamics. Proceedings of the International Society for Magnetic Resonance in Medicine 2012;20:160.

111. Mendes JK, Hanrahan CJ, Layec G, Hart C, Richardson RS, Lee VS. Simultaneous measurement of perfusion and BOLD changes in calf muscle during exercise. Proceedings of the International Society for Magnetic Resonance in Medicine 2013;21:3047.

112. Mendes JK, Hanrahan CJ, Zhang JL, Layec G, Hart C, Lee VS. A novel sequence to simultaneously measure R2, R2*, and perfusion. Proceedings of the International Society for Magnetic Resonance in Medicine 2014;22:4567.

113. Mathewson KW, Haykowsky MJ, Thompson RB. Feasibility and reproducibility of measurement of whole muscle blood flow, oxygen extraction, and VO2 with dynamic exercise using MRI. Magn. Reson. Med. 2015;74:1640-1651. doi: 10.1002/mrm.25564.

114. He X, Yablonskiy DA. Quantitative BOLD: Mapping of human cerebral deoxygenated blood volume and oxygen extraction fraction: Default state. Magn. Reson. Med. 2006;57:115–126. doi: 10.1002/mrm.21108.

115. Zheng J, An H, Coggan AR, Zhang X, Bashir A, Muccigrosso D, Peterson LR, Gropler RJ. Noncontrast skeletal muscle oximetry. Magn. Reson. Med. 2013;71:318–325. doi: 10.1002/mrm.24669.

116. Buck AKW, Elder CP, Donahue MJ, Damon BM. Matching of postcontraction perfusion to oxygen consumption across submaximal contraction intensities in exercising humans. J. Appl. Physiol. 2015;119:280–289. doi: 10.1152/japplphysiol.01027.2014.

117. Zhang JL, Hanrahan CJ, Mendes JK, Layec G, Hart C, Carlston K, Mueller M, Richardson RS, Lee VS. Muscle perfusion reserve (MPR) measured from exercise-recovery MRI: a new functional index for diagnosing PAD. Proceedings of the International Society for Magnetic Resonance in Medicine 2015;23:4248.

118. Criqui MH, Langer RD, Fronek A, Feigelson HS, Klauber MR, McCann TJ, Browner D. Mortality Over a Period of 10 Years in Patients with Peripheral Arterial-Disease. New England Journal of Medicine 1992;326:381–386. doi: 10.1056/NEJM199202063260605.

119. Bragadeesh T, Sari I, Pascotto M, Micari A, Kaul S, Lindner JR. Detection of peripheral vascular stenosis by assessing skeletal muscle flow reserve. JACC 2005;45:780–785. doi: 10.1016/j.jacc.2004.11.045.

120. Lebon V, Carlier PG, Brillault-Salvat C, Leroy-Willig A. Simultaneous measurement of perfusion and oxygenation changes using a multiple gradient-echo sequence: Application to human muscle study. Magnetic Resonance Imaging 1998;16:721–729.

121. Li C, Langham MC, Epstein CL, Magland JF, Wu J, Gee J, Wehrli FW. Accuracy of the cylinder approximation for susceptometric measurement of intravascular oxygen saturation. Magn. Reson. Med. 2011;67:808–813. doi: 10.1002/mrm.23034.

122. van Vaals JJ, Brummer ME, Dixon WT, Tuithof HH, Engels H, Nelson RC, Gerety BM, Chezmar JL, Boer den JA. “Keyhole” method for accelerating imaging of contrast agent uptake. J. Magn. Reson. Imaging 1993;3:671–675. doi: 10.1002/jmri.1880030419.

123. Magland JF, Wehrli FW. Pulse sequence programming in a dynamic visual Environment. Proceedings of the International Society for Magnetic Resonance in Medicine 2006;14:3032.

124. Wu W-C, Wang DJ, Detre JA, Ratcliffe SJ, Floyd TF. Transit delay and flow quantification in muscle with continuous arterial spin labeling perfusion-MRI. J. Magn. Reson. Imaging 2008;28:445–452. doi: 10.1002/jmri.21322.

125. Lu H, Clingman C, Golay X, van Zijl PCM. Determining the longitudinal relaxation time (T1) of blood at 3.0 Tesla. Magn. Reson. Med. 2004;52:679–682. doi: 10.1002/mrm.20178.

126. Gold GE, Han E, Stainsby J, Wright G, Brittain J, Beaulieu C. Musculoskeletal MRI at 3.0 T: relaxation times and image contrast. American Journal of Roentgenology 2004;183:343–351. doi: 10.2214/ajr.183.2.1830343.

127. Versluis B, Backes WH, van Eupen MGA, et al. Magnetic resonance imaging in peripheral arterial disease: reproducibility of the assessment of morphological and

functional vascular status. Investigative Radiology 2011;46:11–24. doi: 10.1097/RLI.0b013e3181f2bfb8.

128. Etsuda H, Takase B, Uehata A, et al. Morning attenuation of endothelium-dependent, flow-mediated dilation in healthy young men: possible connection to morning peak of cardiac events? Clin Cardiol 1999;22:417–421. doi: 10.1109/ieeestd.2008.4475826.

129. Nadel ER, Fortney SM, Wenger CB. Effect of hydration state of circulatory and thermal regulations. J Appl Physiol Respir Environ Exerc Physiol 1980;49:715–721.

130. Bungum L, Kvernebo K, Oian P, Maltau JM. Laser doppler-recorded reactive hyperaemia in the forearm skin during the menstrual cycle. BJOG 1996;103:70–75. doi: 10.1111/j.1471-0528.1996.tb09517.x.

131. Parkes LM, Rashid W, Chard DT, Tofts PS. Normal cerebral perfusion measurements using arterial spin labeling: Reproducibility, stability, and age and gender effects. Magn. Reson. Med. 2004;51:736–743. doi: 10.1002/mrm.20023.

132. Proctor DN, Le KU, Ridout SJ. Age and regional specificity of peak limb vascular conductance in men. Journal of Applied Physiology 2005;98:193–202. doi: 10.1152/japplphysiol.00704.2004.

133. Schulte A-C, Aschwanden M, Bilecen D. Calf Muscles at Blood Oxygen Level–Dependent MR Imaging: Aging Effects at Postocclusive Reactive Hyperemia 1. Radiology 2008;247:482–489. doi: 10.1148/radiol.2472070828.

134. Englund EK, Langham MC, Ratcliffe SJ, Fanning MJ, Wehrli FW, Mohler ER III, Floyd TF. Multiparametric assessment of vascular function in peripheral artery disease: dynamic measurement of skeletal muscle perfusion, blood-oxygen-level dependent signal, and venous oxygen saturation. Circulation: Cardiovascular Imaging 2015;8:e002673–e002673. doi: 10.1161/CIRCIMAGING.114.002673.

135. Anderson JD, Epstein FH, Meyer CH, et al. Multifactorial determinants of functional capacity in peripheral arterial disease: uncoupling of calf muscle perfusion and metabolism. JACC 2009;54:628–635. doi: 10.1016/j.jacc.2009.01.080.

136. Jiji RS, Pollak AW, Epstein FH, et al. Reproducibility of rest and exercise stress contrast-enhanced calf perfusion magnetic resonance imaging in peripheral arterial disease. Journal of Cardiovascular Magnetic Resonance 2013;15:14. doi: 10.1186/1532-429X-15-14.

137. Roberts DA, Detre JA, Bolinger L, Insko EK, Lenkinski RE, Pentecost MJ, Leigh JS. Renal perfusion in humans: MR imaging with spin tagging of arterial water. Radiology 1995;196:281–286. doi: 10.1148/radiology.196.1.7784582.

138. Maccotta L, Detre JA, Alsop DC. The efficiency of adiabatic inversion for perfusion

imaging by arterial spin labeling. NMR Biomed. 1997;10:216–221.

139. Fronek A, Coel M, Bernstein EF. Quantitative Ultrasonographic Studies of Lower-Extremity Flow Velocities in Health and Disease. Circulation 1976;53:957–960. doi: 10.1161/01.CIR.53.6.957.

140. Bernink PJLM, Lubbers J, Barendsen GJ, Van den Berg J. Blood-Flow in the Calf During and After Exercise - Measurements with Doppler Ultrasound and Venous Occlusion Plethysmography in Healthy-Subjects and in Patients with Arterial Occlusive Disease. Angiology 1982;33:146–160.

141. Aslan S, Xu F, Wang PL, Uh J, Yezhuvath US, van Osch M, Lu H. Estimation of labeling efficiency in pseudocontinuous arterial spin labeling. Magn. Reson. Med. 2010;63:765–771. doi: 10.1002/mrm.22245.

142. Englund EK, Langham MC, Li C, Rodgers ZB, Floyd TF, Mohler ER III, Wehrli FW. Combined measurement of perfusion, venous oxygen saturation, and skeletal muscle T2* during reactive hyperemia in the leg. Journal of Cardiovascular Magnetic Resonance 2013;15:1–13. doi: 10.1186/1532-429X-15-70.

143. Magland JF, Li C, Langham MC, Wehrli FW. Pulse sequence programming in a dynamic visual environment: SequenceTree. Magn. Reson. Med. 2016;75:257–265. doi: 10.1002/mrm.25640.

144. Mildner T, Trampel R, Moller HE, Schafer A, Wiggins CJ, Norris DG. Functional perfusion imaging using continuous arterial spin labeling with separate labeling and imaging coils at 3 T. Magn. Reson. Med. 2003;49:791–795. doi: 10.1002/mrm.10438.

145. Wu W-C, Fernández-Seara M, Detre JA, Wehrli FW, Wang DJ. A theoretical and experimental investigation of the tagging efficiency of pseudocontinuous arterial spin labeling. Magn. Reson. Med. 2007;58:1020–1027. doi: 10.1002/mrm.21403.

146. Wong EC. Vessel-encoded arterial spin-labeling using pseudocontinuous tagging. Magn. Reson. Med. 2007;58:1086–1091. doi: 10.1002/mrm.21293.

147. Jain V, Langham MC, Wehrli FW. MRI estimation of global brain oxygen consumption rate. JCBFM 2010;30:1598–1607. doi: 10.1038/jcbfm.2010.49.

148. Rodgers ZB, Jain V, Englund EK, Langham MC, Wehrli FW. High temporal resolution MRI quantification of global cerebral metabolic rate of oxygen consumption in response to apneic challenge. JCBFM 2013;33:1514–1522. doi: 10.1038/jcbfm.2013.110.

149. Barhoum S, Langham MC, Magland JF, Rodgers ZB, Li C, Rajapakse CS, Wehrli FW. Method for rapid MRI quantification of global cerebral metabolic rate of oxygen. JCBFM 2015;35:1616–1622. doi: 10.1038/jcbfm.2015.96.

150. Hirsch AT, Haskal ZJ, Hertzer NR, et al. ACC/AHA 2005 Guidelines for the management of patients with peripheral arterial disease (lower extremity, renal, mesenteric, and abdominal aortic): Executive summary - A collaborative report from the American Association for Vascular Surgery/Society for Vascular Surgery, Society for Cardiovascular Angiography and Interventions, Society for Vascular Medicine and Biology, Society of Interventional Radiology, and the ACC/AHA Task Force on Practice Guidelines (Writing Committee to Develop Guidelines for the Management of Patients With Peripheral Arterial Disease). JACC 2006;47:1239–1312. doi: 10.1016/j.jacc.2005.10.009.

151. Harris LM, Faggioli GL, Shah R, Koerner N, Lillis L, Dandona P, Izzo JL, Snyder B, Ricotta JJ. Vascular reactivity in patients with peripheral vascular disease. American Journal of Cardiology 1995;76:207–212. doi: 10.1016/S0002-9149(99)80066-6.

152. Lijmer JG, Hunink MG, van den Dungen JJ, Loonstra J, Smit AJ. ROC analysis of noninvasive tests for peripheral arterial disease. Ultrasound Med Biol 1996;22:391–398.

153. Hiatt WR. Medical treatment of peripheral arterial disease and claudication. New England Journal of Medicine 2001;344:1608–1621. doi: 10.1056/NEJM200105243442108.

154. Criqui MH, Denenberg JO. The generalized nature of atherosclerosis: how peripheral arterial disease may predict adverse events from coronary artery disease. Vasc Med 1998;3:241–245. doi: 10.1177/1358836X9800300311.

155. Pollak AW, Meyer CH, Epstein FH, Jiji RS, Hunter JR, DiMaria JM, Christopher JM, Kramer CM. Arterial spin labeling MR imaging reproducibly measures peak-exercise calf muscle perfusion in healthy volunteers and patients with peripheral arterial disease. JACC: Cardiovascular Imaging 2012;5:1224–1230. doi: 10.1016/j.jcmg.2012.03.022.

156. Wigmore DM, Damon BM, Pober DM, Kent-Braun JA. MRI measures of perfusion-related changes in human skeletal muscle during progressive contractions. Journal of Applied Physiology 2004;97:2385–2394. doi: 10.1152/japplphysiol.01390.2003.

157. Aboyans V, Criqui MH, Abraham P, et al. Measurement and Interpretation of the Ankle-Brachial Index: A Scientific Statement From the American Heart Association. Circulation 2012;126:2890–2909. doi: 10.1161/CIR.0b013e318276fbcb.

158. Stein R, Hriljac I, Halperin JL, Gustavson SM, Teodorescu V, Olin JW. Limitation of the resting ankle–brachial index in symptomatic patients with peripheral arterial disease. Vasc Med 2006;11:29–33. doi: 10.1191/1358863x06vm663oa.

159. Gardner AW, Katzel LI, Sorkin JD, Bradham DD, Hochberg MC, Flinn WR, Goldberg AP. Exercise rehabilitation improves functional outcomes and peripheral circulation in patients with intermittent claudication: A randomized controlled trial. J Am Geriatr Soc 2001;49:755–762. doi: 10.1046/j.1532-5415.2001.49152.x.

160. McDermott MM, Ferrucci L, Guralnik JM, Dyer AR, Kiang Liu, Pearce WH, Clark E, Yihua Liao, Criqui MH. The ankle-brachial index is associated with the magnitude of impaired walking endurance among men and women with peripheral arterial disease. Vasc Med 2010;15:251–257. doi: 10.1177/1358863X10365181.

161. Szuba A, Oka RK, Harada R, Cooke JP. Limb hemodynamics are not predictive of functional capacity in patients with PAD. Vasc Med 2006;11:155–163. doi: 10.1177/1358863x06074828.

162. Englund EK, Rodgers ZB, Langham MC, Mohler ER III, Floyd TF, Wehrli FW. Simultaneous measurement of microvascular and macrovascular blood flow and oxygenation in the leg. Proceedings of the International Society for Magnetic Resonance in Medicine 2014;22:722.

163. Chance B, Nioka S, Kent J, McCully K, Fountain M, Greenfeld R, Holtom G. Time-resolved spectroscopy of hemoglobin and myoglobin in resting and ischemic muscle. Anal. Biochem. 1988;174:698–707.

164. Mesquita RC, Putt M, Chandra M, et al. Diffuse optical characterization of an exercising patient group with peripheral artery disease. J. Biomed. Opt. 2013;18:57007. doi: 10.1117/1.JBO.18.5.057007.

165. Rodgers ZB, Kini L, Jain V, Langham MC, Magland JF, Wehrli FW. High temporal resolution, simultaneous quantification of intravascular blood flow and oxygen saturation with BRISK k-space sampling. Proceedings of the International Society for Magnetic Resonance in Medicine 2013;21:1351.